Fixed-bed biomass pyrolysis: mechanisms and biochar production

Alba Dieguez Alonso

Technische Universität Berlin
Fakultät III: Prozesswissenschaften
Institut für Energietechnik
Fachgebiet Energieverfahrenstechnik und Umwandlungstechniken regenerativer Energien

Dissertation

Fixed-bed biomass pyrolysis: mechanisms and biochar production

vorgelegt von

Ingeniero Industrial Alba Dieguez Alonso
aus Rodeiro (Galicia, Spanien)

Von der Fakultät III - Prozesswissenschaften
der Technischen Universität Berlin
zur Erlangung des akademischen Grades

Doktor der Ingenieurwissenschaften
– Dr.-Ing. –

genehmigte Dissertation

Promotionsausschuss

Vorsitzender: Prof. Dr.-Ing. George Tsatsaronis
Gutachter: Prof. Dr. Frank Behrendt
Gutachter: Prof. Dr. Douglas Greenhalgh
Gutachter: Prof. Dr. Jacobo Porteiro

Tag der wissenschaftlichen Aussprache: 10. Juli 2015

Berlin 2015

Acknowledgments

I would like to express my gratitude to all those who gave me the possibility to complete this thesis.

I wish to thank:

Prof. Dr. Behrendt, the supervisor of this work, for making it possible in the first place, for the continuous support and confidence and also for the continuous challenges.

Prof. Dr. Porteiro and Prof. Dr. Greenhalgh, the reviewers of this work, for your support.

Dr.-Ing. Anca-Couce and Dr.-Ing. Zobel, for being my mentors.

Dr. Gerardo Ojeda (current affiliation Universidad Nacional de Colombia) and Prof. Dr. (apl) Jörg Bachmann (Institute of Soil Science, Leibniz University of Hannover), for contributing to this work with the characterization of wettability and contact angle of several biochar samples, produced during the realization of this thesis.

Alessandro G. Rombola and Prof. Daniele Fabbri (University of Bologna), for contributing to this work with the characterization of PAHs content and stability with Py-GC-MS for several biochar samples, produced during the realization of this thesis.

Ivo Schneider, Susanne Hoffmann, Uwe Röhr and Birgit Packeiser, simply this thesis would not have been completed without your work, help and support; also because of your patience with my German.

All my master and bachelor thesis students: Laura, Tamara, Amalie, Omar, Daniel, Huong, Kolo, Fabian, Alba II, Naiara, Alberto, Hernán, Pablo, Bernat, you all are part of this work.

All my colleagues at EVUR, for the day-to-day.

Rocío, Johann, Covi, Paula, Carlos and all my friend in Berlin, for sharing my time.

Finally, I would deeply like to thank Sergio, for building a life with me in Germany and my family, for your continuous support and love.

Dedicatoria

Gustaríame adicarlle esta tese a meus pais e ó abuelo, porque fostes e sodes o mellor exemplo de superación.

Abstract

The objective of this thesis is to gain a deeper understanding on the slow pyrolytic conversion of biomass in conditions similar to the ones present at industrial scale. The purpose of this is to contribute to two topics of significant relevance in the biomass thermochemical conversion community nowadays. Firstly, the need for further development of more detailed pyrolysis mechanisms, which account not only for chemical reactions pathways, but also for the influence of transport phenomena on these chemical reactions, enhanced in conditions typical of industrial scale, due to bigger particle and bed sizes. Secondly, the use of slow pyrolysis for production of biochar, in particular, the understanding of how pyrolysis conditions may affect biochar properties and consequently its behavior in soil.

To this end, a technical-scale fixed bed reactor has been built, together with a novel combination of on-line characterization techniques, to perform an exhaustive on-line evaluation of the pyrolysis process. These techniques include temperature measurements inside the bed, characterization of permanent gas composition with gas chromatography - thermal conductivity detection (GC-TCD) and detection of fluorescence emitting compounds with laser-induced fluorescence spectroscopy (LIF). Differentiation between primary pyrolysis and secondary reactions of primary volatiles has been achieved, thanks to the selective detection of targeted species, products of these secondary reactions. Investigation on the source and production enhancement mechanisms of these species has been also carried out.

In a second stage, several characterization methodologies have been developed and applied to get a deep characterization of the solid product (biochar), from two perspectives: structural properties and potential behavior in soil. The objective is to establish clear relations to "engineer" biochar, according to soil application demands and certification requirements. Besides, development of characterization techniques which may lead to a more complete evaluation and therefore better certification of this biochar has been considered, in particular for porosity characterization.

Zusammenfassung

Die Zielstellung dieser Dissertation ist es, ein tieferes Verständnis über die langsame pyrolytische Biomassenkonversion unter Bedingungen zu gewinnen, wie man sie im industriellen Maßstab vorfindet. Hierdurch soll bezweckt werden, auf zwei Feldern von signifikanter Relevanz für die heutige Forschergemeinschaft der thermochemischen Biomassenkonversion einen Beitrag zu leisten. Denn zum einen besteht noch Entwicklungsbedarf für genauere Pyrolysemechanismen, welche nicht nur die chemischen Reaktionsabläufe berücksichtigen, sondern auch den Einfluss durch Transportphänomene auf diese chemischen Reaktionsabläufe miteinbeziehen und angepasst an Bedingungen sind, wie man sie aufgrund von größerer Partikel- und Bettgröße typischerweise im Industriemaßstab vorfindet. Das zweite Feld beinhaltet die Produktion von Biochar durch eine langsame Pyrolyse und soll insbesondere klären, inwieweit die Pyrolysebedingungen die Eigenschaften des Biochars und konsequenterweise deren Reaktionen im Boden beeinflussen. Um dieses Ziel zu erreichen wurde ein Festbettreaktor in Technikumsgröße errichtet und mit einer neuartigen Kombination von on-line Charakterisierungstechniken ausgestattet, welche es ermöglichen, den Pyrolysevorgang umfassend in-situ und on-line zu untersuchen. Diese Techniken umfassen die Temperaturerfassung im Reaktorbett, die Bestimmung der Permanentgaszusammensetzung durch Gaschromatographie-Wärmeleitfähigkeits detektor (GC-WLD) und der Nachweis von fluoreszierenden Verbindungen durch laserinduzierte Fluoreszenzspektroskopie (LIF). Eine Unterscheidung zwischen der primären Pyrolyse und den Sekundärreaktionen der primärflüchtigen Bestandteile war durchführbar, dank der selektiven Bestimmung von Schlüsselverbindungen, welche als Produkte der Sekundärreaktionen entstehen. Fernerhin wurde untersucht, welchen Ursprung diese Spezies haben und welche Mechanismen deren vermehrtes Auftreten fördern.

In der zweiten Phase wurden mehrere Charakterisierungsmethoden entwickelt und angewendet, um das feste Produkt (Biochar) ausführlich in zweierlei Hinsicht zu charakterisieren. Zum einen Hinblick auf die strukturellen Eigenschaften, zum anderen auf das mögliche Verhalten im Boden. Zielstellung war es hier, klare Zusammenhänge

herauszuarbeiten, um einen Biochar zu "konstruieren", welcher den Anforderungen bei Verwendung im Boden und Zertifizierungsvorgaben erfüllt. Außerdem wurde die Entwicklung weiterer Charakterisierungsmethoden geprüft, welche möglicherweise zu einer vollständigeren und daher auch besseren Zertifizierung von diesem Biochar führen, insbesondere in Hinsicht auf die Charakterisierung der Poren.

Contents

List of Figures

List of Tables

Chapter 1

Introduction

In order to meet the goals established by the Kyoto protocol, the European Union has established several tough objectives regarding energy and climate protection by 2020. These include to rise the share of energy from renewable sources in the gross final consumption of energy to at least 20 %; to reach a 20 % improvement in energy efficiency and to reduce the greenhouse gas emissions (GHG) at least 20 % below 1990 levels. Besides this, the share of energy from renewable sources in the transport sector must amount to at least 10 % of the final energy consumption in the sector also by 2020. If we look further ahead, the objectives become even more challenging, aiming at a reduction of 80 - 95 % compared to 1990 levels in greenhouse gas emissions by 2050 [12–14].

With these mid- and long-term objectives, the professionals in the energy sector have the duty and responsibility not only to increase the participation of renewable energies in the energy mix, but also to do it in a sustainable, efficient, economically competitive and stable way.

In order to achieve these goals the main disadvantages of the renewable energy sources must be overcome. Among those, spatial and temporal distribution play a significant role, i.e., the different energy sources are not available everywhere - with transportation not possible in most cases, in opposition to conventional fuels - and, if they are, they may not be available when demanded. Commonly this drawback is overcome by combining several renewable energy sources and prioritizing, when possible, the production of energy from these sources, instead of conventional energy production sources. However, this introduces inevitably instability in the electrical grid and reduces their competitiveness against conventional sources in absence of external support.

It is clear that the solution to this problem is of high complexity, both from a technical, but also from a political point of view, and most probably the global solution would include the combination of several technical approaches, as for example the development of more efficient energy storage systems, together with the development of smart grids.

Another possible contribution to this global solution is the enhancement of energy production from renewable sources which do not show such strong spatial and temporal dependence, such as biomass. This is the only renewable energy source which allows the complete substitution of fossil fuels, in the sense that the same products can be made from biomass as from fossil fuels, including chemicals and transport fuels. At the same time, biomass is a widespread energy source which allows the production of heat (also high temperature heat) and power on demand, as in the case of fossil fuels, and it may be CO_2 neutral if harvested and processed in a sustainable manner [15].

There are several possible biomass conversion routes, depending on the initial feedstock and the desired final product, which can be classified into bio-chemical, physico-chemical and thermo-chemical processes [16].

Bio-chemical - biomass decomposition by microorganisms - and physico-chemical conversion processes constitute nowadays the main pathways for production of biofuels for the transport sector, i.e, bioethanol from fermentation of starch and sugar crops and biodisel from transesterification of vegetable oils or animal fats [17]. These processes, despite being already commercially competitive in some countries, present the shortcoming of employing feedstock which compete directly with food/feed use. Besides, not only biofuels have to be considered, but also the production of electricity, heating and cooling from biomass, which is expected to be a key contribution by 2020 and increase in the post-2020 period [18]. For this reason, up-scaling of bioenergy systems requires: (1) the introduction of alternative and sustainable biomass feedstock, (2) an increase in the efficiency of biomass production, accompanied by a more sustainable land management, and (3) an increase in the conversion efficiency.

A first step to fulfill those requirements is the use of lignocellulosic biomass, since it does not compete directly with food/feed use; it includes agricultural, forestry, industrial, animal and human organic residues and it leads to an increase in the yield of fuel per unit of cultivated area [17].

Then, alternative conversion processes which allow the processing of these materials while increasing the conversion efficiency need to be brought into the game. Biochemical conversion technologies for production of bioliquids, and capable of dealing with these materials, are already available, but they are more technologically demanding and therefore more expensive [17]. An alternative to those processes are the thermochemical conversion processes, which allow not only the production of bioliquids, but also of solid and gaseous fuels, leading to heat and power, while being able to convert all the biomass fractions and therefore to increase the global conversion efficiency. These processes are based on the use of high temperatures (and/or pressures) to break down the biomass macromolecules. They can be mainly classified in: pyrolysis, gasification, combustion and liquefaction [17]. The main energetic applications of these processes are summarized in Fig. 1.1.

Moreover, the up-scaling of any bioenergy system requires, as previously mentioned, more efficient and sustainable biomass production, together with sustainable land management [18]. This will determine, on one hand, if biomass is a sustainable renewable energy source and, on the other hand, it will have a direct impact on the consideration of biomass as a CO_2 neutral energy source, due to the direct and indirect land use change, related to the possible reduction of carbon stocks. Moreover, it may affect biodiversity, land and water quality and increase other GHG emissions besides CO_2 [18]. A solution to this needs to be approached from different fronts, that is to say, selection of more productive feedstock, enhancement of residues use, but also improvement of the soil quality while increasing the soil carbon stocks. It is here where biochar comes into play, which will be discussed in detail in Chapter 7.

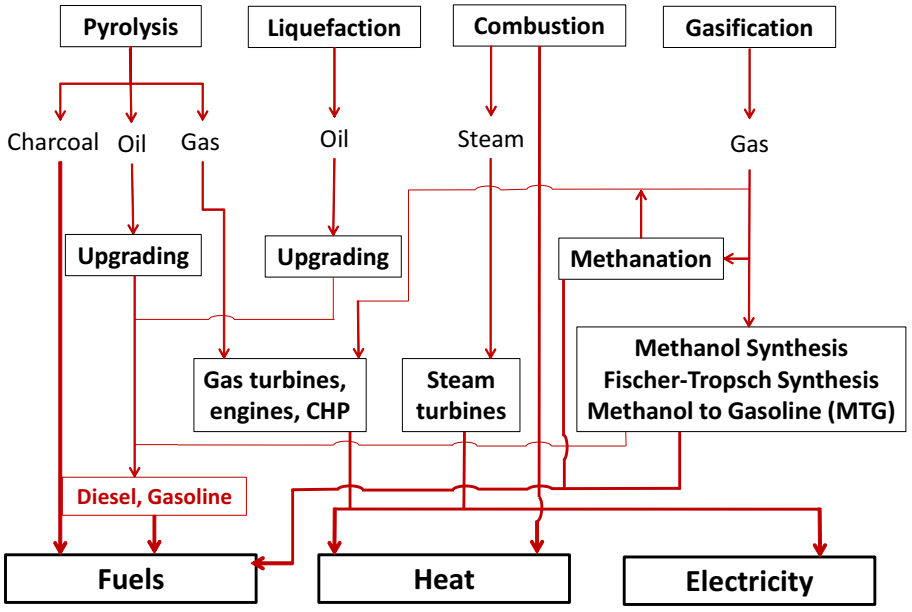

Figure 1.1: *Conversion routes from biomass to biofuels, heat and electricity with thermochemical conversion processes.*

1.1 Thermochemical conversion processes

1.1.1 Combustion

Combustion can be seen as the complete oxidation of the feedstock [15] and constitutes up to now the most employed and commercially competitive thermo-chemical conversion process for biomass utilization, both for heat and for power production [19]. It is also expected to be the main biomass conversion technology in the future [20].

Large-scale ($>$ 20 MW_{th}, classification according to [20]) combustion plants, usually coupled to steam turbines, for power production are a well established technology, especially applied in North American and Scandinavia, with typical capacities between 20 - 100 MW_e [21]. Combustion plants for combined heat and power production (CHP) coupled to steam turbines have shown to be economically and technically feasible for output power $>$ 2 MW_e [1, 21]; while organic Rankine cycles have proven the maturity of the technology in the range of 0.2 - 2 MW_e (medium-scale) [1, 21]. Coupling to Stirling or steam engines is in demonstration status for small-scale CHP plants ($<$ 100 kW_e) [1, 21]. It is in the small-scale combustion systems, mostly used for residential heating, where special attention should be paid, due to the potential growth of this market through direct substitution of fossil fuels, as well as the limitations of the current available technology regarding higher requirements of fuel quality [20] and particle emissions [22].

Several combustion technologies are available in the market, whose selection depends mostly upon the application scale, the feedstock specifications and the affordable investment and operation costs [19]. They have been widely analyzed and reported in literature and they are briefly summarized here, based on [19] and [20]: fixed-bed combustion technologies are available for small (pellets, chips or trunks boilers and stoves), medium (grate-fired furnaces) and large (grate-fired furnaces) scale applications up to 50 MW. The main advantages of these systems are the variability in feedstock humidity, particle size and ash content that they accept, as well as the low investment and operation costs. However, they present lower efficiency due to the requirement of high excess in combustion oxygen and do not deal well with mixing of woody and herbaceous feedstock. Pulverized fuel burners can be used in medium and large applications, allowing in the second case the co-firing with coal up to several 100 MW_{th}. The main advantages are the possible variability in the load and the higher efficiency due to low excess oxygen, but it presents limitations regarding water content and particle size of the feedstock. Fluidized-bed combustion is appropriate only for large-scale applications due to the high investment and operation costs. However, they offer higher efficiency due to lower requirement in oxygen excess and provide better mixing and heat transfer. The accepted particle size range is limited, as well as the ash content and composition due to slagging problems. Besides, the dust load in the flue gas is high, increasing the demand in cleaning systems.

1.1.2 Gasification

Gasification is the thermo-chemical degradation of carbonaceous materials in the presence of an externally supplied oxidizing agent (O_2, H_2O or air) with the objective of producing a gaseous product, composed mainly by CO, H_2, CO_2, CH_4, H_2O and

N_2 (when air is used) [17]. It is therefore a more versatile process in comparison to combustion, since it offers, besides the production of heat and power through direct combustion of gas products, the possibility of producing synthesis gas ($CO + H_2$). This can be combusted in gas engines and turbines in CHP plants, as well as being used for production of methane (methanation) and liquid fuels (BtL). The latter would be achieved with post-processes such as Fischer-Tropsch Synthesis, Methanol Synthesis or Methanol to Gasoline process (MTG) [17], known as Gas/Coal/Biomass to Liquid technology (XtL). Gasification offers therefore a promising alternative for substitution of fossil fuels, both gas and liquid, and consequently brings thermo-chemical conversion processes into the game for biofuels production from ligno-cellulosic materials and waste. However, these technologies are not new at all, experiencing their strong development from the 30s, especially in Germany, for electricity, liquid fuels and chemicals production, based on the use of coal as raw material [23]. Besides, during the Second World War, thousands of cars and trucks were operated in Europe on coal and biomass gasified in on board gasifiers [17] and afterward, during the oil embargo in the 70s, coal gasification recovered its significance being used mainly for heating and production of chemical feedstock [17]. Still nowadays, commercially deployed gasification relies mainly on coal as feedstock, as it is the case of Sasol company in South Africa, based on the Lurgi process (updraft gasification) or new CtL plants in China or India.

Concerning the status of biomass gasification in Europe, gasification technology for heat production up to several hundreds kW_{th} is commercially available and deployed but its contribution to energy production up to now is limited [21]. An example of such application, although pilot plant, is the fluidized bed reactor using steam as gasifying agent at Chalmers University of Technology (Sweden).

CHP gasification plants are mostly in development and demonstration state and have not reached market maturity yet, due to the relatively high costs, critical operational demands and fuel quality requirements [1], although some technologies using gas engines are already on the market [21]. An example is the up-scaling of the Viking gasifier (CHP pilot pant with two-stage gasification technology - screw pyrolysis and downdraft gasification - coupled to gas engines and developed by the Biomass Gasification Group at DTU in Denmark), commercialized for 150 kW_e (demonstration plant in Hadsund, Denmark), 500 kW_e (commercial plant in Hilleröd, Denmark) and 1000 kW_e (not installed so far) by Weiss A/S and COWI A/S [24, 25]. Another example is the Volund gasifier (updraft gasification with moist air), demonstration plant with commercial operation, developed at Harboore by Babcock & Wilcox Volund (Denmark). It is coupled to two gas engines, with a total electrical output of 1.4 MW_e and a thermal power of 3.4 MW_{th} [24,25]. Also the technology developed by Xylowatt reached the market with the NOTAR®gasifier, based on multi-stage downdraft gasification with air or oxygen,

offering capacities of 1 MW LCV, 1.7 MW LCV and 4 MW LCV (oxygas), which can be also combined.

With fluidized bed technology, the Enamora gasification plant (Spain), delivered by Eqtec Iberia, is a commercial CHP plant based on bubbling fluidized bed gasification and coupled to IC turbo-compressed gas engines (from Jenbacher), with an output power of 5.9 MW_e, together with 5600 kg/h of steam at 6 bar(g) and 150 m^3/h of water at 90 °C for the industrial processes at the plant location [25]. Also based on bubbling fluidized bed gasification is the Skive Fjernevarme demonstration plant in Skive (Denmark), based on the Carbona gasification technology (air-blown) and developed by Andritz Carbona as a commercial plant. It operates at pressures between 0.5 and 2 bar and has an output power of 6 MW_e (three gas engines from Jenbacher) and 11.5 MW_{th}, when working in CHP mode; or with a thermal power of 2x10 MW_{th}, when the gas product is alternatively burnt in two gas boilers. In this case, the plant would be included in the classification of heat production (for district heating) [24].

The dual fluidized bed steam gasification technology (gasification zone fluidized with steam and combustion zone fluidized with air), developed at Vienna University of Technology, has been successfully demonstrated in the gasification plant in Güssing (Austria), supplied by AE&E and Repotec, being nowadays commercially operated. It is also a CHP plant with an output power of 2 MW_e and 4.5 MW_{th} [25].

The VIPP gasification unit, developed (pilot plant: VIPP-VORTEX gasification unit of 500 kW_{th}) in collaboration with the Energy Technology Center (ETC) of Pitea (Sweden) and based on an earlier stage of the cyclon gasifier (developed at Lulea Technical University, LTU, Sweden), was brought to a commercialization stage by MEVA Innovation. The demonstration plant is a commercial unit sold to Pite Energi (Hortlax, Sweden) with an output power of 1.2 MW_e and 2.2 MW_{th} [26]. Several CHP demonstration plants, ranging from 1 MW_e to 7 MW_e are in preparation with the MILENA gasification technology, owned by the Energy Research Center of the Netherlands (ECN), coupled to the OLGA gas cleaning system [27].

Gasification technology used in combined cycles for electricity production is in demonstration phase in the range 5-10 MW_e, although it is expected that it can go up to around 200 MW_e [21]. Examples of this technological approach are the gasification plants in Senden (Germany) and Oberwart (Austria), based on the gasification principle of the Güssing plant, but coupled to gas engines and to an Organic Rankine Cycle (ORC), with a total capacity of 5 MW_e and 6.5 MW_{th} and 2.8 MW_e and 4.1 MW_{th} respectively [24, 25].

Regarding gasification technologies for the production of biofuels, GoBiGas in Gothenburg (Sweden) is the first demonstration plant in the world for large-scale production of bio-methane, through gasification of forest residues with a thermal fuel production

power of 20 MW and a thermal output power for district heating of 5 MW. A second phase for commercial application is planned by 2016 with a bio-methane output power up to 100 MW. The technology of this plant is based on gasification and methanation technologies developed in Güssing at pilot scale [25, 28]. Another demonstration plant for the production of bio-methane with a capacity of 4 MW is scheduled for the present year in Netherlands, based on the MILENA gasification technology and the OLGA cleaning system [27].

With respect to the production of liquid transport biofuels, the technology is still moving from pilot scale projects to the construction of the first demonstration plants. One example of pilot plant is the "Bioliq®" process, developed at the Karlsruhe Institute of Technology (Germany) and based on the production of gasoline from methanol through an intermediate step of dimethyl ether synthesis. The idea behind is the decentralized pretreatment of biomass with fast pyrolysis in order to produced a biosyncrude, which can be then economically transported to the core gasification plant. The technology of this plant is high pressure entrained flow gasification for the production of synthesis gas which will be transformed to gasoline [29]. Another example is the pilot plant built in Pitea (Sweden) for production of bio-methanol and bio-DME using black liquor as feedstock, developed under the European BioDME project, as a collaboration of Chemrec, Volvo, Total, Haldor Topsoe, Delphi, ETC and Preem. The gasification technology in this case is based on pressurized oxygen blown gasification with a thermal fuel power of 3 MW_{th} [26]. In the demonstration phase will be the world first commercial biomass to methanol plant, developed by VärmlandsMethanol AB in Sweden and based on HTW (high temperature Winkler) gasification, with a thermal fuel power of 111 MW_{th} [26].

1.1.3 Pyrolysis

Besides gasification, pyrolysis also offers the possibility of producing liquid biofuels from biomass. Pyrolysis is defined as the thermochemical decomposition of carbonaceous materials (such as biomass) either in the total absence of externally supplied oxygen or with a limited supply that does not permit gasification to an appreciable extent [17]. The latter is called oxidative pyrolysis and it has been the technology traditionally used for the production of charcoal, since it turns the process into allothermal due to the heat released during partial combustion. However, new pyrolysis technologies tend to use an inert atmosphere. It usually takes place in the temperature range of 300 - 650 °C [17], giving place to three different products: (a) bio-oil, pyrolysis oil or tar which is liquid at ambient conditions and can be upgraded to transportation fuels, be burnt in a boiler for heat and power production or used for chemicals production; (b) char, which is the solid product and is usually referred to as charcoal, if it is used as a solid fuel or biochar, if it

is used for soil amendment purposes and as carbon sink (introduced in detail in Chapter 7); and (c) permanent gases. Products distribution in pyrolysis depends strongly on the process conditions, specially the heating rate, coupled with the vapor residence time, and the maximum conversion temperature (HTT) [30]. Maximization of liquids yields, optimal for bio-oil production, is achieved with high heating rates ($t_{heating}$ « $t_{reaction}$, i.e., the fuel heating time is smaller than the characteristic pyrolysis reaction time [17]), lower residence time of vapors in the reaction zone, typically between 0.5 - 2 s, and mild temperatures around 500 - 550 °C [31–33]. This process is known as fast pyrolysis. Higher temperatures would lead to secondary reactions of primary tars, causing cracking and polymerization [30], reducing then tar yields while increasing gas yields.

Fast pyrolysis

According to the I.E.A. Bioenergy Task 34 [34], fast pyrolysis bio-oil has been defined as "Liquid condensate recovered by thermal treatment of lignocellulosic biomass at short hot vapour residence time (typically less than about 5 seconds) typically at between 450 - 600 °C at near atmospheric pressure or below, in the absence of oxygen, using small (typically less than 5 mm) dry (typically less than 10 % water) biomass particles". "It typically contains 15 - 30 % water. Common organic components in bio-oil would include acetic acid, methanol, aldehydes and ketones, cyclopentenones, furans, alkyl-phenols, alkyl-methoxy-phenols, anhydrosugars, and oligomeric sugars and water-insoluble lignin-derived compounds. Nitrogen- and sulfur-containing compounds are also sometimes found depending on the biomass source".

Bio-oil can be directly used for combustion in boilers, in order to produce heat and electricity; for indirect production of liquid biofuels, through gasification of bio-oil and following post-processing with Fischer-Tropsch or methanol to gasoline synthesis, as it has been previously presented for the Bioliq®process (biomass pretreatment for supply large biorefineries); or for direct production of biofuels with catalytic upgrading (catalytic hydroprocesses or thermal cracking). Bio-oil can be also integrated in conventional refinery. However, as it has been pointed out by the European Biomass Industry Association (EUBIA) [35], although fast pyrolysis technologies are reaching already the demonstration status, they still have to face significant economic and non-technical barriers which reduce their competitiveness against fossil fuels.

An example of fast pyrolysis for bio-oil production is the technology developed by BTG Biomass Technology Group B.V. (Netherlands) [36], based on a rotating cone reactor (initially developed at the University of Twente) for the production of pyrolysis oil, which can be then directly combusted or upgraded. This company owns a pilot plant with a capacity of 100-200 kg/h of feedstock in Netherlands and built a full scale plant

with a capacity of 2 t/h feedstock (approximate production of 1.2 t/h of pyrolysis oil) to be delivered to Malaysia [36]. BTG is also involved (coordinator) in the Empyro project (financially supported by the 7th Framework Programme of the European Commission) [37], being the objective "to build and demonstrate a 25 MW_{th} polygeneration pyrolysis plant to produce electricity, process steam and fuel oil" in Hengelo (Netherlands). Also at industrial scale, a Finnish Consortium, formed by Fortum, UPM and Valmet developed a fast pyrolysis technology plant (built by Valmet with collaboration of VTT) to integrate to the Joensuu CHP plant (Fortum) for production of heat, electricity and around 50000 tones of bio-oil per year. The bio-oil will be used to replace fossil fuels in the heating plants of Fortrum [38]. The same Consortium started a new five-years project in early 2014 called LignoCat (Lignocellulosic Fuels by Catalytic Pyrolysis) to develop and commercialize integrated catalytic pyrolysis technology for production of high quality biofuels from lignocellulosic materials [39]. Following with the commercialization level, Green Fuel Nordic Oy (Finland) intends to build 20 biorefineries, with a capacity of 90000 tonnes of renewable fuel oil (RFO) each one, using Rapid Thermal Processing (RTP) technology [39]; and Estonia and Latvia plan the construction of two pyrolysis plants, one able to process 130000 tonnes of wood chips in Estonia with fast pyrolysis for the production on bio-oil and another one to integrate in a CHP facility in Latvia, for processing of 100000 tonnes of wood chips [39].

Slow pyrolysis

Slow pyrolysis, on the contrary, is characterized by heating times much longer than the characteristic pyrolysis reaction times (heating rates below 100 K/min), as well as longer residence time of volatiles in the reaction zone, leading to char yields maximization. Slow pyrolysis is the traditional conversion pathway for the production of charcoal, used as solid fuel, or for iron reduction. However, in the present work, slow pyrolysis is the technology considered for the production of biochar, a solid product used for soil amendment purposes and carbon sequestration. A detailed explanation about biochar is given in Chapter 7, however, a short review on the available technologies and companies involved in biochar production nowadays in Europe is given here.

According to the European Biochar Certificate (EBC) Foundation, eight are nowadays the biochar producers certified by the European Biochar Certificate [40] and therefore using different versions of slow pyrolysis (under specific, controlled conditions) as conversion technology. The guidelines of the European Biochar Certificate can be found in [41]. These companies are:

- **Carbon Terra GmbH** [42], which manufactures the Schottdorf-Melier technology, capable of producing 1000 tonnes of biochar per year. The Schottdorf Sys-

tem consists of at least one Schotdorf-Melier, a gas burner (combustion chamber), a steam turbine and a power generator. The Schottdorf Melier is a kiln which works in a counter-current configuration, i.e., the biomass moves from the upper part to the bottom while the oxidazing agent moves in the opposite direction, leaving the reactor in the upper part. The process is a kind of mild gasification with air, with maximum temperatures of 700°C . Each kiln is able to deliver 300 kW of thermal energy through the gas.

- **Pyreg GmbH** [43], specialized in development of equipment for biomass carbonization, including the production of certifiable biochar, with an annual production capacity of around 300 tonnes. The biomass conversion system consists of a screw reactor where the biomass slowly pyrolyzes in absence of O_2. The vapors and permanent gases produced are burnt in a combustion chamber and the thermal energy is used to heat the pyrolysis process and for external heat production.
- **Swiss Biochar GmbH** [44], using also the Pyreg technology. The feedstock used in this case is a mixture of lignin rich wood chips, protein rich fruits residues.
- **Verora GmbH** [45], which also uses the Pyreg technology with temperatures up to 500 - 600 °C. The feedstock used in this case is wood chips from both tree and bush.
- **Sonnenerde** [46], using the Pyreg technology, with a production capacity of around 1500 kg per day. The feedstock used is pulp fiber and cereal husk.
- **Lixhe Compost SA** [47]: no detailed information on the production process is available online yet. The website is provided by the European Biochar Certificate Foundation [40].
- **Fetzer Rohstoffe + Recycling GmbH** [48]: no information available online yet. The website is provided by the European Biochar Certificate Foundation [40].
- **Carmagnola Energie SRL**: no information available online.

Other companies involved in pyrolysis equipment manufacturing for biochar production in Europe, although not certified by the European Biochar Certificate, are [49, 50]:

- **Regenerative Energie Wirtschaftssystem GmbH** [51], specialized in manufacturing equipment for biomass residues (specially wet biomass) processing, including separation, drying, pyrolysis and gasification. The technology for biochar production, based on a screw pyrolyzer (Regenis MAX) has a capacity of around 500 tonnes per year.

- **Black Carbon A/S** [52], which uses the BlackCarbon unit (BC300). This is a CHP unit coupled to a Stirling engine with has a capacity of processing 90 kg/h of biomass. From this it produces 35 kW of electricity, 110 kW of heat for district heating and 110 kW of biochar. The rest of the heat is used to maintain the pyrolysis process.

- **BioMaCon GmbH** [53], which manufactures equipment for biochar production with an annual capacity ranging from 140 to 2000 tonnes. The conversion technology is based on slow pyrolysis in abscence of O_2, taking place in a mono screw reactor and using woody biomass (chips) as feedstock. The system is equipped also with a high temperature reformer (up to 1000 °C) to increase biochar quality and a combustion chamber to burn vapors and gases produced during the pyrolysis process for heat production.

- **Splainex** [54], which is a company with expertise in developing processes and manufacturing equipment for waste treatment, based on pyrolysis technology. The continuous pyrolysis technology they operate with is typically based on a rotatory kiln, in absence of O_2 and up to temperatures of 400 - 600 °C. The produced vapors can be thermally cracked to produce syngas, which is then combusted in a boiler for steam production (MPSC, Modular Pyrolysis Steam Cycle) for power and heat generation. As waste they include different types of wood, agricultural and animal waste, such as poultry litter, for production of biochar.

The previous lists intend to offer a short overview on companies manufacturing pyrolysis equipment or using this technology for biochar production. They have been included either because their biochar production is certified by the European Biochar Certificate or because they have developed interesting slow pyrolysis technologies for biochar production. Information about other companies involved in equipment manufacturing and biochar production and commercialization can be found in [50].

1.2 Next steps. Motivation of this work

The objective of the previous reviews is to offer an overview on the current situation of the main thermo-chemical conversion processes mainly for heat, power and transport fuel production, using biomass as fuel material. As it can be seen, these processes offer a real possibility for progressive substitution of fossil fuels. However nowadays they still present a wide range of technological development degree, from commercially widely deployed large-scale biomass combustion plants for power production, to young demonstration pyrolysis plants for bio-oil or biochar production. This wide range of technological readiness level is a fair reflection of the numerous difficulties that biomass

thermo-chemical conversion processes still need to overcome in order to become a truly competitive energetic alternative. Those include, on a more general level, issues such as the development of sustainable biomass management procedures, sustainable land use or the smart combination of decentralized and centralized applications in order to increase the efficiency of the global system.

In a more technology-related ambit, key issues include: the reduction of contaminant emissions to levels lower than fossil fuels, in both, the biomass conversion step and the subsequent use of the product biofuel; the increase in the conversion efficiency and the potential of the conversion technology to be able to deal with different biomass feedstock (including high ash content biomass), while keeping the operation requirements in an embraceable costs range. These issues are related, to different extents, to the conversion mechanism of the solid fuel under different conditions.

Independently of these process conditions, pyrolysis is always a key stage in thermo-chemical conversion. In this way, and as reported by Di Blasi [30], gas and char yields, as well as char reactivities in processes such as combustion or gasification, are highly affected by the pyrolysis stage, having a direct impact on the conversion efficiency, product quality and emissions [22]. The relevance of the pyrolysis stage in gasification and combustion is illustrated in Fig. 1.2. A deep knowledge of this process is then required in order to improve from the very first principles the performance of these technologies.

However, despite the fact that pyrolysis has been a widely investigated topic in the last decades, as it is shown in Chapter 2, the true pyrolysis mechanism remains still unveiled. This is caused by the high degree of complexity of the chemical reaction network in pyrolysis, yet worsened by the high physical and chemical heterogeneity of biomass feedstock. This leads to the main shortcoming that pyrolysis kinetics, heats of reaction and products distribution and composition are only true for those conditions in which they were experimentally determined, limiting its applicability for "universal" pyrolysis description. As side effect, the optimization of the conversion process, for example in gasification, by optimizing the pyrolysis stage and therefore decreasing the production of tar, main challenge in gasification technologies, is not truly possible when operating conditions are changed. This is yet worsened by the fact that most of the experimental studies on pyrolysis are performed at very small scales, in the range of miligrams to grams, lying far away from conditions corresponding to industrial processes.

It is the objective of the present work to contribute to the further development of detailed pyrolysis mechanisms, as the required step to better understand the pyrolysis process and consequently, to develop models which can be applied in a wide range of conditions. Besides, this investigation is performed in a technical-scale fixed-bed reactor, i.e, in conditions closer to the ones characteristic of industrial applications,

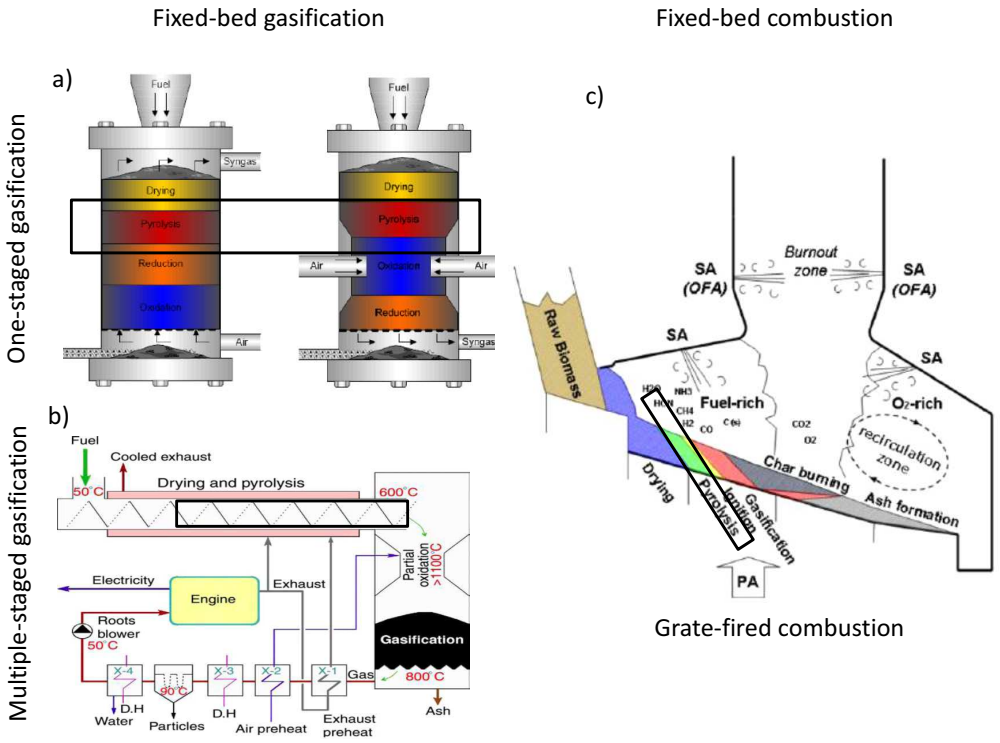

Figure 1.2: *a) Updraft and downdraft gasification configuration [1]. b) Two-staged fixed-bed gasification, Viking gasifier [2]. c) Grate-fired combustion [3].*

where influence of transport phenomena is taken into account. To this end, besides conventional products and temperature characterization methods, a novel technique in the field of biomass pyrolysis is introduced. This characterization method is based on collecting and characterizing the laser-induced fluorescence signal emitted by targeted species, present in the volatiles stream. This technique, as well as its application to pyrolysis characterization, is introduced in Chapter 3. The content of Chapter 3 has been already partially published in [55]. The experimental setup and experimental conditions are described in Chapter 4.

Results describing the process characterization, as well as the knowledge gained on the primary and secondary pyrolysis mechanisms, are introduced in Chapter 5 (content partially published in [55]) and 6 (content partially published in [56]) respectively. Those publications are included in the Publications list of the author, attached to this document.

Finally, this process is evaluated for the production of biochar, which might constitute the connecting piece between biomass utilization for energetic purposes and the improvement of land use management, while increasing the carbon pools. Therefore, biochar production, characterization and application are investigated in Chapter 7 and 8.

Finally a summary of the main conclusions will be presented in Chapter 9.

Chapter 2

Pyrolysis

2.1 Introduction to pyrolysis

Pyrolysis is the thermochemical decomposition of biomass, usually in the absence of externally supplied oxygen, with the objective of producing either liquid (bio-oil) or solid (charcoal) biofuels, or biochar. Besides, it is a stage in gasification and combustion processes as well, influencing char yields and its reactivity and, consequently, the global process performance [30]. Hence, a deep understanding of pyrolysis mechanisms and kinetics is fundamental to evaluate feasibility, design, scaling and optimization of industrial biomass conversion applications [57–59]. However, this is not an easy task due to the high degree of complexity of the chemical reaction network under pyrolytic conditions, together with the effects of interactions between chemical reactions and transport phenomena [60–62], as well as due to the wide heterogeneity of biomass feedstock.

Pyrolysis products are always three, i.e, char, permanent gases and vapor phase volatiles, which are liquid at ambient conditions. However, their final distribution and composition depend strongly on the process conditions, specially the heating rate, coupled with the vapor residence time in the reaction zone and the maximum conversion temperature (HTT) [30]; although other factors also have a significant influence, such as pressure [63], amount and composition of active catalytic ash [30], dependent on feedstock composition, or particle and bed sizes [63], due to enhancement of the influence of transport phenomena.

As it has been already introduced in Section 1.1.3, maximization of liquids yields, optimal for bio-oil production, is achieved with high heating rates, low residence time of vapors in the reaction zone, typically between 0.5 - 2 s, and mild temperatures, around 500 - 550 °C [31–33]. This process is known as fast pyrolysis. Higher temperatures would lead to secondary reactions of primary tars, such as cracking and polymerization [30], reducing then tar yields while increasing gas yields. On the contrary, slow pyrolysis

is characterized by heating times much longer than the characteristic pyrolysis reaction times (heating rates below 100 K/min), as well as longer residence time of volatiles in the reaction zone, leading to char yields maximization [17].

Bigger particle size, higher vapor phase volatiles residence time and concentration, due to lower sweeping flows, and high pressures would also contribute to an increase in char yields. This is driven by an enhancement of the interactions between the solid matrix and primary volatiles, due to an increase in mass transfer limitations (diffusion controlled), which triggers the presence of heterogeneous char-forming reactions, together with the formation of secondary tar [63,64]. These char-forming reactions compete with tar-forming reactions, being enhanced at low temperatures, due to their lower activation energy [64,65]. Char-forming reactions are reported to be exothermic [63,64], in opposition to the endothermicity associated to formation and vaporization of primary tars [64]. Therefore, by controlling those reactions, not only yields, but also the heat of reaction can be optimized. This explains also the wide range of values for heat of reaction reported in the literature for pyrolysis reactions [66,67], and will be further explored in Section 2.2.

In order to properly model these processes, to predict products yields and compositions for design, up-scaling and optimization, it is necessary to understand which kind of chemical and physical phenomena are behind such behaviors. This topic has been widely investigated. However, up to now, "there is little consensus on the mechanisms behind the pyrolysis process", as highlighted by White et al. in [57], as well as on how to model it. In this case, model should be understood as the description of the kinetic rate equation for the pyrolysis reactions [57,68]. Two are the main reasons for the lack of agreement or evolution in this field. On one hand, the fact that pyrolysis of biomass (solid state material) is a heterogeneous chemical reaction, "involving the superposition of several elementary processes such as nucleation, adsorption, desorption, interfacial reaction and surface/bulk diffusion, each of which may become rate limiting depending on the experimental conditions", as described by White et al. in [57]. This is yet worsened by the complexity of biomass feedstock composition, as well as the numerous competitive and concurrent chemical reactions involved in biomass pyrolysis [57], as previously mentioned. The second reason lies on the validity of the most used experimental approach to determine the kinetics of these processes, i.e. thermal analysis, and the mathematical interpretation of the experimental results, instead of focusing "on the reexamination of fundamental solid state reaction theory as it applies to biomass pyrolysis" understanding the chemistry of the solid state reactions, as expressed by Galwey in [68].

Following, a short review on the pyrolysis mechanisms, and models to address them, is presented in order to show the evolution and state of the art in the understanding of the pyrolysis process.

2.2 Pyrolysis mechanisms and models

From the point of view of kinetic studies, ligno-cellulosic biomass decomposition can be either seen as a single component (one-component models) or be treated as a straightforward combination of three reference components: cellulose, hemicellulose and lignin [69–71], assuming non-interaction between them. Due to the complexity in composition of ligno-cellulosic feedstock, the latter approach tends to give better results, i.e., better fitting with experimental data, because of the higher accuracy of the decomposition characterization [15]. Despite this, some studies have shown that there are indeed interactions between the three macromolecules and their intermediate products, affecting the final product distribution and composition, as for example the work of Evans and Milne and Hosoya et al. [72, 73]. This is a very important issue, particularly with respect to the potential influence of inorganics on secondary reactions.

It is generally accepted that the steps involved in biomass pyrolysis are: evaporation of free moisture, degradation of unstable polymers and decomposition of more stable compounds during primary pyrolysis, i.e., in the temperature range between approximately 200 - 400 °C, followed by secondary decomposition reactions occurring in the solid matrix at temperatures above 400 °C, involving aromatization of the char residue formed during the primary stage [57, 74]. While primary pyrolysis usually leads to around 95% [74] of the total mass loss, secondary conversion is much less significant with respect to weight loss and that is why this step is usually ignored or included in primary pyrolysis when modeled [74]. Hence, secondary reactions, specially heterogeneous secondary reactions, are hardly included in pyrolysis models. However, they have a major significance regarding char chemical and physical properties, as well as with respect to the release of some more refractory volatiles [71, 74].

Different classifications of pyrolysis mechanisms can be found in literature, according to several criteria and without true consensus with respect to nomenclature. For the sake of clarity, a classification is also offered in the present work, based mostly on the review works of Di Blasi [70, 71]:

- One-component single reaction mechanisms
- Multi-component parallel single reaction mechanisms
- One component competitive mechanisms
- Competitive detailed mechanisms

One-component single reaction mechanisms of the form Biomass → Char + Volatiles (Tar and Gas) can predict the characteristic time of pyrolysis (the conversion time),

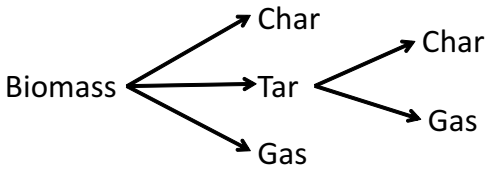

Figure 2.1: *One component competitive reaction mechanism for primary pyrolysis and secondary tar cracking reactions.*

however, they do not "allow the dependence of products yields on reaction conditions to be predicted, as a constant ratio between volatiles and char is assumed", as stated by Di Blasi [70]. This type of model has shown to have a good accuracy reproducing thermogravimetric analysis (weight loss curve) of pure cellulose. For example, Antal et al. [75] claimed that a wide variety of pure cellulose samples can be fitted by an irreversible, single step, first order rate equation with an activation energy of around 238 kJ/mol, when possibility of vapor-solid interactions is minimized. However they do not deliver such good results for biomass. To improve the fitting results of this global models, multi-component parallel single reactions mechanisms can be considered: $\text{Biomass}_i \rightarrow \text{Char}_i + \text{Volatiles}_i$ [15, 57, 76]. Such approaches are usually employed in models for combustion or gasification (specially in fixed-bed due to the fact that devolatilization conditions are comparable to those of thermal analysis, i.e., low heating rates [77]), when the conversion time is the significant variable to be determined [77]. They do not require a deep knowledge of the pyrolysis mechanism.

Therefore, with regard to the development of models for reactor design and optimization, where products yields and composition prediction is needed, as a function of process conditions and biomass composition, another type of models is required. Models based on one component competitive mechanisms seem to be a promising alternative.

In these mechanisms products are lumped in three groups, char, gas and condensable volatiles (tar), including primary and secondary reactions through competitive chemical reaction pathways [57, 70]. An example of such mechanisms is shown in Fig. 2.1. Models based on these mechanisms also allow the coupling of chemical reactions with transport phenomena. Hence, if determination of these primary pyrolysis kinetics is performed in conditions free of transport limitations (small mass samples in the range of

few mg and slow heating rates), i.e., intrinsic kinetics are obtained, and then coupled with transport phenomena in order to include the potential presence of secondary reactions (for example prediction of product yields depending on the residence time of volatiles [78]), models able to describe single particle effects at reactor scale can be developed [70]. Despite the fact that these competitive mechanisms are not of high complexity, kinetics of these schemes are scarce [15]. Besides, the required experimental conditions for their determination are not always reached. Both aspects, combined with ligno-cellulosic biomass heterogeneity lead to a significant disagreement in the predictions of these models, even from a qualitative perspective [70], showing that deep investigation is still needed in this field.

Therefore, further improvement of competitive models requires a deeper understanding of the pyrolysis process. It is in this context where detailed mechanisms appear. In these mechanisms the objective is to understand which type of reactions lead to which products and how and why feestock composition and transport phenomena may affect, or not, products yields and compositions.

One of the main objectives of the present thesis is to contribute to the development of these detailed schemes, with focus on heterogeneous secondary reactions and the pathways leading to the formation of polyaromatic hydrocarbons (PAHs).

In the following section, some of the most relevant competitive and detailed pyrolysis mechanisms are reviewed (Fig. 2.2), showing still at this level the existing disagreement.

2.2.1 Cellulose

Cellulose is the most abundant organic polymer on Earth and is also the main component of ligno-cellulosic biomass. That explains why is the most investigated component, with remarkable difference over hemicellulose and lignin, regarding pyrolysis mechanisms and kinetics.

Broido and his colleagues introduced already during the 70s the foundations of the research work on pyrolysis kinetics carried out up to now [75]. In 1975 [79] they presented a cellulose pyrolysis mechanism (1) in Fig. 2.2) based on two competitive sets of reactions: (1) intermolecular dehydration (cross-linking reactions), leading eventually (anhydrocellulose is the major intermediate product) to char formation and prevailing at low temperatures; and (2) char-free depolymerization (with levoglucosan as intermediate product), leading to the production of volatile tars and governing at high temperatures [79]. They also determined that char yields depend upon the ash content and crystallinity (varied with pretreatments at lower temperatures) of the feedstock as well as on the pressure (they operated in vacuum). Later on, in 1976 [80], Broido upgraded the previous scheme to a multi-step competitive mechanism (2) in Fig. 2.2) to

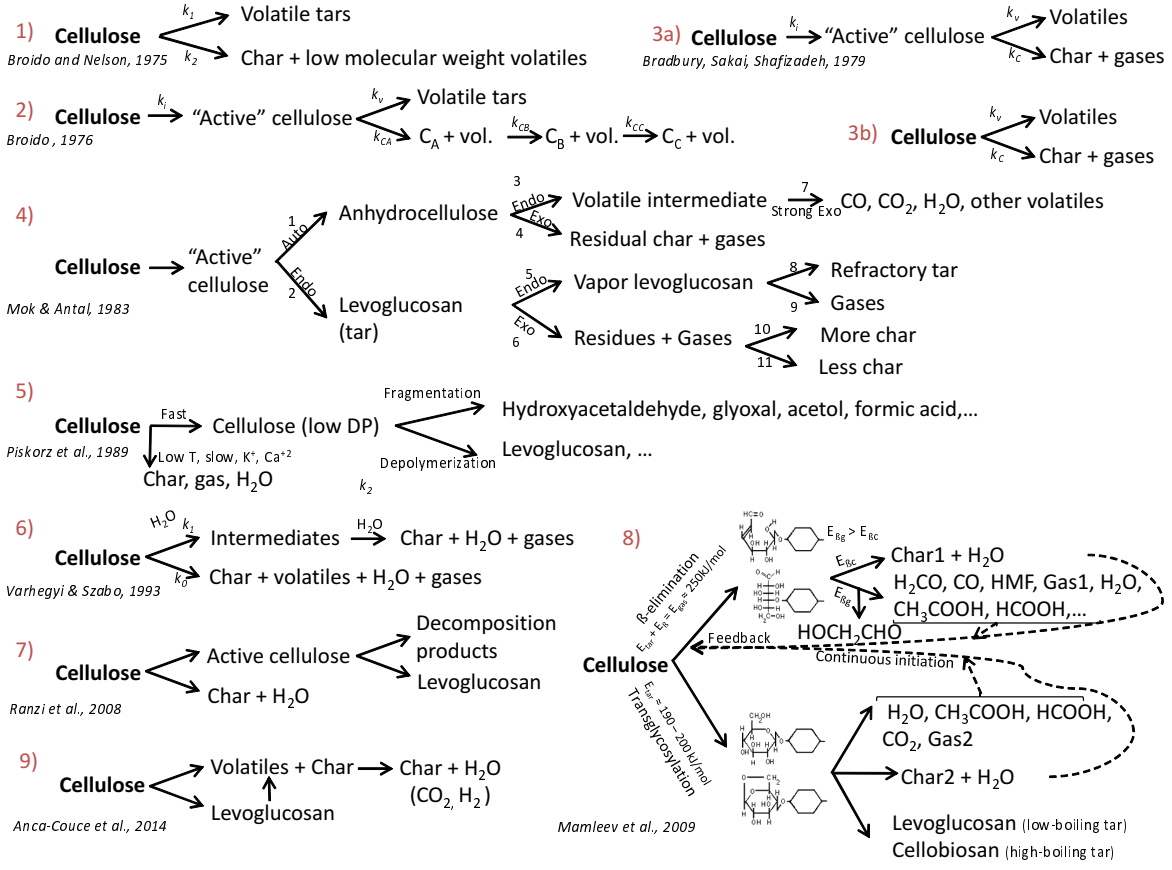

Figure 2.2: *Review on competitive and detailed mechanisms for pyrolysis of cellulose.*

account for secondary reactions taking place in the char and in the vapor phase. Here, he also introduced the concept of "reactive cellulose" to reflect its reactivity at higher temperatures. Noteworthy to mention is that for these experiments they always used a significantly high amount of sample, around 100 mg. Hence, secondary reactions of primary products inside the solid matrix would not be negligible, supporting the multi-step mechanism, in opposition to the later work of Bradbury et al. [81]. However, those kinetics could not be considered as intrinsic.

In 1979, Bradbury, Sakai and Shafizadeh [81] modified the scheme proposed by Broido in 1976, by not taking into account secondary reactions (3a) in Fig. 2.2). They indeed detected that sample size and pressure (experiments carried at atmospheric pressure versus experiments carried out in vacuum) had an influence on char yields. Bigger sizes and higher pressures led to an enhancement of residence time of volatiles in the cellulose matrix and consequently to an increase in char formation. However, as they stated, "products which do not evaporate can not be detected by weight loss" and that is why they did not include the secondary steps in their model [81]. They also distinguished between low temperature pyrolysis (Scheme 3a)), where an activation step was detected, and high temperature pyrolysis (above 300 °C, Scheme 3b)), where pyrolysis degradation could be treated via two competitive first-order reactions. The differences in the pyrolysis mechanisms for temperatures below and above 300 °C were also in good agreement with the results presented by Shafizadeh and Bradbury [82] on decomposition of cellulose in air and N_2. They showed that decomposition rates at temperatures above 300 °C were very similar for both air and N_2; suggesting therefore that pyrolysis in these conditions proceeds via transglycosylation reactions, leading to the formation of anhydrosugars as first product. However, at lower temperatures, oxygen plays a role, being the decomposition rate much faster in an oxidative atmosphere than in N_2. This may indicate that this initiation step involves a free-radical mechanism.

Mok and Antal in 1983 [83] developed an expanded mechanism (4) Fig. 2.2), based on previous works from Broido and colleagues, as well as from Bradbury and colleagues. That is to say, they started with the mechanisms proposed by them, where it is considered that cellulose decomposition follows two competitive pathways, leading to anhydrocellulose production, and eventually to char and permanent gases (dehydration route favored at low temperatures), or to levoglucosan formation with further production of other volatiles and gases (depolymerization route enhanced at higher temperatures), and investigated the effect of pressure and purge gas flow (residence time of volatiles) on secondary reactions of these two main primary products. In particular, reaction possible pathways and heat of reactions. They determined that both, anhydrocellulose and levoglucosan, decompose further following again two competitive pathways, being those highly influenced by the process conditions. The results showed that anhydrocellulose decomposes through an exothermic reaction to char residues and

gas (reaction 4 in mechanism 4), Fig.2.2), being this pathway enhanced by low sweeping flows (higher residence time) and high pressures. However, they also found that anhydrocellulose decomposition involves the formation of intermediate volatiles and that fast removal of these volatiles (for example with high purge flows or vacuum conditions) reduces char formation. At the same time, they can react further in a strong exothemic reaction (reaction 7 in mechanism 4), Fig.2.2) and form permanent gases and other volatiles. Levoglucosan evolves further with either vaporization, endothermic, which gives place to vapor levoglucosan; or through a decomposition pathway, leading to char residues and gases. This pathway is exothermic because involves the formation of char and it is enhanced with higher mass transfer limitations, increasing hence the secondary solid-vapor reactions, i.e., with higher residence time of volatiles in the matrix via lower flows or higher pressures. Vapor levoglucosan can react further in vapor phase to form refractory tar and gases (reaction 8 and 9). Solid residues can also react, leading to char evolution.

In 1989 Piskorz et al. [84] proposed another mechanism for fast pyrolysis, based also on a previous work from Richards [85], where it was suggested the direct formation of low weight compounds, such as hydroxyacetaldehyde or carbonyls, directly from active cellulose decomposition and not from secondary reactions of levoglucosan or other sugars. This pathway would be ring fragmentation, which would compete directly with transglycosylation reactions. The enhancement of these pathways would be highly influenced by the cellulose morphology, in particular the degree of polymerization (low degree of polymerization could increase levoglucosan yields), and by the presence of alkalis, which could inhibit levoglucosan formation, leading to ring fragmentation as main decomposition alternative.

Varhegyi et al. in 1993 [86] investigated the effect of high pressures in closed vessels, as well the presence of water during cellulose pyrolysis, and proposed a new mechanism (5) in Fig. 2.2), since the ones existing did not explain their experimental results. They observed that at moderate heating rates and open vessels, with high purge flow rates, cellulose pyrolysis could be described as a single rate determining reaction, probably due to degradation of cellulose in monomers and oligomers. The observed gases, vapors and chars could be product of secondary reactions of these monomers and oligomers. However, when the volatiles release was hindered due to the use of closed vessels, the reaction mechanisms became more complex. In those conditions they observed that more sample quantity led to higher char yields and reduced the reaction temperature. This behavior had been also reported by other authors, as previously reviewed (for example Mok and Antal in 1983), but in addition, Varhegyi et al. addressed that the experimental results could not be explained by the self-heating of the sample during the exothermic decomposition. As they claimed, "a systematic variation of the experimental conditions and addition of extra water to the sample proved that a major part

of the observed effects are due to the catalytic influence of the water on the reaction". Therefore, in their mechanism they proposed two pathways, the non-catalyzed decomposition (first order kinetics), observed with open vessels (pathway k_0), with very low reaction rate in the lower temperature range of the sealed vessel experiments, and the second reaction pathway in the presence of water. Despite the lower rate of non-catalyzed reactions in the closed vessels, it had to be taken into account due to effect of the produced water on the catalyzed pathway. In the latter pathway, k_1 describes the solid reaction of cellulose in the presence of water, i.e., cellulose hydrolysis and k_2 accounts for the secondary reactions of the intermediates.

Ranzi et al. in 2008 [69] proposed a mechanism for cellulose pyrolysis (6) in Fig. 2.2), where the first devolatilization step would take place through two competitive reactions, one leading to char and water formation and the other one to the formation of active cellulose. This active cellulose would decompose again following two reactive pathways. The one dominating at lower temperatures would lead to the formation of anhydrosugars through chain end depolymerization (rate-limiting step), among which levoglucosan would be the most significant one. Enhanced at higher temperatures, as well as with higher mass transport limitations, β-scission reactions inside the polymer chain, followed by molecular and radical reactions, would lead to the formation of alternative decomposition products, such as hydroxyacetaldehyde, glyoxal, methanol, formaldehyde, CO and CO_2 and char ($< 5\%$) among others. This pathway had been previously introduced and reviewed here with the work of Piskorz et al. [84]. This mechanism was proposed in the framework of the development of a mechanistic model for biomass pyrolysis, which would allow the integration of reaction kinetics and transport phenomena. Special interest was paid to the characterization of volatiles products in order to account for the presence and description of secondary gas phase reactions. However, it is noteworthy to mention that the potential influence of inorganics on these reactions, as well as the possible relevance of secondary charrification reactions, were not considered.

An adaptation of this mechanism was proposed by Anca-Couce et al. [65] (8) in Fig. 2.2), in order to take into account the influence of inorganics (ash) and secondary charring reactions. In this scheme, cellulose devolatilization is described with one single reaction leading to the formation of volatiles and char through a fragmentation pathway. This reaction is described with the kinetic parameters correspondent to active cellulose formation in the original scheme. At the same time, transglycosylation reactions, leading mostly to levoglucosan formation, would be neglected due to the presence of inorganics, which would enhance the fragmentation pathway. Then, secondary char-forming reactions of primary volatiles would lead to the formation of more char and gases. The extent of these secondary reactions would depend mostly on the retention

time and partial pressure of the volatiles in the solid matrix, as well as the presence of minerals.

In 2009, Mamleev et al. [87] proposed a mechanism similar to the one proposed by Mok and Antal in 1983, but with a much deeper insight into the understanding of the chemical reactions taking place, and including the fragmentation competitive pathway already introduced by Piskorz et al [84]. They assumed, as other authors previously reviewed, that cellulose decomposition occurs via two competitive reaction pathways, transglycosylation leading to the formation of levoglucosan or β-elimination, forming char and volatile intermediates. The question they tried to answer at this point was why transglycosylation is the main depolymerization route in cellulose pyrolysis, as well as the rate-limiting step. A possible explanation they proposed for that was that transglycosylation does not need a catalyst, while for example cleavage of pyranose does. However, these catalysts would not be available in the solid matrix. They tried to explain the different phenomena through a two-phase pyrolysis model. The formation of high-boiling liquid tar from tranglycosylation reactions would fill the cellulose cavities and provide volatiles acids, which would act as catalyst for the acid-catalyzed β-elimination reaction. Char would be also produced from secondary reactions in the condensed phase, mainly through the fragmentation pathway. Another interesting affirmation of this work is that dehydration is not a primary step in cellulose pyrolysis, being the primary step of cellulose dehydration to form anhydrocellulose doubtful. Direct dehydration of pyranose rings seems also to be insignificant due to the low concentration of pyrans in the pyrolysate (product of this reaction). They concluded then that rings have first to undergo cleavage and then dehydration can take place. In this way, water is a secondary product of cellulose pyrolysis. Light gases would be produced though breaking of chain ends or components in the tar phase. Hence, they are also secondary products with respect to depolymerization. Besides, they need a catalyst which is provided with the tar. This would explain why tar is a high temperature product.

In a recent work by Carlson et al. [88], it has been also proposed that catalytic fast pyrolysis of glucose would take place in two steps: firstly, the competitive decomposition of glucose to small oxygenates (fragmentation reaction, enhanced at lower temperatures) or the dehydration reaction enhanced at higher temperatures to form anhydrosugars and furans. In a second step aromatics would be formed, being the oxygenates produced during thermal decomposition likely intermediates in these aromatic-forming reactions.

Conclusions on cellulose mechanisms and relation to the present work

After this review on competitive and detailed mechanisms of cellulose pyrolysis, it can be concluded that cellulose may decompose via different competitive pathways, whose

relevance in the global pyrolysis process is highly dependent on the conversion conditions, the potential presence of inorganics and the cellulose morphology. Of high significance is the introduction of the competitive pathways of transglycosylation and ring fragmentation. The first one would lead to the formation of sugars, such as levoglucosan, enhanced at lower temperatures (rate-limiting); and the latter would lead to the formation of low molecular weight compounds, CO, CO_2 and char. This second pathway is said to be enhanced at higher temperatures because it needs a catalyst, which is not available in the solid matrix. Therefore it requires the presence of compounds which can provide this catalyst. This could be done by the high-boiling liquid tar coming from the transglycosylation reactions, which would fill the cavities of the solid matrix and act as electrolyte, enhancing the fragmentation pathway. The presence of inorganics and longer interaction times between the volatiles and the solid matrix (mass transport limitations) would also lead to an enhancement of this fragmentation pathway, as previously introduced, leading not only to the formation of light volatiles but also char. The charrification reactions are reported to be exothermic which could have a significant impact on the global heat of reaction.

Further information is required though on the secondary reactions, i.e., once the intermediate products are formed, either through fragmentation or transglycosylation reactions, how they react further, forming products such as PAHs, and which are the main parameters influencing these secondary reactions.

In the present thesis, further investigation on these secondary reactions, enhanced by the ash content and leading to products such as PAHs is performed. Besides, influence of these secondary reactions on char structure and composition (biochar) is considered.

2.2.2 Hemicellulose and lignin

Hemicellulose is a radom-structured amorphous matrix of polysaccharides formed by several monomers, including glucose, xylose, mannose, galactose, arabinose and other polysaccharides [89], which makes it the least stable of the three wood macromolecules, reacting typically in the temperature range of 200 - 300 °C. For kinetic studies, usually xylan is used as its representative component.

In comparison to cellulose, hemicellulose has been much less investigated. Therefore, few results are available in the literature regarding hemicellulose pyrolysis mechanisms and kinetics. Although one-step global reaction models for hemicellulose description have been reported in literature, they do not show such good comparison with experimental results as for cellulose [65]. Indeed, several thermal degradation studies on representative compounds of hemicellulose, such as xylan, have shown the presence of two reaction zones (two peaks in the DTG curves), suggesting the existence of a

two-step (two successive reactions or at least two rate-limiting successive reactions) decomposition mechanism [89, 90].

Koufopanos et al. [91] proposed a mechanism for hemicellulose decomposition based on competitive reactions, as they did for cellulose. The experimental results were obtained in isothermal conditions with negligible mass and heat transfer limitations, therefore they claimed that the process was kinetically controlled. In their scheme, a first zero-order Arrhenius reaction, with an activation energy of 72.4 kJ/mol, or pre-pyrolysis phenomena, would lead to changes in the original material, i.e., sort of an activation step. This would be followed by a reaction leading to the production of char and other pyrolysis products, responsible for most of the weight loss, in competition with a third phase, where decomposition of char would take place. The second and third reactions would be 1.5 order reactions with activation energies of 174.1 and 172 kJ/mol respectively. However, as later discussed by Di Blasi et al. [89] about these results, the fact that the activation energies for both reactions were practical identical suggests that they were not truly competitive reactions.

As it has been aforementioned, such models do not allow the prediction of products yield distribution. Hence, a new mechanism, and subsequent model, was proposed by Di Blasi et al. in 1997 [89] (based on xylan pyrolysis), so that "it could be integrated in more complex kinetic schemes and coupled to the equations of transport phenomena, to simulate the dynamics of chemical reactors and, in particular, the variations in product distribution, as the reaction conditions are varied", as claimed by the authors. This mechanism is shown in Fig. 2.3, 1) and consists of a two-stage mechanism. In each step, two competitive reaction pathways leading to the formation of volatiles or solid (char) are suggested. The first stage is supposed to be very fast and it is also associated to a high volatile release. At around 270 °C further degradation of the solid intermediate product is observed, producing charred residue and further volatiles.

Ranzi et al. proposed in 2008 [69] another competitive scheme, shown in Fig. 2.3, 2). In this scheme, hemicellulose evolves to two different types of active hemicellulose (HCE1 and HCE2), decomposing HCE2 with delay with respect to HCE1. This is done to reproduce the two-stage mechanism observed by previous authors. The decomposition of HCE1 is very fast and similar to the one for cellulose, since it takes place through two competitive reactions, one leading to the formation of xylose (sugar) and the other one producing char and light volatiles, through a fragmentation pathway. HCE2 decomposes following a similar path as for fragmentation of HCE1. The pathway leading to the formation of xylose is expected to loose relevance when secondary charring reactions are enhanced or minerals are present, as stated by Anca-Couce et al. [65].

With respect to lignin, it presents "a complex structure of racemic polymers mainly derived from hydroxycinnamyl alcohol monomers with different degree of methoxylation",

as highlighted by Ranzi et al. in [69]. It decomposes over a wide range of temperatures, from approximately 250 °C to 700 °C. Hence, it can be easily assumed then that its decomposition takes place in several successive steps. At low temperatures, the least stable functional group bonds break, emitting low molecular weight compounds, such as CO [76]. At higher temperatures, dissociation of more stable bonds leads for example to the production of CH_4, through release of weakly bonded methoxy groups. Above 500 °C, the aromatic rings in the solid fraction are rearranged and condensed releasing H_2 [65, 76, 92]. Lignin is also the main source of char in ligno-cellulosic materials pyrolysis.

The structural complexity of this macromolecule, together with the variability in stability of its chemical bonds, hinders even more the development of an appropriate pyrolysis mechanism, as basis for a well founded model. As for the cases of cellulose and hemicellulose, single first-order reaction models have been developed also for lignin, as reviewed in [92], with low activation energies, as for example the ones reported by Varhegyi et al. [76], in the range of 34 - 65 kJ/mol.

On the contrary, kinetics based on the competitive scheme proposed by Koufopanos et al. [91] (the same as the ones proposed for cellulose and hemicellulose, previously described) are significantly higher, i.e., 147.7 kJ/mol for the first "activation" reaction; 137.1 kJ/mol for the 1.5 order reaction, leading to the formation of volatiles and 122.1 kJ/mol for char formation.

Caballero et al. [93] developed a model assuming that lignin (and other biomasses that, as lignin, decompose over a wide range of temperatures) is formed by a great number of fractions, whose decomposition starts only when a threshold temperature is reached. The model is based on a function of distribution of solid decomposition. In this case, activation energy values between 72.4 and 174 kJ/mol were obtained.

Ranzi et al. [69] proposed also a quite detailed model, able to predict products yields, assuming that lignin can be represented by the combination of three different units: LIG-C (rich in carbon), LIG-O (rich in oxygen) and LIG-H (rich in hydrogen). The scheme is shown in Fig. 2.3, 3). The three reference compounds decompose to char, volatiles and intermediate compounds, which further react in one-step or competitive reactions. The latter is the case of LIG, which decomposes through a competitive pathway to produce phenolic compounds or char and gas. This resembles the competitive schemes for cellulose and hemicellulose, previously explained.

Zobel et al. [4] introduced recently a quite detailed mechanism for lignin, adapted from the work of Asmadi et al. [5], and focused on the evolution of volatiles, where they took into account primary pyrolysis, as well as further gas phase and heterogeneous secondary reactions of these intermediates. The scheme is shown in Fig. 2.3, 4). In this mechanism, they described the evolution of primary tars, coming from primary pyroly-

sis of lignin, towards the formation of PAHs, either enhanced by high temperatures in the gas phase or by the solid matrix in heterogeneous secondary reactions. Secondary tars would be described as the intermediate products of these secondary reactions.

These mechanisms proposed for lignin will be the foundation of the detailed mechanism for lignin proposed in the present work. Both mechanisms, i.e., the detailed mechanism for cellulose pyrolyis, with focus on secondary reactions, leading to the production of PAHs, as explained in Section 2.2.1; and the detailed mechanisms of lignin decomposition (also producing PAHs), will be combined to further understand the pyrolytic behavior of wood.

2.2.3 Products of pyrolysis

Pyrolysis products of ligno-cellulosic materials, as previously said, can be lumped in char, permanent gases and tar, term which includes in the present work all condensable volatiles at ambient conditions. A deep explanation of char properties will be given in Chapter 7. Permanent gases are mainly CO_2, CO, CH_4 and H_2. The main source of CO and CO_2 is the primary thermal cracking of carbonyl and carboxyl groups present in cellulose and hemicellulose, as reported by Yang et al. [94], while the main source of CH_4 is related to reactions such as the cracking of methoxyl-O-CH_3 functional groups in lignin decomposition [95]. H_2 release is mostly related to cross-linking and condensation reactions in the solid phase [96]. CO, CH_4 and H_2 are also the main gas products of homogeneous secondary reactions of primary tar.

Tar is the most complex product, from a composition, but also from a characterization point of view in pyrolysis. According to Evans and Milne [72], tars can be classified in primary tars or mixed oxygenates, secondary tars or hydrocarbon zone and aromatic or tertiary tars. Primary oxygenates are formed typically [15, 97] by acids, sugars, ketones, aldehydes, alcohols and furans, coming from cellulose and hemicellulose; as well as guaiacols, syringols and other more complex compounds, such as pyrolytic lignin. Tertiary tars are polyaromatic hydrocarbons (PAH), such as naphthalene, phenanthrene or anthracene. Secondary tars are all intermediate compounds between primary and tertiary tars. Evans and Milne [72] also proposed temperature ranges for each tar zone. In this way, primary tars would be produced from 400 to about 700 °C, secondary tars would evolve between 700 and 850 °C and PAH would be formed above 850 - 1000 °C. However, this classification was proposed based on experimental results where very low sample mass was used (10 - 1000 mg), together with high heating rates > 30 °C/s and small gas phase residence time (< 1 s) and particle size (< 250 μm). In these conditions, evolution of tars to secondary and tertiary species would only take place in gas phase reactions. Other authors [33, 98, 99] have reported, however, the presence of phenols, cresols and cathecols, considered typical products of secondary reactions,

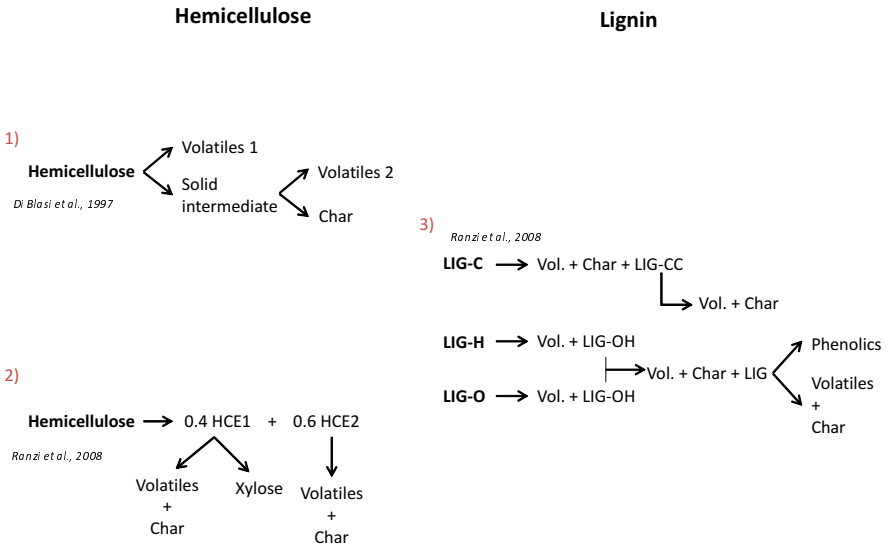

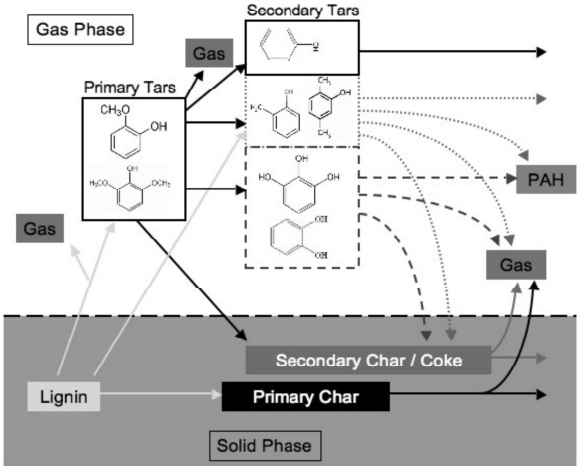

Figure 2.3: *Top: review on competitive and detailed mechanisms for pyrolysis of hemicellulose and lignin. Bottom: scheme developed by Zobel et al. [4], adaptation from a work of Asmadi et al. [5] for evolution of lignin products due to secondary reactions.*

at lower temperatures ($\leq$ 600 °C), as well as the presence of PAHs in slow pyrolysis of big particles [100], and even the direct formation of PAHs from cellulosic materials in the temperature range of 400 - 600 °C for slow pyrolysis [100, 101]. It is intended with this to show that even tar classification is not an easy task, and the reason is that tar evolution depends not only on gas phase reactions but also on heterogeneous reactions, strongly determined by transport limitations. In previous sections, it has been extensively highlighted the relevance of including these secondary reactions when describing pyrolysis of lignocellulosic materials, due to their influence on products yields and heat of reactions; but it is also needed to follow the evolution in composition of these products. For that, characterization of these products is needed.

Nevertheless, efficient and trustful characterization of pyrolysis products, specially tars, must face two significant drawbacks: the wide range of chemical species that are present in pyrolysis tars [33, 72, 98], many of them with high structural complexity, which makes them non-detectable for standard methods, such as gas chromatography [102]; and the instability of pyrolytic oil, which may induce erroneous characterization in off-line analysis techniques, due to sampling and preparation. For instance, the high reactivity of some oxygenated compounds, the volatility of species such as benzene or repolymerization due to aging effects [97]. Besides, off-line characterization does not give information about the transient behavior of tar species depending on the process conditions and conversion degree, fundamental to develop control and optimization techniques.

Consequently, on-line techniques which support off-line methods are needed. These techniques should avoid, as much as possible, modifications in the volatiles composition, caused by sampling and conditioning. Spectroscopy techniques, such as Laser-Induced Fluorescence (LIF), may be an alternative. This is a non-intrusive, in-situ technique, which allows high temperature detection with significant sensitivity, in the order of tens or hundreds ppb [103] in gas phase and even larger in liquid phase [104]. It is also a selective technique, by choosing the excitation wavelength it is possible to excite and consequently analyze specific groups of molecules. As an example, formaldehyde is mainly excited at 355 nm [105] while 1 and 2 rings aromatics compounds present the most efficient fluorescence behavior with an excitation wavelength of 266 nm [106].

Chapter 3

Laser-Induced Fluorescence

3.1 Introduction

Briefly explained, fluorescence is the emission of light (photon) by a compound, when an electron from an excited electronic state (excited singlet state) comes back to the ground state. This process is very fast (spin allowed), being the lifetimes of the excited electronic states in the order of 10^{-8} s [107]. This excitation is produced by previous absorption of light, being the emitted light less energetic (due to the higher efficiency of vibrational relaxation) and having therefore a longer wavelength than the absorbed light, also known as Stokes shift [107]. Further characteristics on the fluorescence phenomenon will be given along this chapter, applied to the present case of study.

In laser-induced fluorescence (LIF), the excitation light is provided then by a laser. This spectroscopy technique has been largely used in combustion for identification of pollutants coming from incomplete combustion, such as CO or oxygenated compounds, or to assess flame structure [8, 108]; for detection of PAHs [103, 108, 109] or for characterization of particles formation in flames in combination with LII (Laser-Induced Incandescence) and fluorescence lifetimes measurements [110, 111]. It has been also applied in gasification processes for PAHs detection [112]. However, in the field of pyrolysis its application is scarcer. It has been used for on-line tar characterization in single particle pyrolysis, as reported by the studies of Brackmann et al. [113] and Zobel and Anca-Couce [4,114]. In the first case, absorption and fluorescence emission studies were carried out. Absorption results showed a nearly featureless absorption in the ultraviolet spectral region, with a continuously stronger absorption for shorter wavelengths; while fluorescence measurements were done using different excitation wavelengths, observing broad-band fluorescence spectra in the region from 300-500 nm, associated with larger hydrocarbons. Zobel and Anca-Couce [4, 114] carried out fluorescence emission measurements of single wood particles using an excitation wavelength of 355 nm. It was stated that the composition of the volatiles leaving the particle -analyzed by fluo-

rescence emission in the close particle vicinity- strongly depended on the particle size and heating rate, indicating the presence of heterogeneous secondary reactions of primary and secondary tars, for a particle size of 25 mm diameter, while no hint of these reactions was observed for particle sizes of 0.5 and 1 mm. LIF has been also applied for detection of CO and formaldehyde in flash pyrolysis carried out in a heated grid reactor, with samples in the range of 3 - 6 mg [105]; and to study the evolution of aromatic ring systems present in bio-oil from fluidized-bed fast pyrolysis [115].

As the next step, laser-induced fluorescence is applied in the present work for on-line characterization of tar evolution in a technical-scale (1 m height, 22 cm of internal dia-meter) fixed-bed pyrolysis process, using thermally thick wood particles. In these conditions, the extent of mass and heat transport limitations become more significant due to the larger scales. Therefore, as it has been explained in Chapter 2, it is more likely that secondary reactions - mainly heterogeneous - occur, leading to a change in products yields and composition, including the potential formation of PAHs [4,100,114]. These are the conditions which are mostly encountered in industrial applications. However, just a few studies can be found in literature regarding products composition characterization at this relevant scale [100, 116]. In these conditions, typical primary tars from lignin such as guaiacols and syringols (Section 2.2.2) may further evolve through cracking reactions and changes in the functional groups composition towards tertiary tars precursors and eventually the formation of PAHs [117]. Schröder [116] carried out pyrolysis in a fixed-bed reactor with 2 kg of beech wood cubes. Tar characterization in this study was focused on tar elemental composition, water content and calorific value as function of maximum pyrolysis temperature. Fagernäs et al. [100] carried out slow pyrolysis of birch wood for charcoal production at big scale, in the order of hundreds of kg. They separated the liquid product in settled tar and aqueous phase by decantation and extracted then the aqueous phase, using water, into water soluble and water non-soluble fractions. Each fraction was analyzed in different ways. For the aqueous phase, water content, pH, total organic content, total carbon content, chemical oxygen demand and total acid number were studied, together with the quantitative analysis in a GC-FID/MS for the main water soluble organic compounds present in this fraction. The presence of PAHs in the aqueous phase was also analyzed by using GC-MS/SIM techniques. In the settled tar fraction, water content, solids content, elemental composition, calorimetric and effective heating values and viscosity were analyzed. PAHs and other organic compounds were also studied using the same procedures as for the aqueous phase. However, despite the deep tar characterization in both studies, off-line methods were employed and consequently no information about the dynamic behavior of the process was given, in particular regarding volatiles composition, which would be a prerequisite for any optimization strategy.

Therefore, it is the objective of the present work to gain insight into on-line volatiles characterization by applying laser induced fluorescence spectroscopy. The influence of process conditions and raw material on the evolution of volatiles composition is studied. To this end, the fluorescence signal emitted by targeted species, present in the volatiles stream, is collected and compared to the spectra of representative pure species, in order to develop a qualitative characterization tool for these volatiles. The experimental setup used to carry out the fluorescence measurements is described in Section 3.2. The reactor set up used in the pyrolysis experiments is shown in Section 4.1.1. Further information on the species to be characterized is presented in Section 3.3.

3.2 Experimental setup for fluorescence measurements

The LIF system used to carry out the fluorescence measurements was previously developed in this research group and introduced already in a previous work [6, 106], where it was applied to characterization of synthetic mixtures of pure PAH species. The measuring cell consists of a stainless steel cube with two holes in one side to let the tar vapor enter and leave the cell. In two of the other sides, opposite to each other, two holes are placed, which let the laser beam pass through the cell. After the cell, a powermeter is placed to measure the laser power. The tar vapor path and the laser path inside the cell are parallel. The emitted radiation is collected at 90° with respect to this path. The cell, as well as the inlet and outlet pipes, are heated up to at least 300°C, to avoid tar condensation.

The light source used to excite the molecules is a pulsed Nd:YAG Laser (6FQSS266-50 of CryLas GmbH, Berlin, Germany). The fourth harmonic (266 nm) is used with a repetition rate of 100 Hz. The laser pulse energy in the experiments is set to 64 μJ. The laser beam is guided to the measuring cell from the laser head with two mirrors.

Fluorescence signal is guided to a compact spectrometer with a CCD camera integrated (Maya 2000; Ocean optics) by an 1000 nm inner diameter optical fiber. The spectrometer integration time is set to 30 s. Between the cell and the lens used to collect the fluorescence signal, a cooling system consisting of an aluminum cylinder with flippers is placed to avoid damaging the lens.

A scheme of the setup is shown in Fig. 3.1.

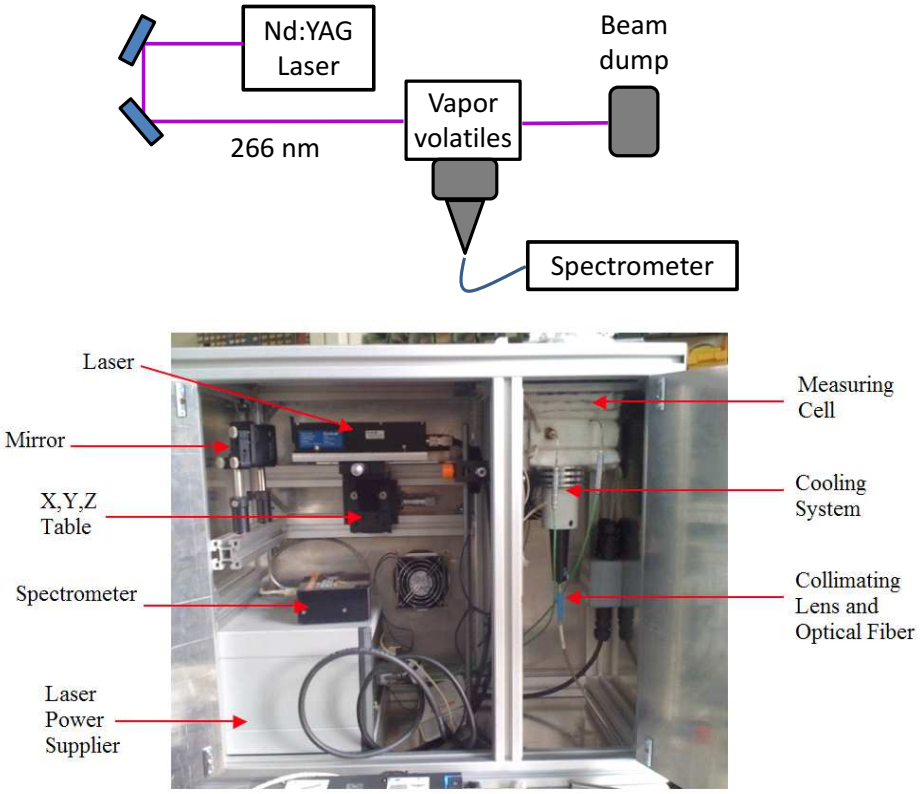

Figure 3.1: *Experimental setup of the LIF system [6].*

3.3 Fluorescence of single pyrolysis species

In order to characterize the composition evolution of the produced volatiles during the pyrolysis process, by analyzing the emitted fluorescence signal, two main factors must be taken into account: the species that may be present in the volatiles vapor under these pyrolytic conditions and the capacity of these species to emit fluorescence with the measurements conditions applied in the LIF system. This capacity is determined by the absorption cross section, the quantum yield and the fluorescence lifetime of each species, which depend mainly on the nature of the molecule, the applied excitation wavelength and the temperature and environment (composition of the vapor stream going through the LIF system, geometry) of the measurements, due to the potential presence of quenching phenomena such as: (i) collisional quenching, due to the presence of quencher substances - such as oxygen, halogens or heavy atoms -, (ii) static quenching, due to the formation of new compounds between the fluorophores and the quenchers or (iii) non-molecular quenching, due to decrease in the excitation light power by other absorbing species or the fluorophore itself [118].

As previously introduced, pyrolysis primary tars (acids, sugars, alcohols, ketones, aldehydes, phenols, guaiacols, syringols and furans, as reported by Milne and Evans [97]), coming from primary devolatilization of biomass, may evolve homogeneously (in gas phase inside the pores or outside the particles, mainly at temperatures above 550 - 600 °C [15, 119]) or heterogeneously (due to interaction with the solid matrix, being dominant these reactions at temperatures below 450 °C, as reported by [119, 120]) giving place to secondary tars, permanent gases and secondary char, as shown for example in Fig. 2.3 for the case of lignin. These secondary tars, formed mainly by phenol, cresol, catechol and derivates, which come mostly from the lignin fraction, may react at higher temperatures to form tertiary tars (PAHs), more permanent gases and char. Asmadi and co-workers [5] suggested the formation of some PAHs (naphthalene, anthracene and phenanthrene) from pyrolysis intermediates formed from syringyl and guaiacyl units and Hajaligol et al. [101] suggested the formation of some PAHs from direct cellulose and hemicellulose decomposition. Under the experimental conditions developed in this study, heterogeneous secondary reactions are the most likely pathway for tar evolution, since the high temperatures required for homogeneous secondary reactions and are not reached. Besides, heterogeneous reactions are highly enhanced here due to the big particle and bed sizes [121, 122].

It is also necessary to pay attention to which species present in pyrolysis volatiles are likely to emit fluorescence under the conditions appled in the LIF system. That is to say, an excitation wavelength of 266 nm, a temperature of 300 °C and the use of N_2 as carrier gas.

As reported by Skoog et al. [107], "the power of fluorescence emission is proportional to the radiant power of the excitation beam that is absorbed by the system", as Equation 3.1 shows:

$$F = \phi_f K"(P_0 - P) \tag{3.1}$$

where F is the power of fluorescence emission, P_0 is the power of the incident beam on the species, P is the power of the beam after crossing a defined length of the sample, K" is a constant which depends on several factors, such as geometry, and ϕ_f is the quantum efficiency of the fluorescence process [107]. The light power absorbed by the sample will depend on the molar absorptivity of the species, their concentration and the path length along which the light interacts with the sample. This relation is known as the Beer′s law and it is shown in Equation 3.2 [107]:

$$\frac{P}{P_0} = 10^{-\epsilon lc} \tag{3.2}$$

where ϵ is the molar absorptivity (also known as molar attenuation coefficient), l is the path length and c is the concentration of the species [107]. The molar absorptivity is related to the absorption cross section (also known as attenuation or capture cross section) as it is shown in Equation 3.3:

$$\epsilon = \frac{N_A \sigma}{ln10} \tag{3.3}$$

with σ being the absorption cross section of the species in [cm^2/molecule], N_A the Avogadro constant and ϵ the molar absorptivity in [cm^3/(mol cm)]. Molar absorptivity and therefore absorption cross section are intrinsic properties of a molecule [107].

It is also reported in literature [107] that fluorescence is more frequently observed, and with higher intensity, in substances containing functional groups with low-energy $\pi \rightarrow \pi^*$ transitions, although compounds with aliphatic and alicyclic carbonyl structures, or highly conjugated double-bond structures can also show fluorescence.

Looking at pyrolytic tars, this would mean mainly small cyclic aromatic compounds, and species with carbonyl groups such as ketones and aldehydes [113]. However, as previously pointed out, their capacity to emit fluorescence depends on the absorption cross section of these compounds with 266 nm excitation wavelength and the quantum yield. Among these species, polycyclic aromatic hydrocarbons present the highest absorption cross section, with values ranging from the order of 10^{-18} cm^2/molecule (for example anthracene [123]) to 10^{-17} cm^2/molecule (values in this order of magnitude were reported for naphthalene, without significant influence of measurement temperature on the absorption cross section [123–125]) and even up to 10^{-16} cm^2/molecule (as

reported for pyrene [123]). Monoaromatic compounds report typically lower adsorption cross sections. For phenolic compounds, relevant products in pyrolysis of lignocellulosic materials, absorption cross sections in the order of 10^{-18} cm^2/molecule have been reported in literature [123, 125], without significant influence of measurement temperature. These values go down to the order of 10^{-19} cm^2/molecule for compounds such as toluene or xylene and even to lower values (10^{-20} cm^2/molecule) for benzene. Regarding ketones and aldehydes, values in the order of 10^{-18} cm^2/molecule have been reported for aromatic ketones and aldehydes [123], while values down to the order of 10^{-20} cm^2/molecule are typical for aliphatic ketones and aldehydes [123].

Regarding the quantum yield, it is defined as the ratio of the number of photons emitted to the number absorbed [118] or, in other words, the relation between the energy vanished through radiative decay in comparison to the energy vanished through radiationless decay. It is usually favored by an increase in the structural rigidity (for example fluorene presents a quantum yield close to 1 while biphenyl presents a quantum yield of 0.2 [107]), since the possibility of undergoing radiationless decay is lower. On the contrary, an increase in temperature decreases the quantum yield, due to the higher probability of collisions and consequently deactivation by external conversion. In the same way, the presence of quenching agents as O_2, halogens or heavy atoms decreases the quantum yield [107, 118]. The decrease in intensity due to collisional quenching is described by the Stern-Volmer equation 3.4 [107]:

$$\frac{F_0}{F} = 1 + K[Q] = 1 + k_q \tau_0 [Q] \tag{3.4}$$

where K is the Stern-Volmer quenching constant, k_q is the bimolecular quenching constant, τ_0 is the unquenched lifetime and [Q] in the quencher concentration.

According to the previous introduction, it is expected that aromatic compounds emit the highest fluorescence intensity in pyrolytic tars. But this intensity will depend, as aforementioned, on both absorption cross section and quantum yield, therefore, the fluorescence emission signal for each species, even with the same concentration, will be different, making tar quantification in mixtures of several species very challenging. Fluorescence emission signals of PAHs are usually broad and rather structureless spectra. However, depending on the number of rings they emit fluorescence in a specific wavelength. The higher the number of rings, usually the more red-shifted the signal [126]. In this way, the peak position can be related to certain groups of species. Other features, such as functional groups attached to the main aromatic structure, are not possible to identify in a mixture of several substances due to signals overlapping. The fluorescent behavior of aromatics will be further discussed in Section 3.4.

Other compounds such as ketones and aldehydes may also contribute to the global fluorescence signal, and therefore emission spectra, from pyrolysis, specially at earlier

stages of the conversion process. For this reason, their behavior regarding characteristic emission wavelengths must be also known, to be able to distinguish them from aromatic compounds in case of overlapping.

Somersall and Guillet [127] studied the absorption and emission fluorescence spectra of several simple ketones as well as of ketones polymers. They observed that all these compounds, at room temperature, absorb radiation in the wavelength range of 250 - 325 nm, having all of them the absorption peak around 280 nm (double efficient for ketones polymers), which in principle makes them suitable to be excited with the 266 nm wavelength used in this study. Besides this, it was stated - using an excitation wavelength of 310 nm - that fluorescence spectral distribution was very similar for all the simple ketones - with the maximum around 400 $\pm$ 5 nm -, suggesting that in these compounds the characteristic fluorescence emission is due to the carbonyl bond. For polymeric ketones, the fluorescence emission was however blue-shifted between 10 - 20 nm with respect to the simple ketones - maybe due to interaction of other close carbonyl groups -, presenting all of them very similar fluorescence emission distribution.

Similar fluorescence behavior was observed by de Joannon et al. in [8], using an excitation wavelength of 266 nm. In this study it was stated that fluorescence emission in carbonyl compounds is due to the electronic transition n $\rightarrow \pi^*$, which characterizes the fluorescence spectra, independently of the molecule to which the carbonyl group is attached to. However, the type of atoms bonded to the carbonyl functionality may also affect these fluorescence spectra, resulting in the presence of other structural characteristics besides the one representative of the carbonyl group [8]. In their study, the representative spectra for several alipahtic ketones (with one carbonyl group) showed the maximum intensity wavelength peak around 420 nm. They also affirmed that this characteristic behavior was observable in aldehydic compounds. In these compounds, besides the carbonyl functionality, it is necessary to take into account other electronic transitions due to the aldehydic group (-CHO), which could cover the wavelength region from ultraviolet to infrared. Related to this, they showed that the maximum of these characteristic fluorescence emissions were located at 320 - 330 nm and 380 nm. Similar behaviors to those reported for ketones were also observed by Hansen et al. in [128] for linear aldehydes regarding emission spectra, with a maximum intensity peak of the fluorescence emission around 420 nm. However, the maximum intensity absorption cross section was observed at 290 - 295 nm, while for ketones was observed, by the same research group at 276 nm - significantly nearer the used one in the present study - and the quantum yields for aldehydes were observed much lower than those for ketones.

To conclude, aliphatic ketones fluorescence behavior is explained due to the electronic transition n $\rightarrow \pi^*$, characteristic of carbonyl groups, giving place to a very similar fluorescence behavior for a large family of ketones, locating the maximum intensity

peak of the fluorescence emission in the range of 420±40 nm. This variation may be due to the length of the ketone side chain, the position of the carbonyl group in the molecule and the presence of a second carbonyl groups in the molecule, near enough to interact with the first carbonyl group, giving place to other red-shifted structures, as well as due to the measurement conditions. Aliphatic aldehydes present also similar fluorescence behavior in comparison with ketones due to this carbonyl group, having the maximum intensity peak around 420 nm. Besides this n $\rightarrow \pi^*$ electronic transition, aldehydes may also emit fluorescence due to other electronic transitions in the aldehydic group (-CHO), which gives place to emissions from ultraviolet to the infrared region. However their quantum yields are significantly lower than those for ketones.

3.4 LIF spectra of pure species

Measurements with representative pure species were done before carrying out on-line measurements in pyrolysis experiments, to determine which species can be seen with the LIF system and at which wavelengths each one of them emits fluorescence under the measurements conditions, that is to say, in gas phase at at least 300 °C in a N_2 atmosphere. As pointed out in Section 3.3, each aromatic group - according to the number of rings - emits fluorescence intensity in a characteristic wavelength range. Hence, from a global fluorescence spectrum, it may be possible to determine which aromatic groups are present. To this end, representative species for each group of aromatic compounds should be selected.

In this study, as it can be seen in Fig. 3.2, the chosen species are guaiacol (1 ring) as representative of aromatic primary tars, naphthalene (2 rings), fluorene (2 rings connected by a rigid structure), phenanthrene (3 rings) and pyrene (4 rings) for PAH compounds, xylene as representative of BTX and acetone for ketones as compounds including carbonyl groups. It is observed that the bigger the aromatic compound, the more red-shifted (lower energy) the fluorescence spectrum, with characteristic wavelength regions for each group. This result is very important to characterize the family of PAH that are present in the volatiles stream. Fluorene is an exception to this behavior, since it emits fluorescence at lower wavelengths, similar to guaiacol, despite being formed by two benzene rings linked with a rigid structure. This fact is also mentioned by Sirignano et al. [111], where it is said that "aromatics linked together with σ-bonds should exhibit fluorescence spectra typical of the PAHs of which they are composed". This fact is very significant regarding characterization and, above all, differentiation of pyrolytic lignin. According to literature [102], complex molecules called pyrolytic lignin may be formed through thermal release and recombination reactions during pyrolysis. In these molecules several benzene rings may coexist, which are linked by different chemical structures. The fluorescence spectra of pyrolytic lignin compounds should be

more similar to the spectra of monoaromatic compounds than to PAHs as reported in [111]. It is also necessary to point out that these representative species exhibit different fluorescence intensities, although in Fig. 3.2 normalized spectra are shown. This is observable in the noise that guaiacol and acetone signals present in comparison with other spectra. This fact is due to the different capacities that the species have to emit fluorescence, as pointed out in Section 3.3.

The LIF system behavior is validated by comparing some of these fluorescence spectra with other measurements from literature [7, 8], as shown in Figure 3.2, where the top figure includes the measurements carried out in the LIF system, while the bottom figure shows spectra from literature for xylene, naphthalene, phenanthrene, fluorene, pyrene and acetone. Although the spectra are not obtained mostly in the same conditions as for the LIF system, they exhibit very similar behavior regarding the fluorescence peak wavelengths.

3.5 LIF analysis

In this Section, the procedure to analyze the fluorescence signals is presented. The total fluorescence intensity (TFI) evolution is determined as the integral of the fluorescence intensity signal over the wavelengths range under study (266 - 780 nm) at each time step. This fluorescence is emitted by the species passing through the measuring cell in the LIF system.

$$TFI = \int_{266nm}^{780nm} I(\lambda) d\lambda \tag{3.5}$$

To identify which species are emitting fluorescence, single pyrolysis spectra are fitted to spectra of representative pure species which emit fluorescence with an excitation wavelength of 266 nm and may be present in the volatiles stream. These species could be [55]: species containing carbonyls groups, such as ketones and aldehydes, 1-ring aromatic compounds, mainly phenolics and 2-, 3-, and 4-ring aromatic compounds.

In Fig. 3.2, the spectra of representative pure species are shown. These spectra are obtained by analyzing the pure species in vapor phase and in a N_2 atmosphere passing through the cell at 300 °C, except for the case of the carbonyl group. This spectrum has been taken from the initial wood devolatilization spectrum, which is typical of species containing carbonyl groups, such as aldehydes [4, 55]. As it can be seen in Fig. 3.2 phenolic compounds, which have typical fluorescence behavior of one-ring aromatic compounds, emit fluorescence at the lowest wavelengths of all the species analyzed in the present work. Then, the higher the number of rings of the aromatic compound, the

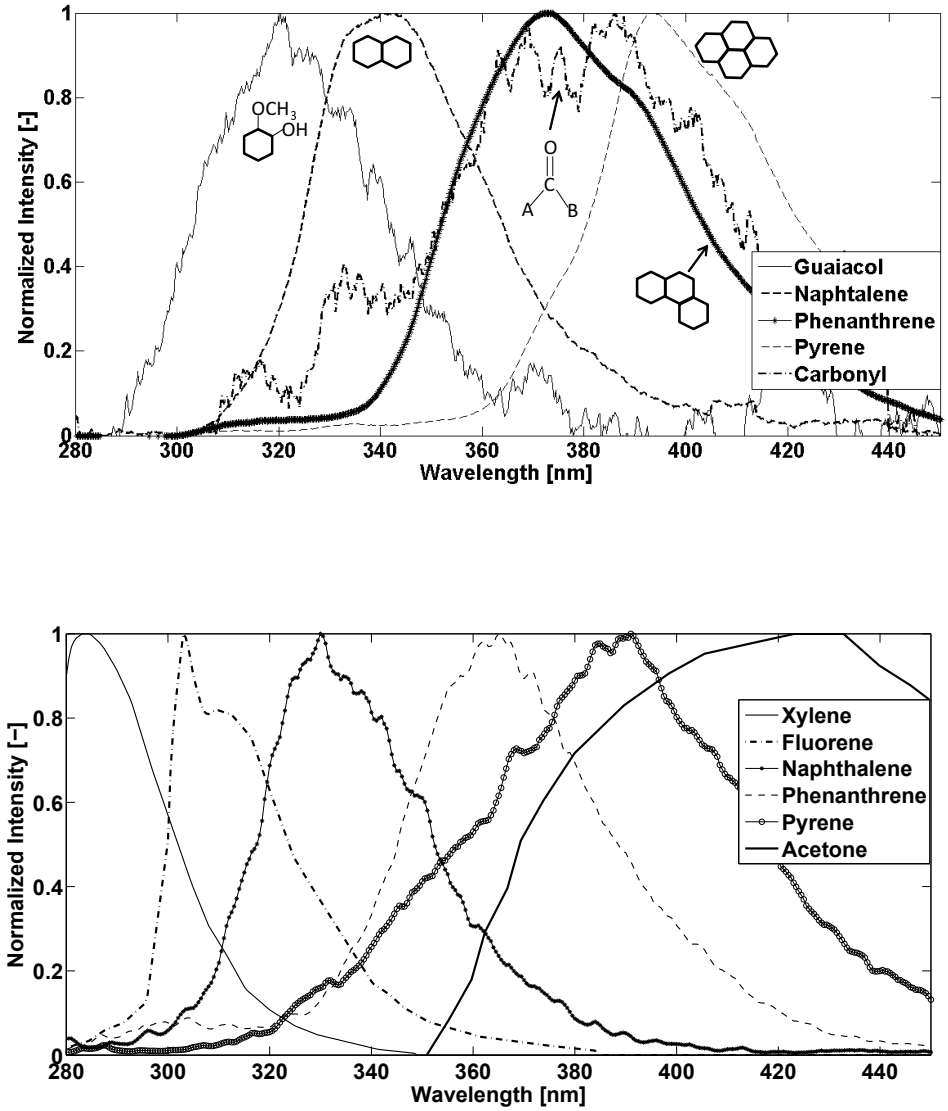

Figure 3.2: *Top: spectra of selected pure species measured in the LIF system in the same conditions as the pyrolysis experiments. Bottom: spectra of pure species from literature [7]. Xylene is measured in cyclohexane solution with 265 nm excitation wavelength, fluorene is also measured in a cyclohexane solution with an excitation wavelength of 262 nm, naphthalene in gas phase at 400 K with 266 nm excitation wavelength, phenanthrene in gas phase (266 nm), pyrene in gas phase (266 nm) and acetone in water solution with an excitation wavelength of 266 nm [8].*

more red-shifted the peak of the fluorescence intensity. Compounds including carbonyl groups present the peak of the fluorescence spectrum close to 400 nm.

Chapter 4

Experimental setup and conditions

4.1 Experimental setup

4.1.1 Reactor

A technical-scale fixed-bed reactor has been developed during the present work in order to investigate and characterize in detail the conversion process of slow pyrolysis, in conditions similar to the ones encountered in industrial applications.

The reactor itself is a cylindrical container made of stainless steel with 102 cm height and 22 cm of internal diameter. Inside the reactor, a second cylindrical container is placed, where the biomass is placed/falls in, depending on the reactor operation mode. That is to say, the reactor can work in batch or semi-continuous mode. This container is 56 cm height and 21 cm of internal diameter. The bottom of the container is a stainless steel mesh, placed on another mesh alike which constitutes the bottom of the reactor. The objective is that N_2 entering the reactor from the bottom has an uniformly distributed flow. The reactor is externally heated by a wire heater, with a maximum power of 3000 W placed on the external reactor wall. Both flanges in the reactor are also heated and insulated to reduce heat losses. The N_2 flow is preheated before entering the reactor as well. The temperature operation of this preheater is 600 °C.

The temperatures are measured inside the reactor at three different heights: 0, 5, 10 and 30 cm above the grate. At each height, three thermocouples are also placed at three radial positions: 0, 5 and 10 cm from the container wall. The reference pyrolysis temperature referred to in the present work (if not specified anything else) is defined as the temperature measured by the central thermocouple at 10 cm above the grate (bottom of the reactor). Heating rates between 1 and 10 K/min approximately are obtained depending on the stage of the pyrolysis process.

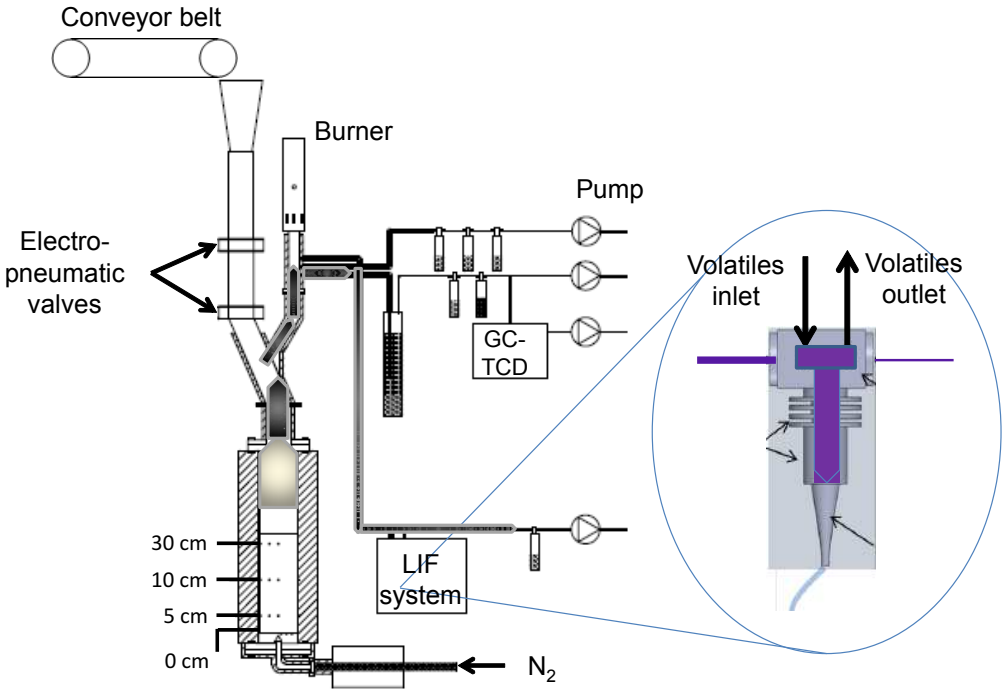

Figure 4.1: *Scheme of the reactor setup.*

The gas outlet is placed at the top part of the reactor. From the main line, which leads directly to the burner, a sampling line, heated above 300 °C, is attached, which lead to the analytical devices for volatiles characterization: permanent gases and condensable volatiles (tar). These devices are the gas-chromatograph termal-conductivity-detector (GC-TCD) and the LIF system respectively.

The feeding system is also placed at the top of the reactor. It is formed by a hopper, a conveyor belt to carry the particles into the reactor and two electro-pneumatic valves in series that work sequentially. The idea behind is to keep the reactor always isolated from the environment during feeding.

In Fig. 4.1 a scheme of the reactor is shown.

4.1.2 Analytical part

In this Section, the analytical devices attached to the reactor, excluding the LIF system, are presented.

Sampling line

The sampling line has the following elements:

- A stainless steel pipe connecting the outlet of the reactor with the LIF system, heated above 300 °C in order to reduce as much as possible tar condensation.
- The LIF system, also heated above 300 °C and explained in Section 3.2.
- The condensation system.
- A manometer to measure and control the pressure in the sampling system. If a clogging of the pipe or condenser should happen, it would be detected by the pressure measured at this point. It also works as splitting point in two different lines. One of them would go directly to the GC-TCD and the second to the main pump.
- The main pump is a membrane pump and is responsible for sucking the gas from the reactor. The flow extracted from the reactor is controlled through by-passing of this pump with a valve. Depending on the opening degree of this valve, the pump is able to suck different flows. Afterward a gas clock is placed to measure continuously the flow going through the sampling system.
- The line leading to the GC-TCD includes a glass wool filter and a particle filter before letting the gases get into the GC-TCD. After the GC-TCD, a second membrane pump is placed, which has the aim of sucking the gas used for analysis from the splitting point. The flow sucked by this pump is also controlled by a by-pass of the pump. After it, a second gas clock is placed to measure the flow passing through the GC-TCD.

The condensing system includes the following parts:

- A stainless steel condenser with several liters capacity filled with toluol, approximately 500 g of toluol in each experiment. This condenser is inside a cold bath kept below -15 °C.
- Several smaller glass condensers filled with isopropanol, silica gel and activated carbon/cotton wool. These condensers are kept in an ice bath. The silica gel has the main function of removing the water than is not previously condensed, as well as the solvent taken away from the condensers by the gas stream. The activated carbon has the aim of adsorbing also part of this solvent and small hydrocarbons which are not able to be condensed in the condensers. However, this activated carbon also adsorbs part of the CO_2, therefore it cannot be used when determining

permanent gas yields. In this case, cotton wool is used. However, it is not as efficient as activated carbon for adsorbing these volatiles and consequently lower tar (condensable volatiles) yields are obtained.

GC-TCD

The GC-TCD system is based on gas-solid chromatography (adsorption) for separation and qualitatively characterization of the different compounds present in the gas stream; followed by thermal conductivity detection for quantitatively analysis of the gas molecules. The columns are packed columns 60/80 Carboxen-1000. In one of the columns, N_2 is used as carrier gas and in the second one He is used. The reason for that is to be able to detect H_2 in the column using N_2 as carrier gas.

The sampling system for the GC-TCD is formed by two electro-pneumatic valves. Once the signal is given to take a new sample, these valves lead the gas stream into the sampling loop for several seconds and them back to the normal position. The GC-TCD is calibrated with two different known compositions of synthetic gas mixtures, air and pure N_2. One gas mixture includes: 13% H_2, 53% N_2, 16% CO, 5% CH_4 and 13% CO_2. The second gas mixture includes: 10% CO, 60 % CH_4, 10% CO_2, 10% C_2H_6 and 10 % C_2H_4.

Analysis of condensable volatiles

The volatiles condensed in the stainless steel condenser (toluol), as well as in the glass condensers (isopropanol) are used to determine liquid/tar mass yields for the mass balances. For that, all the cold parts are weighted before and after the experiment, including the used solvent.

Then these volatiles are analyzed in a gas-chromatograph mass-spectrometer detector (GC-MS), equipped with a column Ultra 2 (Cross-Linked 5% Phenyl Methyl Silicone), 25 m x 0.2 mm and 0.3 μm film thickness. The carrier gas used is He. Several fractions of the volatiles are analyzed. First of all, a sample is analyzed, as it is taken from the condensers, including the solvent and without any further treatment. Then the volatiles condensed in the toluol condenser are separated in two phases by decantation; one phase is toluol miscible and the other phase cannot mix with toluol but it condensed due to the low temperatures. Then the solvent is evaporated from each phase in a rotary evaporator, at a temperature of 40 °C and at different degrees of vacuum. Typically, isopropanol evaporates at 100 mbar while toluol requires 40 mbar to evaporate. Then the gravimetric tar (tar which did not evaporate) is solved again in isopranol for further analysis in the GC-MS. The solvent fractions are also analyzed. A sample of the gravimetric tar, before dilution with isopropanol is taken for elemental analysis.

4.2 Experimental conditions

4.2.1 Materials and experimental conditions

The materials used in the experiments reported in the present work are: pine wood chips - approximate average size 3 cm x 2 cm x 0.5 cm - provided by Robeta Holz OHG, Milmersdorf, Germany; cellulose with high ash content (h.a.c. cellulose), cellulose with low ash content (l.a.c. cellulose), both obtained from disposable plates cut in pieces - approximate average size 5 cm x 5 cm x 0.2 cm -; cellulose obtained from cotton wool; powder kraft lignin (Protobind 2000); bio-waste, a mixture of cellulose and food waste; beech wood spheres of 25 mm of diameter; and corn digestate. The corn digestate was provided by ATB Potsdam, in particular by Dr. Axel Funke.

The disposable plates are referred to as cellulose, since it is mostly a cellulosic material, except in Chapter 6, where pyrolysis mechanisms of lignocellulosic materials are studied, based on the pyrolytic behavior of their main macromolecules. In this case, they are referred to as holocellulose, since they can also contain significant amounts of hemicellulose [129]. This is due to the fact that pulping removes nearly all the lignin but just partially the hemicellulose, leading to hemicellulose contents that can be higher than 10%. Besides, the pyrolysis mechanism of hemicellulose is consider to be quite similar to the one of cellulose, therefore the main conclusions from cellulose can be extrapolated to hemicellulose [130].

In Table 4.1, the proximate and elemental composition of the materials used in the following experimental investigations on the pyrolysis process and biochar production are shown. In Table 4.2 the experimental conditions for the different experiments are summarized.

(wt%,db)	**Volatiles%**	**Ash%**	**C%**	**H%**	**N%**	**O%**
Pine chips	86.00	0.19	49.38	6.61	0.05	43.78
	±0.95	±0.04	±0.40	±0.02	±0.01	±0.43
Beech spheres	86.78	0.30	47.92	6.64	0.26	44.83
	±0.76	±0.05	±0.44	±0.03	±0.23	±0.25
Cellulose	94.68	0.11				
L.a.c. cellulose	86.47	0.94	47.26	6.61	0.15	44.99
(low ash content)			±0.15	±0.05	±0.01	±0.17
H.a.c. cellulose	72.87	15.70	39.00	5.57	0.20	39.31
(high ash content)			±0.20	±0.01	±0.01	±0.25
Lignin	74.20	1.40	63.17	6.06	0.75	27.50
			±0.06	±0	±0.01	±0.14
Corn digestate	64.24	19.57	40.67	5.45	2.36	31.68
	±0.05	±0.04	±0.69	±0.11	±0.05	±0.76
Heptane-washed	86.60	0.21	49.77	6.53	0.04	43.41
pine chips	±0.17		±0.13	±0.06	±0.01	±0.11
HCl-washed	88.71	0.01	50.09	6.43	0.04	43.41
pine chips			±0.02	±0.04	±0.01	±0.05

Table 4.1: *Proximate and elemental analysis of the raw materials used in the experiments. Oxygen content is determined as: 100%-(C%+H%+N%+S%+ash%). The volatiles and ash content was determined following the DIN norms, DIN 51720 and DIN 51719 respectively. The elemental composition was determined used an elemental analyzer Vario EL III.*

Experiment	Material	Temp.*	Flow N_2	Mass	Application
PW600-20	Pine chips	600 °C	20 Nl/min	1500 g	V., B., M.
PW600-40	Pine chips	600 °C	40 Nl/min	1500 g	V., B., M.
PW500-50	Pine chips	500 °C**	50 Nl/min	800 g	V.
PW400-20	Pine chips	400 °C	20 Nl/min	1500 g	V., B.
PW400-40	Pine chips	400 °C	40 Nl/min	1500 g	V., B.
BS500-50	Beech spheres	500 °C	50 Nl/min	750 g	V.
CD600-20	Corn digestate	600 °C	20 Nl/min	1500 g	B.
CD600-40	Corn digestate	600 °C	40 Nl/min	1500 g	B.
CD400-20	Corn digestate	400 °C	20 Nl/min	1500 g	B.
CD400-40	Corn digestate	400 °C	40 Nl/min	1500 g	B.
CELash	L.a.c.cellulose	600 °C	20 Nl/min	500 g	V., B.
Cellulose	L.a.c.cellulose	360 °C	10 Nl/min	500 g	B.
CEL	Cellulose	600 °C	20 Nl/min	500 g	V., B.
CELash+	H.a.c.cellulose	600 °C	20 Nl/min	500 g	V., B.
Waste	Bio-waste	360 °C	10 Nl/min	500 g	B.
Lignin	Lignin	400 °C**	20 Nl/min	500 g	M.
Washed-wood	Water-washed PW	600 °C**	20 Nl/min	1000 g	V., B.
Washed-wood1	Heptane-washed PW	600 °C**	20 Nl/min	1000 g	V., B.
Washed-wood2	HCl-washed PW	600 °C**	20 Nl/min	1000 g	V., B.
Wood20	Pine chips	600 °C**	20 Nl/min	1000 g	V.
Wood10	Pine chips	550 °C**	10 Nl/min	1000 g	V.
WoodSPS	Pine chips	560 °C**	20 Nl/min	1000 g	V.
BW600-20	Beech spheres	600 °C	20 Nl/min	3500 g	B.
BW340-50	Beech spheres	340 °C	50 Nl/min	750 g	B.

Table 4.2: *Summary of the experiments carried out. *Temperature measured in the reference position as specified in Section 4.1.1. **In these experiments, the final bed height is lower than 10 cm, therefore, the reference temperature is taken at 5 cm from the bottom of the reactor. V.: experiment used for volatiles characterization (Chapter 5). M.: experiment used for investigation on pyrolysis mechanisms (Chapter 6). B.: experiment used for biochar characterization (Chapter 8).*

Chapter 5

Volatiles evolution

In this chapter, volatiles produced during slow pyrolysis of wood are characterized, both on-line and off-line, as a mean of getting a deeper understanding of the pyrolysis process, in particular in conditions closer to industrial applications. The influence of particle size, retention time and concentration of volatiles in the reaction zone, as well as alkali content in the raw material, will be also studied.

On-line characterization is performed through analysis of permanent gases in a GC-TCD, as well as characterization of species emitting fluorescence with LIF spectroscopy (see Section 3.3). This is accompanied by on-line characterization of temperatures evolution inside the bed. Off-line characterization is performed by collecting the condensable volatiles after the pyrolysis process and subsequent analysis of compounds in a GC-MS (see Section 4.1.2). With the measured gas evolution, integrated over time, and the condensed volatiles, the total volatiles mass released from the bed can be estimated. This mass, together with the mass of the solid char remaining in the reactor, allows mass balances determination.

The content of this chapter has been partially published in [55], included in the Publications list of the author, attached to this document.

5.1 Permanent gases evolution

Four are the main permanent gas species present in the pyrolysis product of lignocellulosic or cellulosic materials: CO_2, CO, CH_4 and H_2 [96,131,132], being CO_2 and CO the main gas compounds produced during primary pyrolysis, while CH_4 is released in smaller quantities [120]. The evolution of these three species can be correlated with the fuel mass loss during primary pyrolysis [120], while H_2 release at higher temperatures is mostly related to progressive aromatization of the solid phase [96].

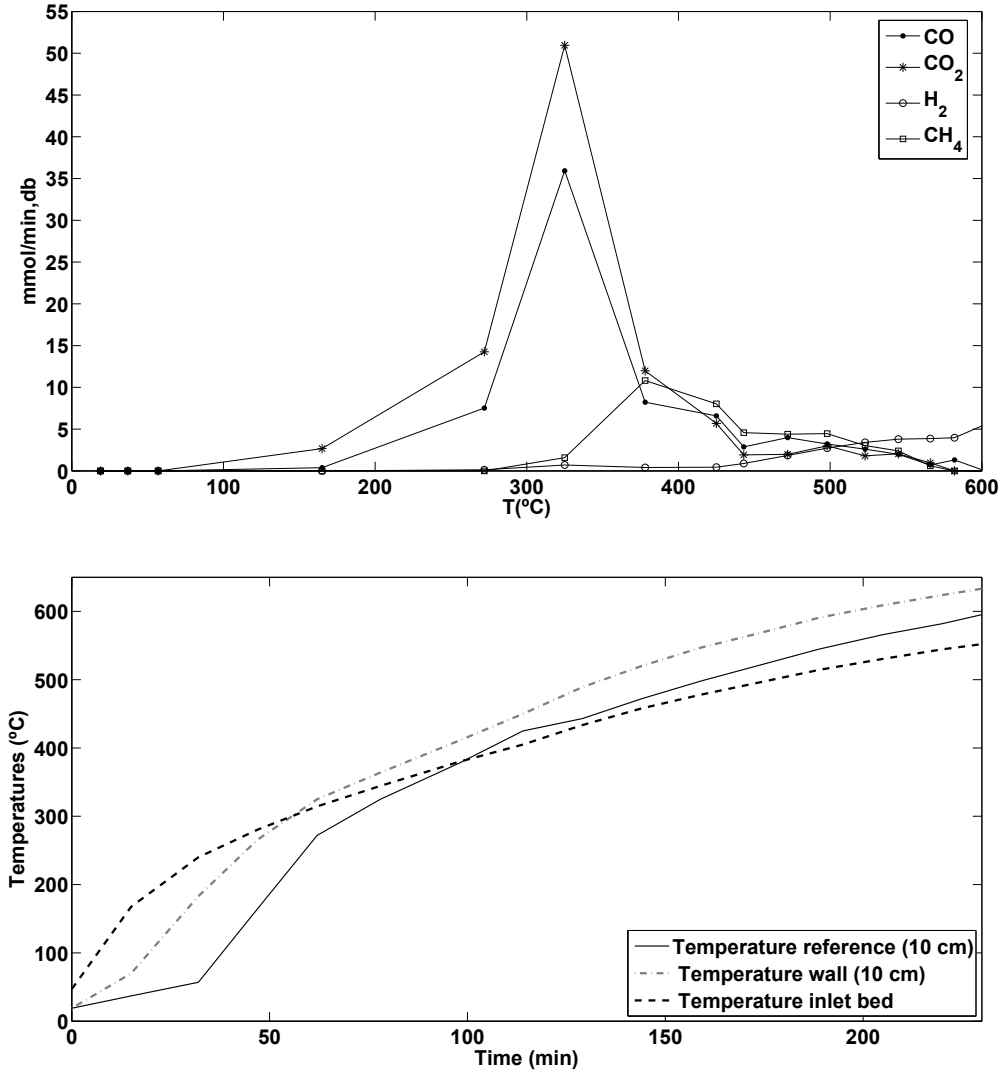

Figure 5.1: *Top: evolution of the main permanent gases present in the volatiles stream vs. temperature during pyrolysis of pine wood chips, 600 °C, 40 l/min (PW600-40), measured in the reference position (Section 4.1.1). Bottom: temperature evolution in different positions inside the bed for the same experiment.*

In Fig. 5.1, the evolution of these four species during the pyrolysis of pine wood chips up to 600 °C (measured in the reference position, Section 4.1.1), with a N_2 sweeping flow of 40 l/min is shown, together with the temperatures evolution inside the bed. This experiment corresponds to PW600-40 (Table 4.2).

The relatively high concentrations of CO and CO_2 observed at temperatures around 200 °C, when pyrolysis should be insignificant, according to literature and previous results on devolatilization kinetics of this material with similar heating rates [133], may be explained due to the inhomogeneity in temperature distribution inside the bed, especially at this early stage. That is to say, in other parts of the bed, the temperature is almost 300 °C, according to Figure 5.1 (bottom). The major release rate of CO and CO_2 takes place at temperatures around 325 °C in the reference position. At this point, the temperatures inside the bed are quite homogeneous, being the maximum internal temperature gradient approximately 50 °C. At higher temperatures, around 400 °C, CO and CO_2 concentrations decrease while CH_4 emission increases, reaching similar molar release rates as the ones for CO and CO_2. Similar behavior is also observed by Ryu et al. [134] and Wang et al. [96], where in both cases pyrolysis of pine wood at different scales is carried out, although in the case of Ryu et al. CO is the major gas component (in molar fraction) instead of CO_2. Above 450 °C H_2 becomes significant, being the main gas species at temperatures above 500 °C. The gas species behavior allows identification of different stages in the pyrolysis process.

CO and CO_2 are produced in primary pyrolysis mainly due to thermal cracking of carbonyl and carboxyl groups present in cellulose and hemicellulose, as reported by Yang et al. [94], which is consistent with their maximum release at low temperatures; while CH_4 and H_2 appear at higher temperatures, above 350 °C. CH_4 release may be related to reactions such as the cracking of methoxyl-O-CH_3 functional groups during lignin decomposition [94, 95], while H_2 formation is related to the cracking and deformation of C=C and C-H [94] bonds, as well as due to restructuraction and aromatization of the solid matrix at higher temperatures [96]. Yang et al. [94] also pointed out that CH_4 is released in two stages: at low temperatures mostly from hemicellulose primary pyrolysis around 280 °C, behavior that is not detected in the present study, and at higher temperatures, between 500 and 600 °C from lignin, most probably due to secondary reactions. Since CH_4 in the present study is detected only at temperatures around 400 °C, this could be an indication of the presence of heterogeneous secondary reactions enhancing its emission. Granada et al. [135] carried out TGA experiments coupled with FTIR to analyze CO, CO_2 and CH_4 release rates under different heating rates for pine wood. It was observed that with slow heating rates (10 °C/min), CH_4 had its maximum release rate at temperatures around 450 °C, with values (in mass) one order of magnitude lower than CO maximum release and two orders of magnitude lower than CO_2. However, by increasing the heating rates, CH_4 was the species that

mostly increased its release, followed by CO, while CO_2 remained constant. These results may be also an indication of the fact that CH_4 release is related to the presence of secondary reactions. In this case, higher heating rates mean more residence time at high temperatures and, consequently, higher possibility of undergoing secondary reactions. Neves et al. [120] also reported that CO and CH_4 were major species coming from secondary reactions of tars, increasing significantly their release at temperatures above 600 °C and being CH_4 yields always an order of magnitude (in mass) below CO yields.

In the present study, this behavior is further validated with the fact that around 400 °C, the release rate (in mol) for CH_4 is similar than those for CO and CO_2, that is to say, it supposes approximately a third (in mass) of CO_2 release and slighlty above half of the CO release. This behavior is in good agreement with the work from Asmadi et al. [5], who proposed a possible pathway for CH_4 formation based on the demethylation of cresols/xylenols as intermediate products from primary pyrolysis. Boroson et al. in [136] also affirmed that, despite observing some modest emissions of CH_4 from primary pyrolysis, it was definitively a secondary product from homogeneous tar cracking reactions, together with CO and H_2; while CO_2 was detected as a truly product from primary pyrolysis. In [122], where tar cracking reactions over a char bed were studied, CO and CO_2 were also detected as definite products of tar heterogeneous secondary reactions. This behavior could be related with the similar release rates that CO, CO_2 and CH_4 experience at temperatures above 400 °C.

Other authors like Gilbert et al. [137] reported that both, homogeneous and heterogeneous secondary reactions give place to the formation of CH_4, CO and H_2. Aguiar et al. studied in [132] the effect of temperature and particle size on gas product composition in fixed-bed pyrolysis of orange peel residues, concluding that H_2 production was enhanced with increasing particle size and pyrolysis temperatures, while CH_4 and CO_2 productions were just affected by the particle size and not by the pyrolysis temperature, suggesting therefore a possible enhancement in heterogeneous secondary reactions, giving place to these species.

To sum up, CO_2 is reported to be a product of primary pyrolysis or produced during heterogeneous secondary reaction of tars. CO is a product from primary pyrolysis, but it is also a very important product of both homogeneous and heterogeneous secondary reactions of tar. CH_4 can be detected in small quantities during primary pyrolysis, around 2 orders of magnitude below CO_2 (in mass) and it is also a clear product of secondary reactions, mainly through demethylation reaction. In the present study, at temperatures around 400 °C, CH_4 release rate (in mass) was around half of that from CO and above one third of CO_2. Since at those temperatures homogeneous secondary reactions of tars should be almost negligible, these yields must be explained through

the presence of heterogeneous secondary reactions, enhanced by big particle and bed sizes.

5.2 Influence of process conditions on volatiles evolution

New experiments were performed in order to further confirm the previous assumption: permanent gas characterization allows distinguishing two phases in slow pyrolysis of wood, a primary pyrolysis stage where CO and CO_2 are the dominant species, and a second stage, where the release of CH_4 becomes significant, indicating the presence of heterogeneous secondary reactions. In these experiments, the residence time and concentration of volatiles inside the bed were changed, as well as the particle size and the alkali content of the initial feedstock. The experiments presented in this Section have been carried out in the framework of the master thesis from Pablo Cabaleiro, of which I am coordinator (in submission).

In Fig. 5.2, the comparison of two pyrolysis experiments, using pine wood chips as feedstock, with an initial bed weight of approximately 1000 g, is shown. The figure on the top is correspondent to a N_2 flushing rate of 20 l/min (experiment Wood20), that is to say, lower retention time of volatiles inside the bed, as well as lower concentration of these volatiles. The figure on the bottom shows the results with a flow rate of 10 l/min (experiment Wood10).

It is observed that the release of CO, CO_2 and CH_4 is significantly higher in the experiment with lower flow rate (10 l/min), and that these maximum release rates take place with temperatures inside the bed ranging from 350 - 500 °C, meaning that homogeneous secondary reactions should be negligible. Looking at Fig. 5.4 (top), it is observed that the CO_2 yield increases from around 10 to 14% (wt, db), the CO yield from 5 to 9% approximately and the CH_4 yield from 1.2 to 1.8 % roughly, when residence time and concentration of volatiles are increased. This happens even when the final temperature of the experiment, with a flow rate of 20 l/min, is slightly higher (600 °C, measured at 5 cm from the bottom of the reactor) in comparison with the final temperature for the experiment Wood10 (560 °C, measured at 5 cm from the bottom of the reactor). This suggests that heterogeneous secondary reactions are being enhanced.

In Fig. 5.3 the experiments with pine wood chips, using beds of 1000 g and N_2 flow rates of 20 l/min, but with small particle size (WoodSPS) and with HCl washed wood (Washed-Wood2), are compared. For the experiment with small particle size (top), maximum release rates similar to those for Wood10 (flow of 10 l/min) were obtained. In principle, it should be said that the observed behavior is exactly the opposite as expected. However, it must be taken into account that with smaller particle size the bed turned to be much more compact, with significantly higher bulk density. For this

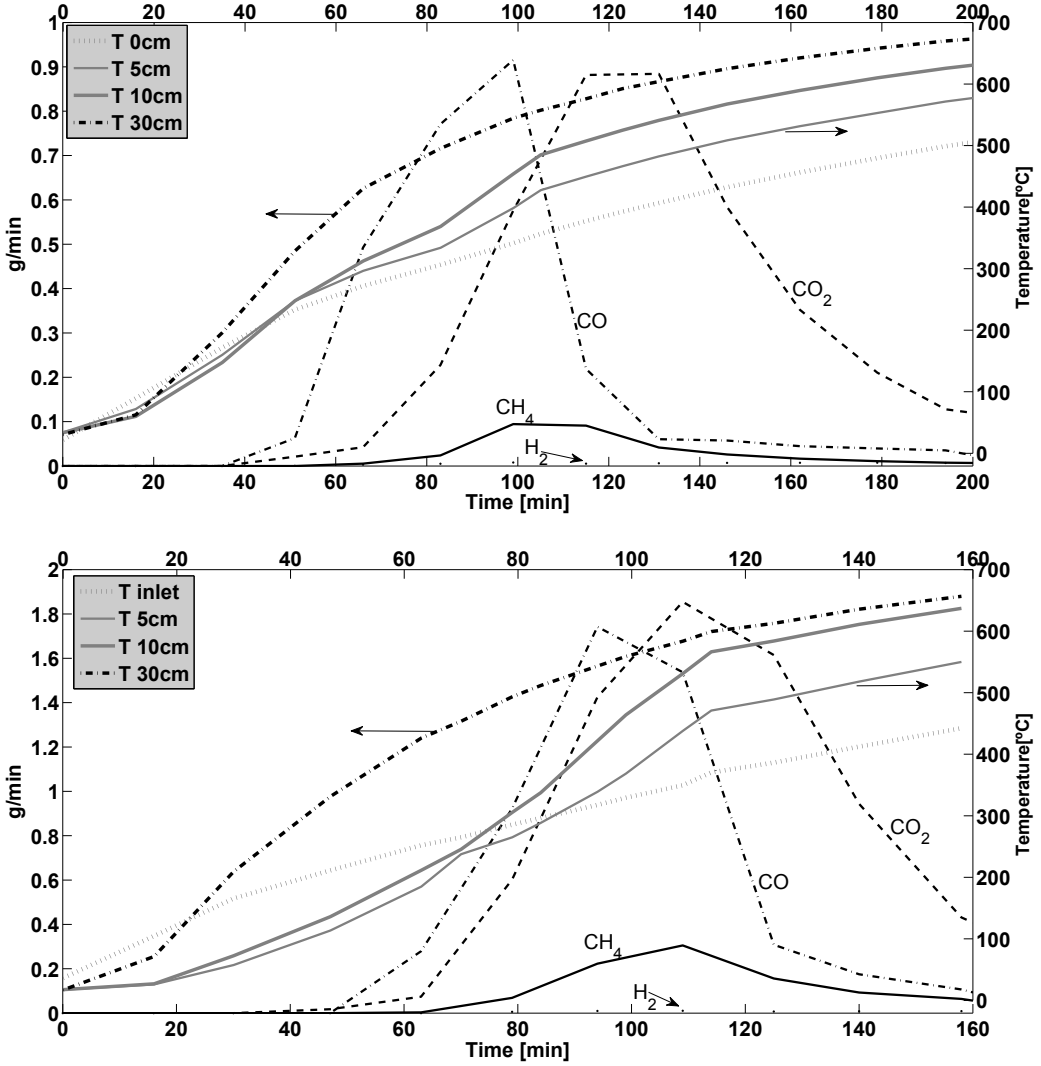

Figure 5.2: *Top: transitory behavior of permanent gases and temperatures for wood pyrolysis (Experiment Wood20) with a N_2 flow rate of 20 l/min. Bottom: transitory behavior of permanent gases and temperatures for wood pyrolysis (Experiment Wood10) with a N_2 flow rate of 10 l/min.*

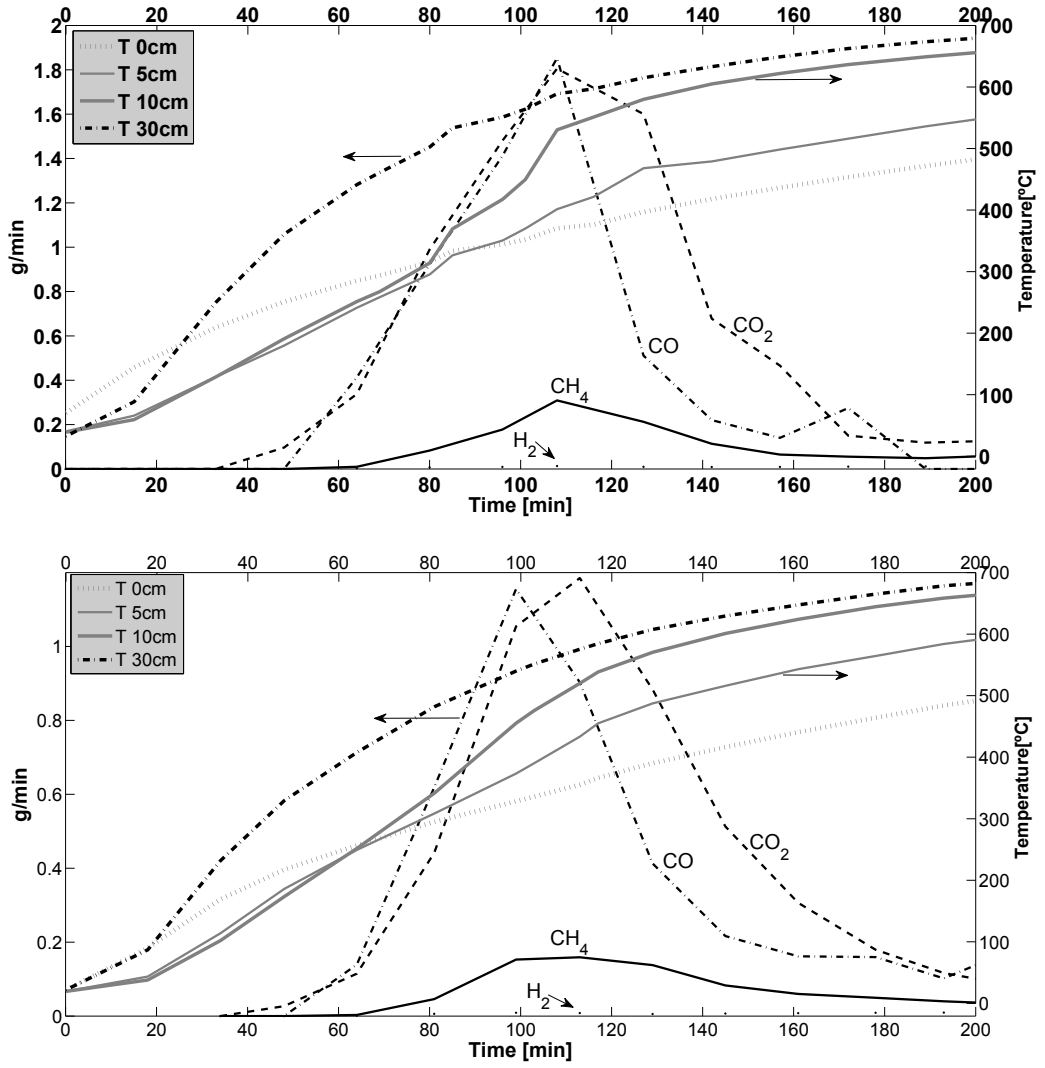

Figure 5.3: *Top: transitory behavior of permanent gases and temperatures for wood pyrolysis with small particle size (Experiment WoodSPS) with a N_2 flow rate of 20 l/min. Bottom: transitory behavior of permanent gases and temperatures for HCl washed-wood pyrolysis (Experiment Washed-wood2) with a N_2 flow rate of 20 l/min.*

reason it is believed that in these conditions the bed, due to the high compaction, and not the particle size, was enhancing secondary reactions. This is further validated with the fact that, in these conditions, the maximum release of CO and CO_2 takes place at the same time, similar to the case for lower flow rate. For HCl washed wood (Washed-Wood2), similar values were obtained as for wood with 20 l/min (Wood20), indicating that the removal of alkali content does not have a significant impact on these products yields. Slightly more CO is obtained.

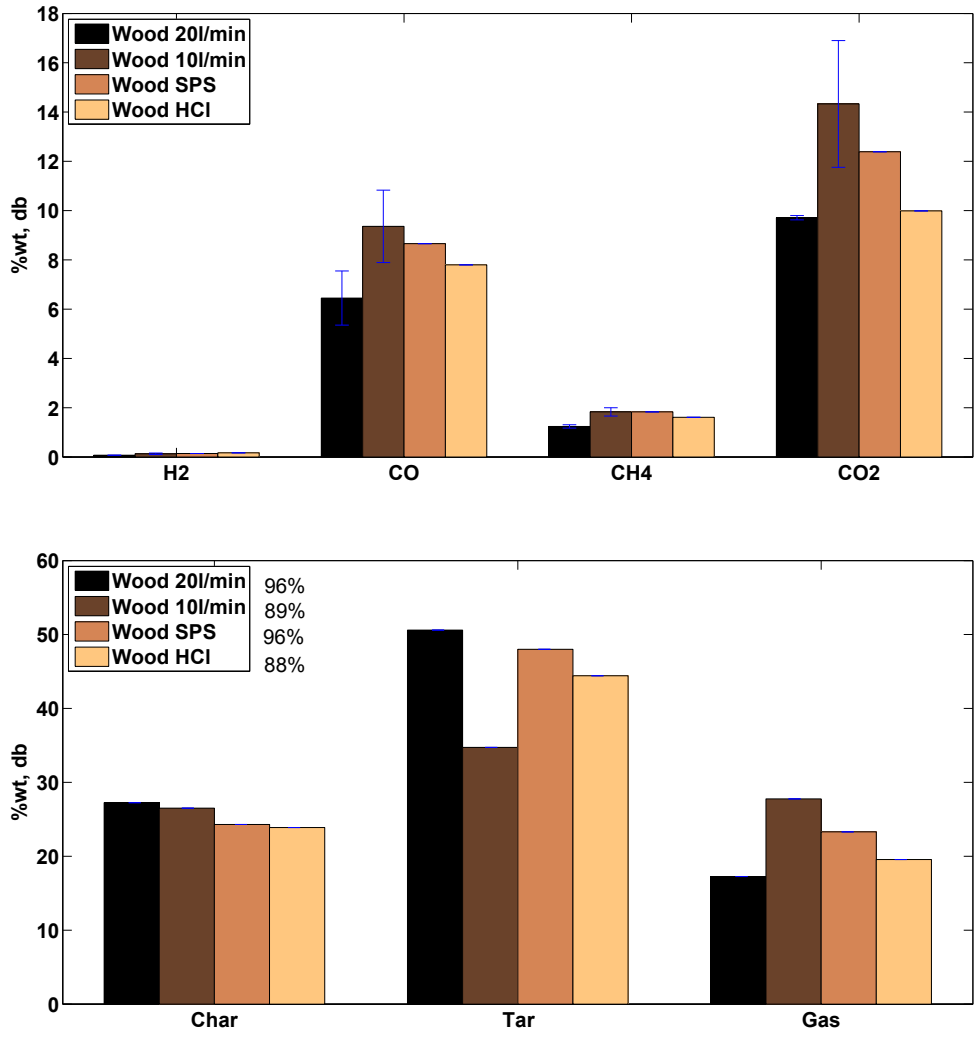

Figure 5.4: *Permanent gas species yields (top) and products distribution (bottom) for the experiments Wood20, Wood10, WoodSPS and Wood-washed2. The percentages in the bottom figure represent the total mass balance for each experiment.*

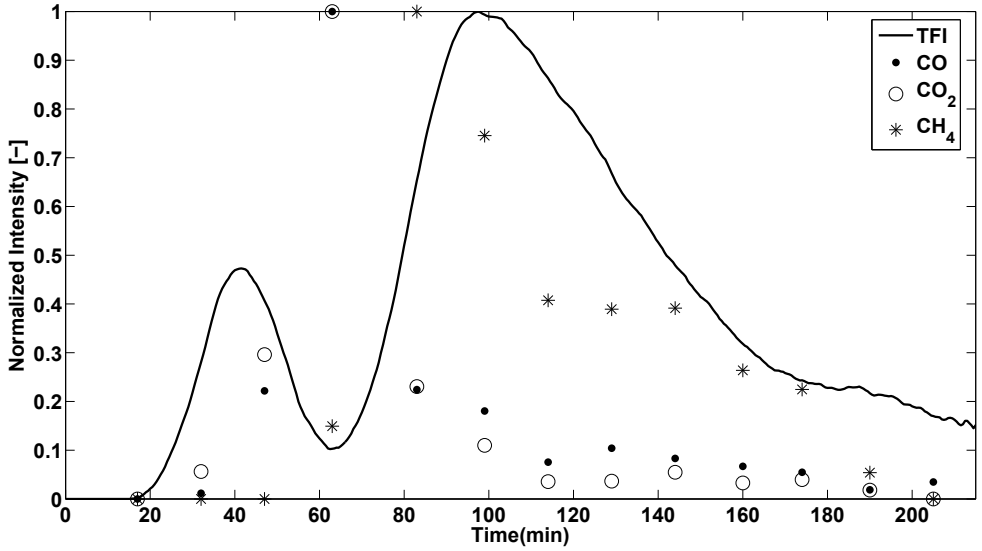

Figure 5.5: *Comparison of the normalized total fluorescence intensity (TFI) and the normalized evolution of the main gas species CO, CO_2 and CH_4 for experiment PC40.*

5.3 Laser-induced fluorescence applied to volatiles characterization

With the objective of learning more about the probable presence of these heterogeneous secondary reactions, on-line characterization of volatiles with laser-induced fluorescence (LIF) was performed, following two complementary paths: by analyzing the evolution of the total fluorescence intensity (TFI) (explained in Section 3.5) and by characterizing qualitatively the spectra evolution. The analysis of the LIF signal is performed as explained in Section 3.5.

In Fig. 5.5, the normalized TFI evolution is compared with the normalized gas species evolution for experiment PW600-40, as in Section 5.1. An attenuation in the TFI is observed, coincident with the maximum release of CO and CO_2, that is to say, with the maximum volatiles release; while CH_4 release occurs later and it is coincident with the second peak in fluorescence intensity after the signal is recovered.

If the TFI evolution is also compared with the total gas release for other experiments, such as PW600-20 and PW500-50, as it is shown in Figure 5.6, the same behavior is observed. It is important to say that these experiments present different process conditions - bed heights and N_2 flow rates - which lead to different retention times of the volatiles inside the bed and different dilution degrees in the volatiles stream passing through the LIF system. However, in all of them the same attenuation phenomenon, coincident with the major gas species release, is observed. Together with this fluorescence intensity decrease, a significant reduction in the laser intensity at a wavelength

of 266 nm, measured after passing though the measurement cell, takes place. Both behaviors are due to the high tar concentration present in the LIF cell in this stage of the pyrolysis process. The question now is if the actual maximum of the TFI would happen during this signal attenuation, being not visible due to the attenuation phenomenon, or if it would actually correspond to the second peak observed in Fig. 5.6, after fluorescence intensity recovery. In the first case it would mean that the TFI evolution resembles the primary pyrolysis process, while in the second case, it would imply that it mostly follows secondary reactions, supported by the CH_4 behavior. With the objective of clarifying this question, the TFI evolution is divided by the laser intensity at a wavelength of 266 nm measured after the measurement cell (TFILI). It is expected that this value (TFILI) accounts better for substances that emit fluorescence since it takes into account how much light has been absorbed. Due to the absorption phenomenon that the laser beam also experiences during this pyrolysis stage, a low-limit value of 250 counts in laser intensity is selected. In Fig. 5.7 the comparison of TFI and TFI divided by the laser intensity (TFILI) is shown. The tendency of TFILI is to increase when the attenuation in the fluorescence intensity takes place and to decrease when the second TFI peak appears. This result would mean that the actual maximum in the TFI evolution, if there was no attenuation (for example with a higher dilution), would be approximately coincident with the major volatiles release, resembling hence primary pyrolysis.

The comparison of total gas and TFI evolution also shows that after the major volatiles release, with temperatures above 400 °C, the TFI is still significantly high, presenting similar qualitative behavior to CH_4 release. This could be another hint of the presence of heterogeneous secondary reactions. This similarity is further analyzed with the ratio CH_4 / TFI - both signals normalized - for experiments PW600-20 and PW600-40. This ratio presents quite constant values, between 0.35 and 0.5 for PW600-40 and 0.15 and 0.3 for PW600-20. The lowest value in PW600-20 may be due to the fact that longer residence times give place to a higher quantity of bigger PAHs as shown Sections 5.3.1 and 5.3.2, which present higher fluorescence intensity as already commented.

The next step would be the analysis of the signal spectra at different stages of the pyrolysis process, to get more information about tar evolution regarding its composition during the pyrolysis process. To this end, two different stages were considered separately. The first stage, before signal attenuation, considers the fluorescence spectra at low temperatures, up to 300 °C approximately, that is to say, the beginning of the pyrolysis process. The second stage, after signal attenuation, refers to tars at higher temperatures, after maximum volatiles release rates, and shows the possible tar composition evolution due to the presence of heterogeneous secondary reactions. Both stages are discussed in the next Sections 5.3.1 and 5.3.2.

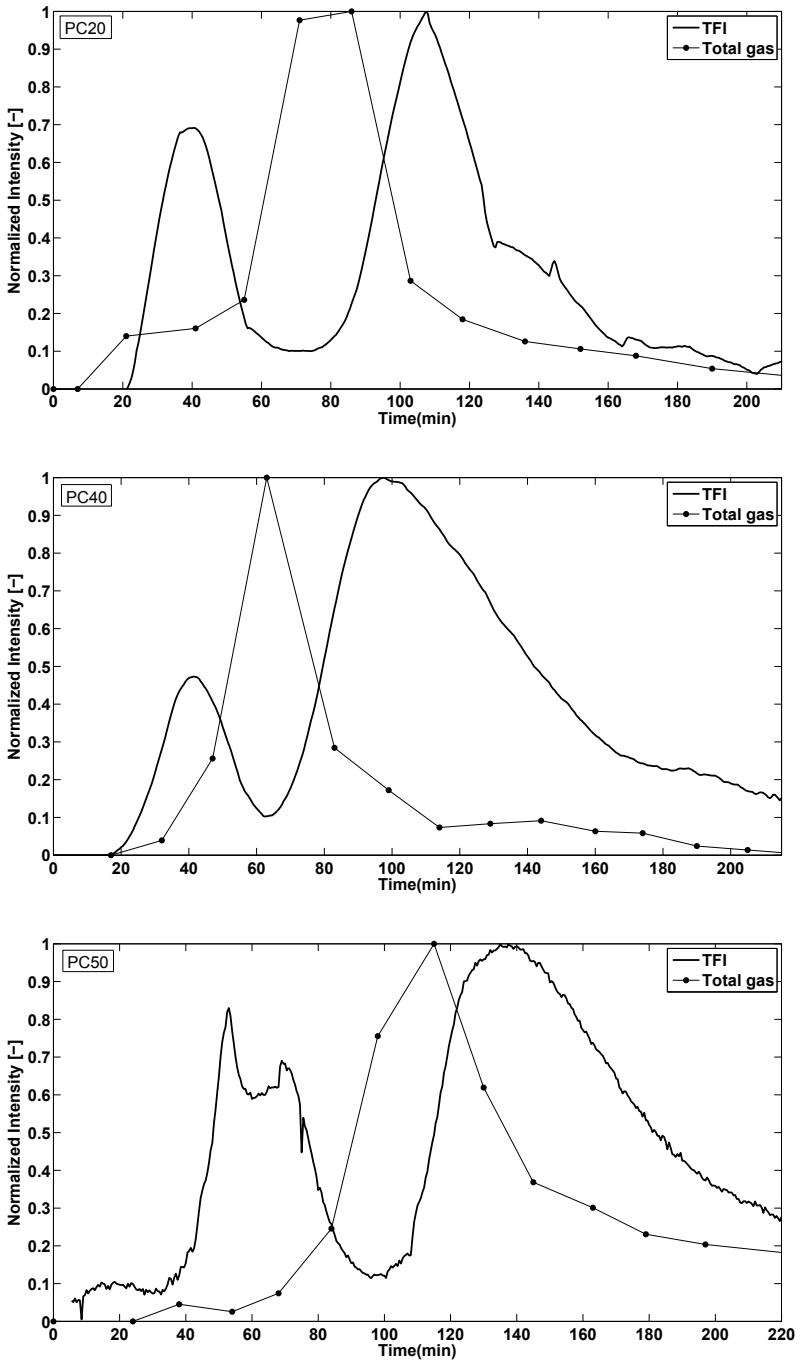

Figure 5.6: *Comparison of the total fluorescence intensity (TFI) and the main gas species CO, CO_2 and CH_4 for experiments PW600-20, PW600-40 and PW500-50.*

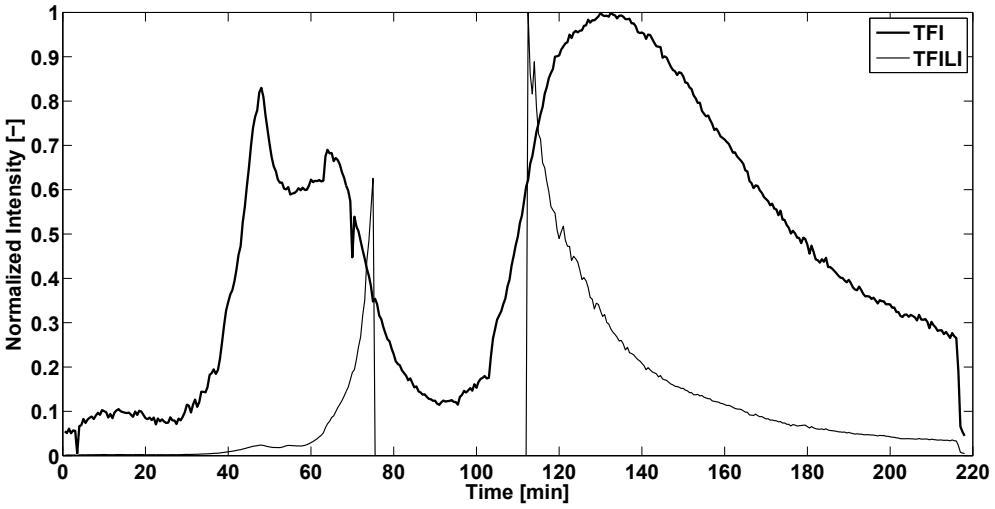

Figure 5.7: *Comparison of the total fluorescence intensity (TFI) and the TFI divided by the laser intensity at 266 nm (TFILI) for experiment PW600-40.*

5.3.1 Qualitative tar characterization at early pyrolysis stages: before attenuation

In this Section, several fluorescence spectra, correspondent to pyrolysis of pine chips and beech spheres under different experimental conditions, are compared and discussed. In Fig. 5.8 the fluorescence spectra at different temperatures below 300 °C are shown for experiments PW600-20 and PW600-40. The only difference in these experiments was the flow rate, 20 and 40 l/min, respectively. Lower flow rate means higher retention time of volatiles inside the bed and, consequently, higher possibility of undergoing secondary reactions, leading to a potential change in tar composition.

The most significant phenomenon observed in this case is the blue-shift of the fluorescence spectra between 190 °C and 280 °C, from 390 nm approximately to around 350 nm. This behavior is observed for the experiment PW600-40 but not for PW600-20, due to an earlier signal attenuation. However, similar behavior is expected in this case, since at 190 °C the spectra in both experiments are very similar.

The explanation for the presence of the peak at 390 nm at low temperatures is not clear. It is not probable that it belongs to ketones - aliphatic -, since they emit fluorescence at higher wavelengths, as it has been reported in Section 3.3 (Figure 3.2). However, it could have its origin in some electronic transition from aldehydic groups, although in this case the absorption cross section and quantum yield with this excitation wavelength should be low. For further interpretation of this behavior, the author now refers to the results of experiments PW500-50 and BS500-50 in Fig. 5.9. If the fluorescence spectra evolution of pine chips is compared with the one for beech spheres, it can be observed

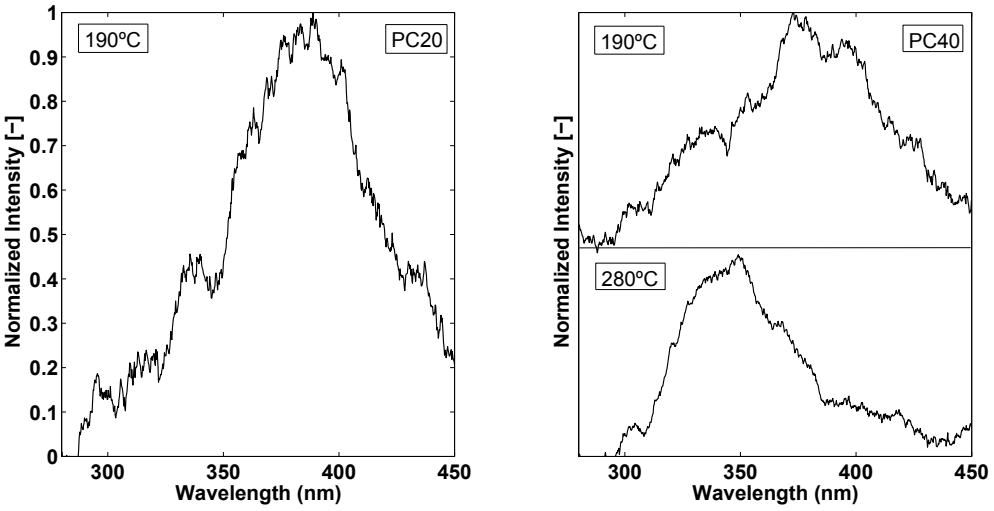

Figure 5.8: *Left: fluorescence spectrum at 190 °C in PW600-20. Right: fluorescence spectra at 190 °C and 280 °C for experiment PW600-40.*

that the peak shift from 390 to 340 nm is not present for beech wood, having similar fluorescence peaks for 250 °C and 275 °C.

These results are also consistent with experiments at particle level for both, pine chips and beech spheres, using in this case an excitation wavelength of 355 nm. The results for single particle pyrolysis of beech spheres have been already reported in a previous work of this group [4]. New experiments using pine chips (the same type as the chips used for the reactor level experiments, with the same setup used in the aforementioned study and similar process conditions) are added to investigate if this behavior is also observable at particle level with different wavelengths (355 nm excitation wavelength for particle level and 266 nm excitation wavelength for reactor level). As it can be seen in Fig. 5.10, a blue-shift in the fluorescence signal is also observed in the case of single pine chip particle, although the emission fluorescence wavelengths are different due, probably, to the different excitation wavelengths. It is also worthy to mention that, in the first red-shifted signal from pine, the characteristic structure of formaldehyde fluorescence is observed on top. This would be in good agreement with the hypothesis that the fluorescence peak may be due to aldehydic groups.

The spectra from pine chips shown in Fig. 5.10 indicate a change in volatiles composition. The authors interpret this behavior as due to the presence of extractives, which is not reflected by the spectra from beech spheres, or even due to the different composition in hemicellulose from both wood species, since one is softwood and the other one hardwood. The same interpretation can be applied to the results of the technical-scale pyrolysis shown in Fig. 5.8 and Fig. 5.9, where a blue-shift of the peak from 390 nm to 350 nm can be observed only for the experiments with pine chips but not for beech spheres.

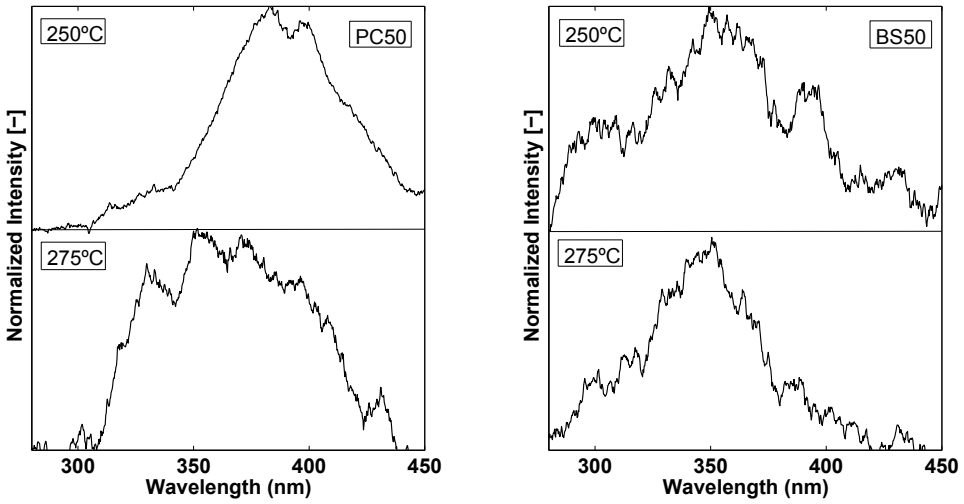

Figure 5.9: *Left: fluorescence spectra at different temperatures for pyrolysis of pine chips with N_2 flow of 50 l/min (PW500-50). Right: fluorescence spectra for beech spheres pyrolysis under the same conditions as the previous one (BS500-50).*

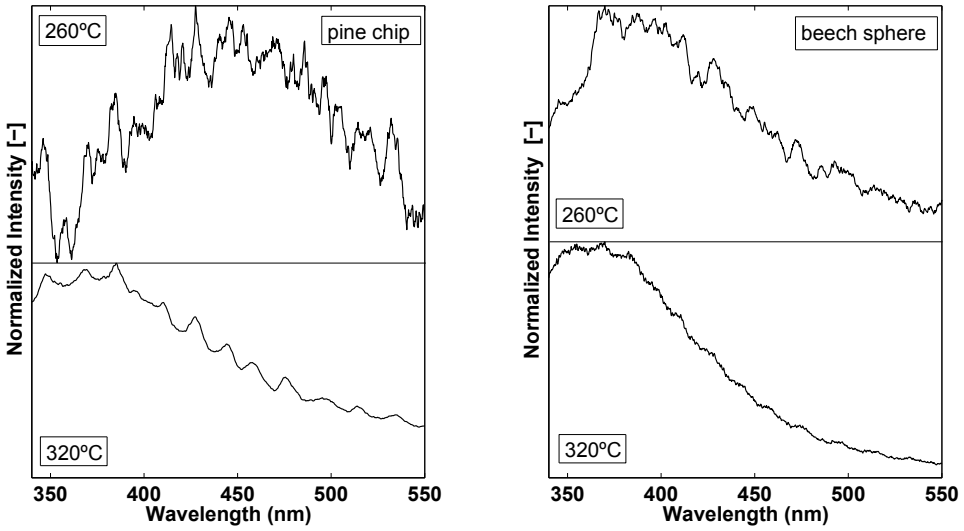

Figure 5.10: *Left: fluorescence spectra at two different temperatures for a particle of pine wood. Right: fluorescence behavior for a sphere of beech wood [4].*

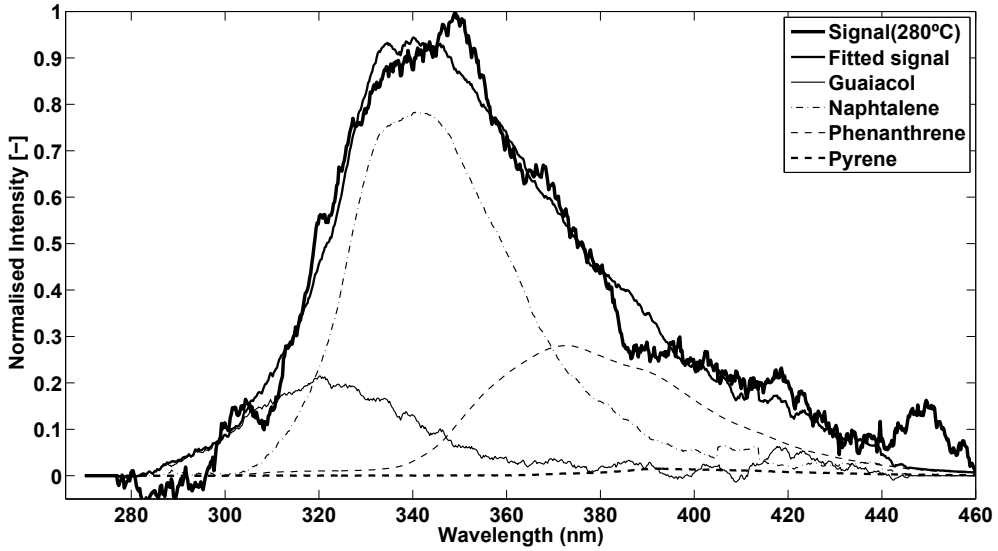

Figure 5.11: *Fitted signal with pure species guaiacol, naphthalene, phenanthrene and pyrene for the spectrum at 280° C from experiment PW600-40.*

Coming back to the second peak observed in Fig. 5.8 and 5.9, in all the cases it appears around 350 nm, independently of the process conditions and raw material. This means that, in this stage, volatiles composition is not affected by the retention time of volatiles inside the particle or bed and neither by the wood type. This could suggest that they come from primary decomposition of cellulose, hemicellulose and lignin, which is also consistent with the low temperatures at which they appear. By fitting this spectrum with the pure species spectra, obtained as previously reported, the qualitative composition of the volatiles leading to this spectrum can be seen. As shown in Fig. 5.11, the main species are guaiacol, as representative of 1-ring aromatic compounds, naphthalene for 2-ring aromatic compounds and phenanthrene for 3-ring aromatic compounds.

5.3.2 Qualitative tar characterization at later pyrolysis stages: after attenuation

The objective of this Section is to discuss the evolution in tar composition during the pyrolysis process at higher temperatures, through the analysis of fluorescence spectra, and determine how process conditions may affect this evolution, regarding the possible enhancement of heterogeneous secondary reactions with higher residence times and concentration of volatiles, as well as bigger particle and bed sizes. To support this, comparison in evolution for each one of the chosen pure species, as representative of n-ring aromatic groups (guaiacol: 1 ring; naphthalene: 2 rings; phenanthrene: 3 rings;

pyrene: 4 rings) is done [106, 126]. For this purpose, the spectra are fitted with the representative pure species, as done in Fig. 5.11.

The main drawback regarding qualitative characterization is that the observed fluorescence signals are broad-band featureless spectra, characteristic which has been also shown for spectra of some PAHs mixtures [126]. Hence, the presence of a specific species can not be reliably deduced from these spectra, as done for example in [113] with formaldehyde. However, characterization of tar composition and evolution can be done based on the fact that each representative species has its fluorescence intensity peak at a specific wavelength, together with the fact that the bigger the aromatic compound, the more red-shifted the fluorescence spectra [126].

In Fig. 5.12 the influence of flow rate on volatiles composition evolution is studied, comparing the spectra at 440 °C - measured in the reference position, as explained in Section 4.1 - for experiments PW600-20 and PW600-40. As previously explained, lower flow rate means higher residence time and higher volatiles concentration in the reaction zone and, consequently, potential wider extent of heterogeneous secondary reactions. It can be observed that in the case of PW600-20 - lower flow rate - there is a slight red-shift of the signal by approximately 10 nm with respect to PW600-40 - higher flow rate -. At the same time the curve correspondent to PW600-20 presents higher intensity at wavelengths corresponding to 3- and 4-ring aromatic compounds than PW600-40. As shown in Fig. 2.3, PAHs are possible products of secondary reactions. Hence, the observed red-shift and higher intensity at higher wavelengths may be attributed to the higher extent of secondary reactions in the case of PW600-20.

This can be further observed by comparing the relative evolution of the representative pure species for PAHs, guaiacol, naphthalene, phenanthrene and pyrene, over time. To carry this out, every normalized single spectrum is fitted with these pure species, as it has be done in Fig. 5.11. The results of this fitting are summarized in Fig. 5.13. As it can be observed, naphthalene, as the representative species of 2-ring PAH group, is the main species present during the whole process. This is in agreement with the measurements presented by Fagernäs et al. [100], Srinivasan et al. [138] and Ahrenfeldt et al. [139], where naphthalene was reported to be the main aromatic compound. It can be also observed that around 85 min approximately a significant increase in the relative concentration of phenanthrene occurs. This increase takes place after the signal attenuation, that is to say, it is coincident with the second peak of fluorescence as seen in Fig. 5.6. This phenomenon is also coincident with the increase in CH_4 release. This could mean that this second peak in the TFI, after the signal attenuation during primary decomposition, could be due to the presence of heterogeneous secondary reactions leading to a more complex structure in aromatic compounds. As the process is more evolved - around 130 min - a slight decrease in the relative concentration of

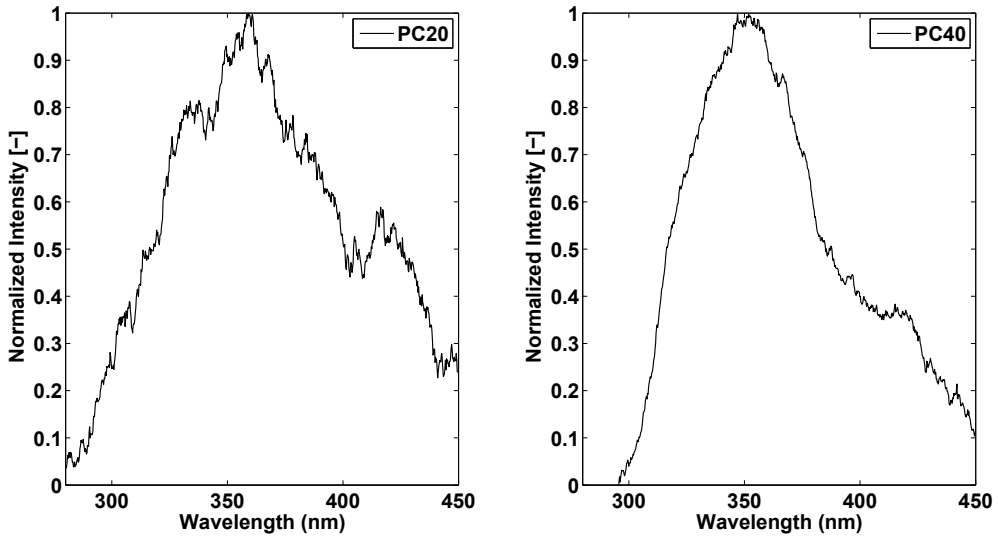

Figure 5.12: *Comparison of volatiles spectra under two different flow rates (20 and 40 l/min) at 440 °C.*

phenanthrene can be observed. At the same time, the relative concentration of pyrene increases slightly.

The next step would be to compare the effect of raw material on tar composition evolution in this temperature range, after attenuation. Comparing the fluorescence spectra at 300 °C for wood chips and beech spheres under the same pyrolysis conditions, no clear variation in tar composition can be found as shown in Fig. 5.14. This is in agreement with the fact that both wood types have very similar chemical composition which is illustrated by the proximate and ultimate analysis shown in Table 4.1.

5.4 Conclusions

Laser-induced fluorescence (LIF) has been applied to tar on-line characterization in a technical scale - 1 m high, 22 cm of internal diameter and bed weights in the range of kg - fixed-bed pyrolysis process of two woody species - pine and beech -. The evolution of total fluorescence intensity (TFI) is measured during the pyrolysis experiment and compared to on-line gas evolution characterization and total gas release rate. Analysis of fluorescence single spectra, based on the characteristic spectra of representative species, are carried out to qualitatively determine tar composition in terms of n-ring aromatic groups.

CO_2 and CO are the main species ejected during the pyrolysis process, having their maximum release rate at around 325 °C, measured in the reference postion. These species come mostly from decomposition of cellulose and hemicellulose, thus, they are

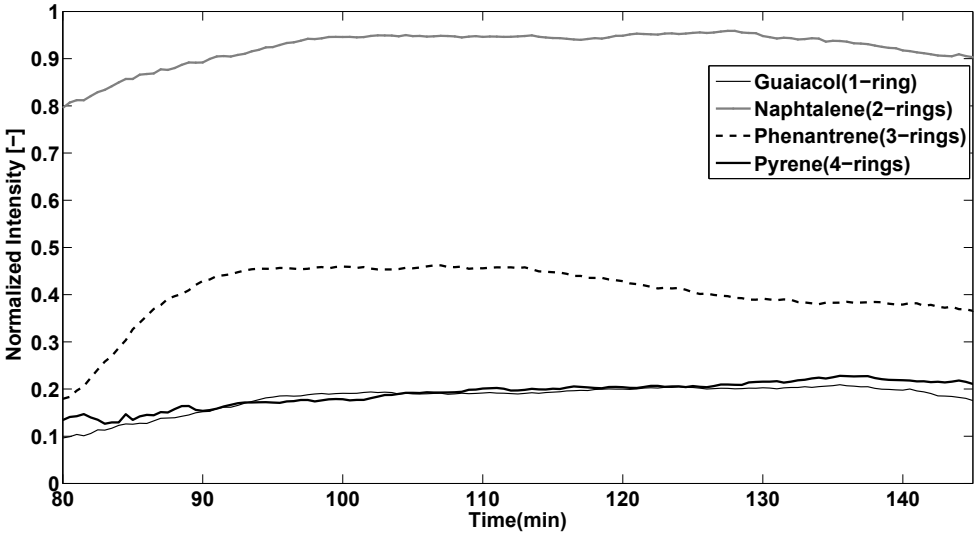

Figure 5.13: *Comparison of main representative species evolution after fitting with normalized spectra for experiment PW600-40.*

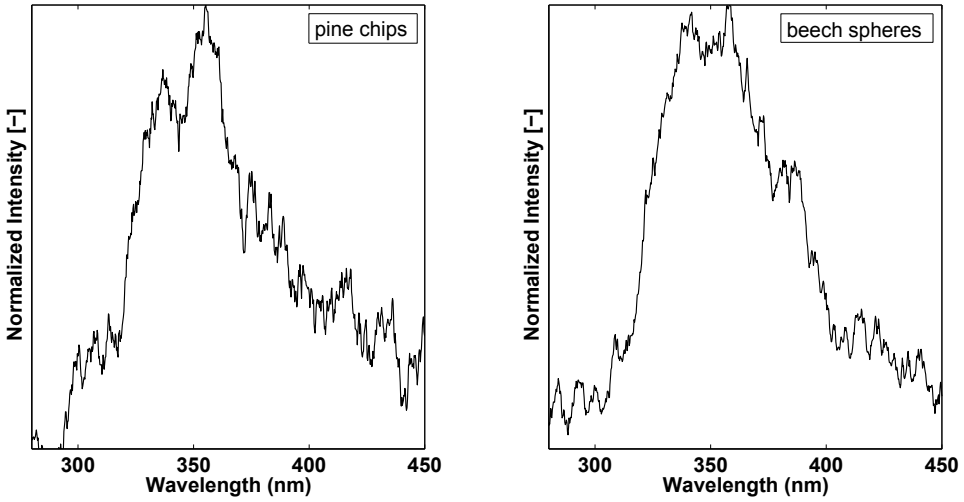

Figure 5.14: *Spectrum of tar fluorescence at 300 °C from pine wood chips and beech wood spheres pyrolysis with a flow of 50 l/min.*

considered representative of the weight loss or major volatiles release during primary pyrolysis. CH_4 and H_2 releases, however, take place at higher temperatures. Their release may be related to the presence of secondary reactions. Higher residence time and higher concentration of primary volatiles in contact with the solid matrix leads to enhancement of CO, CO_2 and CH_4 production, as well as a decrease in the liquid yields.

If the TFI evolution is compared with the total gas release rate, an attenuation in the fluorescence signal is observed, coincident with this major gas release, independent of the process conditions. This is due to strong absorption of the laser light, but also of the fluorescence emitted, as consequence of the high tar concentration in the LIF cell. The TFI divided by the laser intensity at 266 nm (TFILI), measured after the cell, shows that the actual peak of the TFI, if there was no attenuation phenomenon, would be approximately coincident with the major volatiles release, resembling then primary pyrolysis.

Qualitative characterization of fluorescence spectra is divided in two parts: before and after attenuation. Before attenuation, early fluorescence emissions are observed for pine wood pyrolysis, in both, reactor level - 266 nm excitation wavelength - and particle level - 355 nm excitation wavelength - experiments, exhibiting behaviors distinctive of aldehydic groups. However, these emissions are not observed in the case of beech wood. Hence, their presence may be attributed to the release of extractives present in pine, or even due to the different composition in hemicellulose between both species. This is also consistent with the low temperature at which they are observed, below 200 °C in the reference position.

After this early fluorescence emission, a blue-shifting of the fluorescence peak is observed in the case of pine wood, towards characteristic wavelengths of monoaromatics - guaiacol - and small PAHs - naphthalene and phenanthrene -. This behavior shows that PAHs of 2- and 3-rings are already released during primary pyrolysis. After attenuation, it is observed that process conditions affect tar composition. Higher retention times lead to a slight red-shift in the fluorescence intensity peak and also to an increase in intensity at wavelengths characteristic of 3- and 4-ring aromatic species. This could suggest an enhancement of secondary reactions with higher retention times.

Tar qualitative characterization during this second stage of the pyrolysis process is further studied by fitting all the fluorescence spectra with the selected representative species for 1-, 2-, 3- and 4-ring aromatic compounds. It is observed that the main components are 2-ring aromatic compounds, which is in good agreement with results from literature. It is also observed that an increase in phenanthrene relative composition occurs after major volatiles release, being coincident also with the major CH_4 emission. This could also be a proof of the presence of heterogeneous secondary reactions. At

the end of the process, a decrease in phenanthrene and an increase in pyrene relative composition is observed. In this second stage of the pyrolysis process no influence of the raw material is observed.

Chapter 6

Primary and secondary pyrolysis mechanisms

In this chapter, the experimental setup presented in Chapter 4 and applied in Chapter 5, with on-line characterization of permanent gases and targeted tar compounds, is used to get a deeper understanding of the pyrolysis mechanism of lignocellulosic materials. Experiments are performed for wood and its two main macromolecular components, holocellulose and lignin, to try to explain the behavior of biomass, based on the behavior of its main components [72], in conditions similar to the ones encountered in industrial applications. The experimental conditions and raw materials properties are reported in Section 4.2.

The content of this chapter has been partially published in [56], included in the Publications list of the author, attached to this document.

6.1 Results and discussion

6.1.1 Holocellulose

In this Section, results of holocellulose pyrolysis are presented. As it has been explained in Section 4.2, holocellulose is referred to as the combination of hemicellulose and cellulose. Holocellulose h.a.c. stands for holocellulose with high ash content and l.a.c. holocellulose stands for low ash content cellulose.

In Fig. 6.1 the temporal evolution of temperatures, permanent gases, and TFI are shown for h.a.c. holocellulose (a) and b)) and l.a.c. holocellulose (c)and d)). It is observed that the main permanent gas species are CO and CO_2, resulting mainly from decarboxylation, decarbonylation and dehydratation reactions as reported in literature [94, 140]. A source of controversy is, though, the emission rates of these species at different temperatures during the pyrolysis process. Shen et al. [141] reported that CO is the main permanent gas species (% mass) in fast pyrolysis, performed in a

fluidized bed reactor. On the other hand, Xin et al. [140] reported higher CO_2 (% mass) production rates compared with CO for a slow pyrolysis process of cellulose in fixed-bed, with temperatures lower than 550 °C and masses around 1 g. In both works, with higher conversion temperatures, the CO yield increased while the CO_2 total yields kept almost constant. This increase in CO production is probably due to the presence of homogeneous secondary tar cracking reactions, which take place mostly at temperatures higher than 500 °C and produce CO as major product [136]. Yang et al. [94] reported a slightly higher weight percentage for CO_2 than CO in a fixed-bed experiment over a wide temperature range.

The release patterns obtained in the present study are similar to those reported by Yang et al. [94] from a qualitative point of view, that is to say, the peak production rate of CO is obtained at lower temperatures than the peaks of CO_2 and CH_4. The total mass yield of CO_2 is higher than the one for CO, in agreement also with Xin et al. [140]. Therefore, the present results supported by literature analysis, suggest that CO is a product of primary pyrolysis, since homogeneous secondary reactions of primary volatiles are not expected to happen at the temperatures reached in the current experiments, with maximum temperatures inside the solid bed around 400 °C at the moment of maximum CO release rate (Fig. 6.1, b)). CO_2 is also a product of primary pyrolysis, but its production may be enhanced as a product of heterogeneous secondary char-forming reactions. It is proposed in literature [64, 65, 75] that char is a secondary product of cellulose pyrolysis resulting from secondary reactions in vapor and solid phases. The residence time of the volatiles inside the matrix, more than the temperature or heating rate, is the determining factor for the char yield. In this char-forming reactions CO_2 and water are proposed as the main byproducts [64,65,75], together with the production of aromatic compounds [88].

In the present study a higher char yield (around 32 % mass, d.b.) is obtained for h.a.c. holocellulose than for l.a.c. holocellulose (around 20 % mass, d.b). CO_2 release rate follows the evolution of the TFI signal, as shown in Fig. 6.1 a) and c), with temperatures inside the solid bed between approximately 350 and 450 °C at the time of maximum release rate. These temperatures are higher than those for the CO peak emission rate, as well as for the usual cellulose peak decomposition.

In the case of TFI evolution for l.a.c. holocellulose (Fig. 6.1, c) and d)), it can be seen that there is a first peak between 30 and 60 min, which is not observed in the case of h.a.c. holocellulose. This peak is produced by an early decomposition of the feedstock at low temperatures, probably due to the presence of hemicellulose or some extractives and it will be discussed in more detail in Section 6.1.3.

Comparison of single spectra from both holocelluloses (Fig. 6.4, a) and c)) shows a very similar behavior for the spectra produced at 90 and 106 min, i.e., the fluorescence

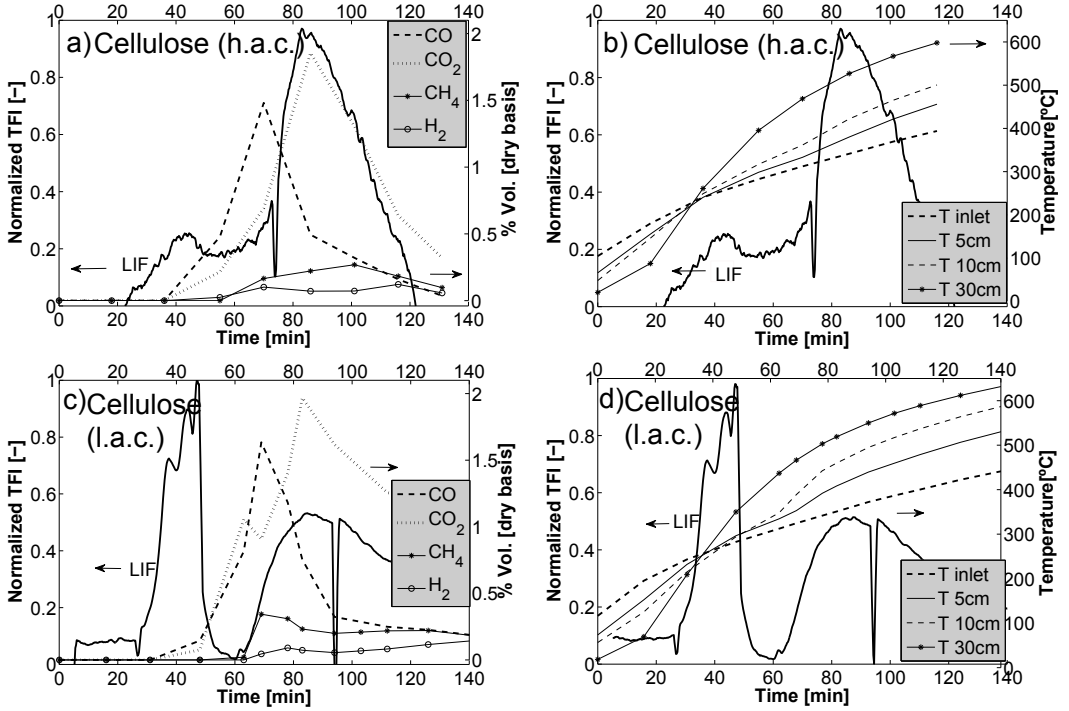

Figure 6.1: *TFI and permanent gases evolutions for h.a.c. holocellulose* **a)**, *l.a.c. holocellulose* **c)**. *TFI and temperature evolutions for h.a.c. holocellulose* **b)** *and l.a.c. holocellulose* **d)**.

spectra obtained at advanced pyrolysis stage and coincident with the second peak in the TFI evolution for the case of l.a.c. holocellulose. On the other side, early spectra for the case of l.a.c. holocellulose, represented in Fig. 6.4 c) (48 min), coincident with the maximum of the first TFI peak, show slightly different shape, which could be considered more similar to fluorescence signal from species containing carbonyl structures. The fitting of these spectra (90 and 106 min) to representative pure species (Fig. 6.4, b)) for h.a.c. holocellulose may indicate that 2-ring aromatic compounds (naphthalene) are present. Therefore, the release of CO_2 would follow the formation of aromatic compounds, probably due to secondary char-forming reactions. Besides this, fluorescence at longer wavelengths than those typical of 2-ring compounds is also observed. Which species cause the longer wavelengths fluorescence intensities may be a matter of controversy. According to Fig. 3.2, both phenanthrene and what is has been considered as species containing carbonyl groups emit fluorescence in the same region. Aromatic compounds with three or more aromatic rings are reported to be produced from cellulosic materials at low temperatures, but in very low concentrations and, at least, one order of magnitude lower than 2-ring aromatic compounds [88, 101, 142]. As several compounds containing carbonyl functional groups are produced from cellulose, including intermediates in charring reactions [88], this region of the spectrum at longer wavelengths is fitted to a considered representative spectrum of these compounds. These carbonyl species emit lower fluorescence intensity than naphthalene, but since their concentrations are higher [100], it is possible that similar fluorescence

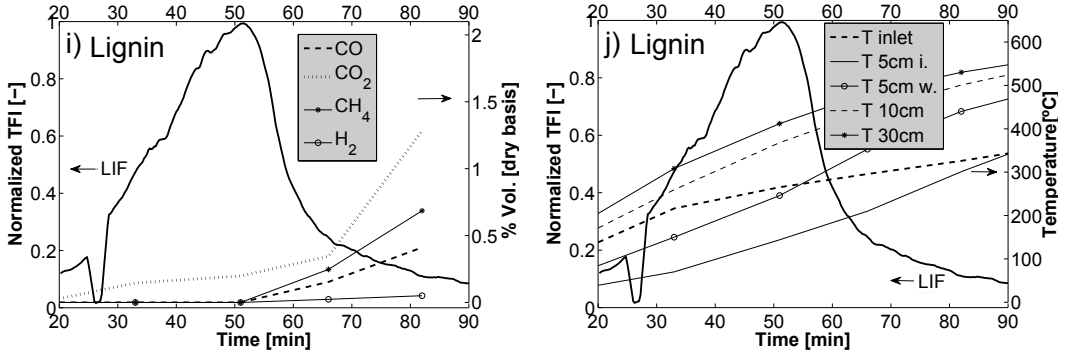

Figure 6.2: *TFI and permanent gases evolutions lignin* ***i)****. TFI and temperatures evolutions for lignin* ***j)****.*

intensities are observed. It is also observed that the fluorescence spectra obtained during the advanced pyrolysis stage (> 60 min) do not experience a significant qualitative evolution, that is to say, the fluorescence emissions take place always in the same wavelength range. It is then interpreted that the fluorescence observed during cellulose pyrolytic decomposition is due to the presence of species containing carbonyl groups, as well as 2-ring PAHs, produced in heterogeneous secondary char-forming reactions, and that these species do not evolve significantly at higher temperatures to bigger PAHs.

6.1.2 Lignin

Lignin decomposes slower over a much wider temperature range (150 to 750 °C) than cellulose or hemicellulose, as known from literature [72]. In the present study, the whole range of lignin decomposition is not considered, but just the temperature range where also the cellulose and main wood decompositions are observed. It is also the time range when fluorescence signal is observed. This is why the evolution of permanent gases shows the highest release rate at the end of the experiment, as opposite to cellulose and wood. The evolution of lignin pyrolysis products is also very complex due to the complexity of the initial matrix, leading to the formation of a wide range of products, from reactive intermediate to more stable aromatics [72].

Comparing the temporal evolution of the permanent gases (Fig. 6.2, i)) with results from literature for temperatures below 450 °C, similar patterns are observed [94, 140]. At low temperatures CO_2 is the main gas species followed by CH_4 and CO. The production of CO_2 may be related to the breaking of some more labile oxygen containing functional groups during the initial devolatilization of lignin. According to Fig. 6.2, i), a significant fluorescence signal is observed simultaneously with the initial formation of CO_2. Aiming at analyzing the origin of this fluorescence, in Fig. 6.4 e) every single spectrum measured during the TFI peak (30 - 70 min) is fitted with the representative pure species (as done for holocellulose in Fig. 6.4, b)) for 1-, 2-, 3- and 4-ring aro-

matic compounds (guaiacol, naphthalene, phenanthrene and pyrene respectively), giving place to a qualitative temporal evolution of the representative fluorescence-emitting species. The fitting values are plotted together with the 95% confidence intervals for each species. The selection of these species is based on the expectation that phenolics and PAHs would contribute mostly to the fluorescence emissions in lignin pyrolytic decomposition, while the presence of species containing carbonyl groups would be much lower due to the initial structure of lignin.

Looking at the species qualitative evolution (Fig. 6.4 e)), it is observed at early pyrolysis stages (before the peak of the TFI evolution, with temperatures inside the bed below 300 °C - T inlet and T 5cm, Fig. 6.2, j) -) that the main species contributing to fluorescence are 1- and 2-ring aromatic compounds. According to literature, primary devolatilization of lignin gives place mainly to monomers with just one aromatic ring (phenolics) - e.g., for coniferyl alcohol [72] - or conglomerates of these monomers in polymers - pyrolytic lignin -, which would exhibit similar fluorescence as 1-ring aromatic compounds [111]. Hence, it is expected the presence of 1-ring aromatic compounds to be significantly higher than 2-ring aromatic compounds, despite the higher fluorescence intensity of 2-ring aromatic compounds (Fig. 6.4, e)). This higher fluorescence intensity observed for 2-ring aromatic compounds is due to the higher absorption cross section and quantum yield of these compounds in comparison to 1-ring aromatic compounds with 266 nm as excitation wavelength, leading to higher fluorescence intensity, as it has been explained in Section 3.3. 1-ring aromatic compounds without oxygen content (BTX) are also produced but in much lower quantities than phenolics [100] and, as these individual compounds, have a similar fluorescence intensity to phenolics, BTX are not considered in the discussion.

PAHs, on the other hand, will be the product of secondary reactions [4, 5]. This is in good agreement with the volatiles behavior observed at higher temperatures, when the emission of CH_4 and CO starts and the TFI evolution peak is reached, accompanied by a red-shift in the spectra towards wavelengths characteristic of 2-, 3- and 4- ring aromatic compounds, as shown in Fig. 6.2 i) and 6.4 d). Evans and Milne [72] reported that the only source of CH_4 that they observed (excluding homogeneous secondary reactions at higher temperatures) is the breaking of methoxy groups at later stages of the pyrolysis process. In the present work this delayed CH_4 emission is observed accompanied by the onset of 4-ring aromatic compounds emission, together with an increase in the release of 3-ring aromatic compounds, while 1-ring aromatic compounds (phenolics) decrease significantly. That could mean that parallel to these functional-groups breaking reactions also repolymerization may occur, promoted by the higher residence time of the volatiles in contact with the solid, resulting in 2-, 3- and 4-ring aromatic compounds.

The fact that phenanthrene fluorescence spectrum is similar to the one of species containing carbonyl groups, as discussed in the previous section 6.1.1, may lead to question the origin of lignin red-shifted fluorescence signal. Aiming at clarifying this issue, in Table 6.1 the maximum TFI is compared for the different cases. It is observed that for lignin the maximum intensity is higher than for cellulose, despite the fact that the concentration of compounds containing carbonyl functional groups is expected to be more significant in the case of cellulose, mainly due to its chemical composition. This could mean that the volatiles passing through the cell emit more fluorescence intensity in the case of lignin than for cellulose, leading to the conclusion that the origin of this fluorescence should be 3-ring aromatic compounds, with higher absorption cross section and quantum yield than carbonyl structures with an excitation wavelength of 266 nm.

6.1.3 Wood

In Fig. 6.3 e) the TFI and the evolution of the main permanent gases is plotted during pine wood pyrolysis. With respect to the TFI, a first peak between 20 and 65 min is observed (as in the case of holocellulose), followed by a damping of the signal between approximately 65 and 90 min, and a recovery of the fluorescence intensity and second peak between 90 and 140 min. This signal attenuation in the middle of the experiment has been already reported in Chapter 5 and in [55], and it is partially attributed to the high volatiles concentration in the measuring cell (many of these compounds can absorb the fluorescence light), since it was coincident with the major volatiles release (CO and CO_2 peak), i.e. with the peak of the primary pyrolysis devolatilization. The results from this study, done with 900 g of wood, and the previous study, shown in Chapter 5 and [55], done with 1500 g of wood, are very similar. The main gases are CO_2 and CO in both studies, being the weight yields for CO_2 higher than for CO, as also reported in the literature [120]. In the present study, however, a slightly delayed CO_2 emission is observed, partially coincident with the second TFI peak. This CO_2 delay was not observed before, and it may be due to different dynamics in the bigger bed. In the current experiments, as a lower initial mass of wood is employed with the same N_2 flow, lower concentrations of volatiles inside the bed, and consequently in the measuring cell, should be obtained. This leads, first, to a lower attenuation than in the previous study and, second, and earlier recovery of the fluorescence signal.

In Fig. 6.4 f) spectra at different stages of the wood pyrolysis process are shown. Initially a spectrum which could come from species containing carbonyl structures is observed (36 min). This spectrum is coincident with the first peak in the TFI of wood (Fig. 6.3 e)) and it is also observed during holocelulose pyrolysis, coincident with the first early peak in the TFI evolution (Fig. 6.3 c)). Then, at 51 min, the obtained spectrum is similar to the ones obtained for lignin with similar temperatures inside the

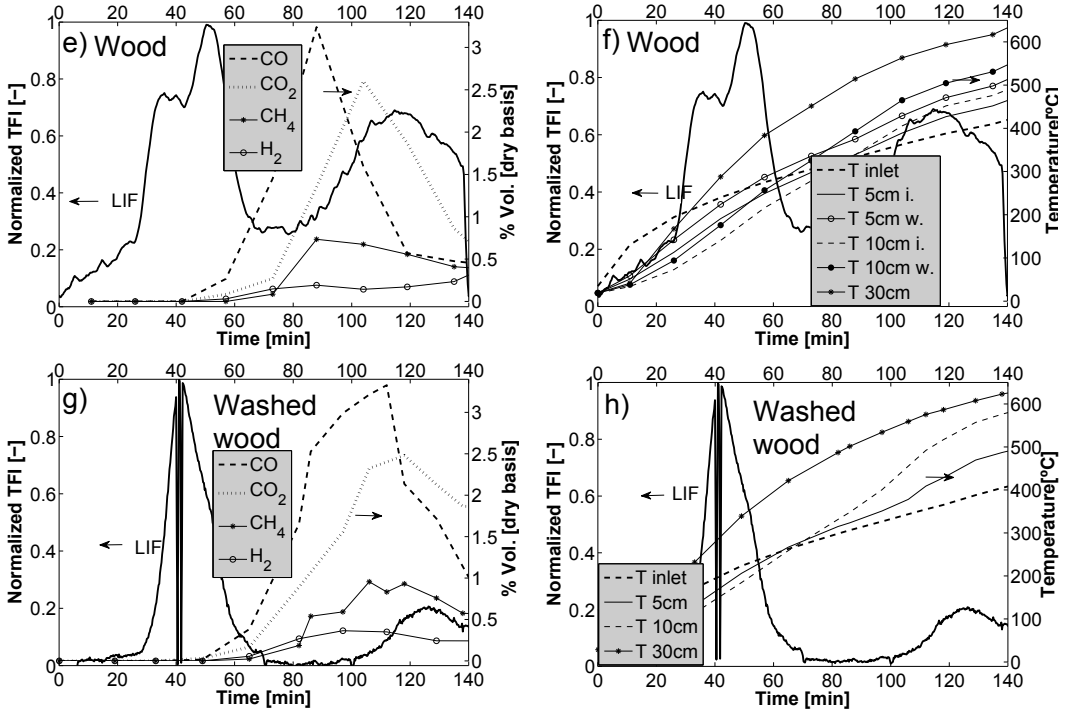

Figure 6.3: *TFI and permanent gases evolutions for wood* ***e)*** *and HCl+water washed wood* ***g)****. TFI and temperatures evolutions for wood* ***f)*** *and HCl+water washed wood* ***h)****.*

bed (53 min for lignin). This signal, obtained before the TFI attenuation, should come from the products of early lignin decomposition, including phenolics and small PAHs. After the fluorescence intensity attenuation, spectra similar to the ones observed at later stages of lignin decomposition are observed. That is to say, there is a red shifting of the signal due to the production of bigger PAHs, with more rings, at higher times and temperatures.

The origin of the early fluorescence signal during wood and holocellulose pyrolysis (Fig. 6.3, c) and e)) may be due to both an early hemicellulose decomposition or emission of extractives as previously said. In order to further investigate this, the same experiment has been performed with wood, previously washed with HCl (500 ml of HCl 37% vol. in 10 l of distilled water for 24 hours) and distilled water (for 24 hours). The results of this experiment are shown in Fig.6.3 g) and h). As it can be seen, after the washing, the first TFI peak persists while the second one is reduced. These results show two facts. Firstly, the first fluorescence peak, with spectra that could belong to species containing carbonyl groups, is not produced by extractives susceptible of being dissolved in water or acid, since the peak does not disappear after the washing. On the other hand, this washing reduces the TFI correspondent to the formation of PAHs, i.e., the second peak. This can be explained by the reduction in ash content (< 0.05 % mass d.b.) in the wood after the pretreatment. Besides this, in previous experiments presented in Chapter 5 and [55], performed with beech wood (hardwood), this early peak with potential carbonyl structure was not observed. We can conclude that the

		Holocel. (h.a.c.)	Holocel. (l.a.c.)	Lig.	Wood
Char(%,d.b.)		33.38	21.76	50.36	23.37
TFI peak	Early peak	-	$8*10^5$	-	$8*10^5$
(a.u.)	Main peak	$2*10^5$	2-3$*10^5$	$9*10^5$	$4*10^5$

Table 6.1: *Char yields and maximum fluorescence intensities for holocellulose, lignin and wood.*

early fluorescence signal arises from pine and washed pine (softwood) and in some cases from holocellulose but not from beech (hardwood) [55]. This indicates that this signal may come from a specific type of hemicellulose, although lipophilic extractives can not be disregarded. With respect to the second peak in the TFI evolution, we can conclude that acid washing decreases the alkali content in wood, which catalyzes the formation of PAHs, reducing therefore the formation of these species and consequently the fluorescence intensity.

Biomass pyrolysis can be considered as the sum of its macrocomponents pyrolytic behaviors, as suggested in literature, although there are some interactions among them [72]. In this case, the evolution of the fluorescence intensity from wood is mainly dominated by the fluorescence from lignin (except at the very beginning), as could be expected due to the higher fluorescence intensities for lignin than for cellulose (Table 6.1), i.e., aromatic compounds of one to four rings dominate the spectrum during conversion. However, the fluorescence intensity obtained from wood is lower than the one for lignin (Table 6.1), probably due to the higher concentration of volatiles species that can absorb the laser light and the fluorescence emission in the case of wood. Another possible explanation could be the lower quantity of lignin (as a macromolecule of wood) in the experiments with wood (900 g of wood) than in the case of pure lignin (500 g). In comparison to holocellulose, the intensity obtained for wood is higher, despite the attenuation of the signal, although a small contribution from hollocellulose is also present.

6.2 Off-line validation with GC-MS

In this Section, GC-MS analysis of the condensed volatiles (as explained in Section 4.1.2) are presented as a means to support the fluorescence results previously shown, i.e., detect the presence of PAHs in the condensed phase. In Fig. 6.5, the results from the analysis of condensable volatiles produced during pine wood pyrolyis are shown, for both toluol and isopropanol phases. As it can be seen, among many other species, naphthalene (the presence of this species could be enhanced due to potential contamination of the system during calibration of the LIF system), phenanthrene or anthracene, methyl-naphthalene and fluorene are present. Besides, other species with

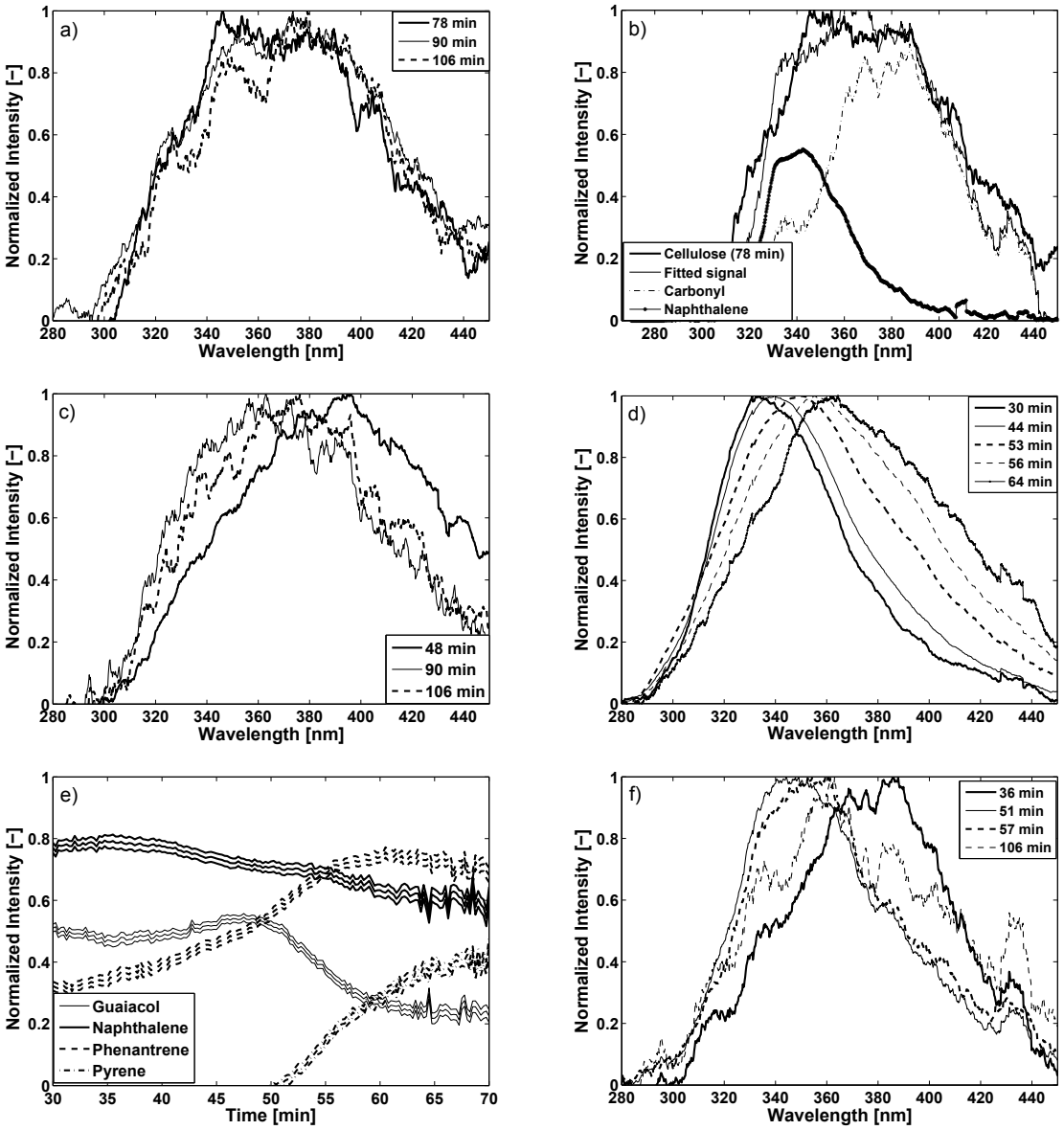

Figure 6.4: ***a)****: H.a.c. holocellulose fluorescence spectra at beginning (78 min), peak (90 min) and attenuation (106 min) of the TFI curve.* ***b)****: Fitting of the fluorescence spectrum at 78 min as a mixture of naphthalene (2-ring aromatic compounds) and a spectrum probably coming from species containing carbonyl groups.* ***c)****: L.a.c. holocellulose fluorescence spectra during the first TFI peak (38 min), and during the second peak (90 min, 106 min) of the TFI curve.* ***d)****: Spectra evolution for lignin at several pyrolysis stages.* ***e)****: Qualitative evolution of the representative pure species (guaiacol, naphthalene, phenanthrene and pyrene) with confidence intervals (95% confidence interval) for lignin obtained by fitting every single spectra (30 - 70 min).* ***f)****: Spectra evolution for wood.*

3-ring aromatic compounds have been detected, which could give place to fluorescence at higher wavelengths.

In Fig. 6.6, the results for heptane washed wood pyrolyis are shown. As it can be seen, in this case naphthalene and phenanthrene/anthracene are also present, but in lower concentrations in comparison with to wood pyrolysis (qualitative comparison with respect to other species). This confirms the results observed with LIF spectroscopy.

In Fig. 6.7, the condensable volatiles composition for holocellulose experiments with low ash content is shown. It can be observed that naphthalene and methyl-naphthalene are present, however bigger PAHs are not detected. This is in good agreement with the conclusions reached based on the LIF results.

6.3 Conclusions

The conclusions are summarized in Fig. 6.8, where the primary and secondary reactions of the pyrolysis process of the three different materials, and the identification of possible fluorescence sources, are schematically represented. Dashed lines correspond to fluorescence from holocellulose, solid lines to fluorescence from lignin and dotted lines to fluorescence from hemicellulose or extractives.

During holocellulose primary decomposition a small quantity of char ($\downarrow$) is formed, together with permanent gases and other condensable volatile species. The main permanent gas is CO, being CO_2 and CH_4 also released. Some of the condensable volatiles species may then undergo heterogeneous secondary reactions to produce more char, secondary condensable volatiles species and more permanent gases. The main secondary permanent gas species would be CO_2, being CO, CH_4 or H_2 also produced. Fluorescence comes from species belonging to the group of secondary condensable volatiles. According to the spectra analysis, they include 2-ring aromatic compounds (PAH), as naphthalene, and compounds with species containing carbonyl groups. Regarding lignin decomposition, compounds emitting fluorescence are already produced in the zone dominated by the primary devolatilization. These are mainly 1-ring aromatic compounds (phenolics) which appear together with 2-ring aromatic compounds (PAHs). In this zone CO_2 is also formed. At higher temperatures, heterogeneous secondary reactions become significant, being coincident with the onset in the emission of CH_4, CO and H_2 and giving place to a shifting in the fluorescence spectra to longer wavelengths, due to the formation of PAHs with three and four rings. For pine wood, a fluorescence signal is already observed at very early stages of the pyrolysis process and it is attributed to species with carbonyl structures present in extractives or hemicellulose. This signal appears also occasionally in holocellulose. Wood pretreatment

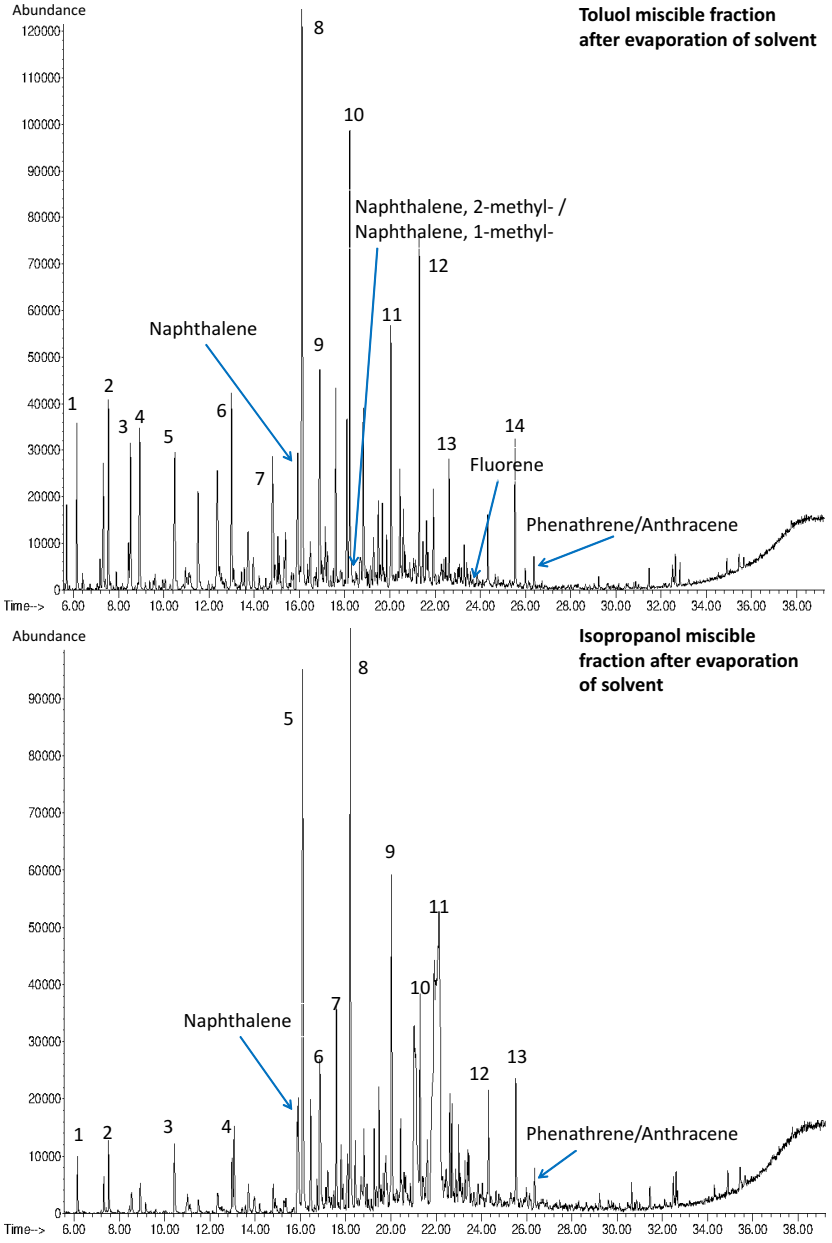

Figure 6.5: *GC-MS analysis of the toluol (top) and isopropanol (bottom) phases for wood pyrolysis experiments.*

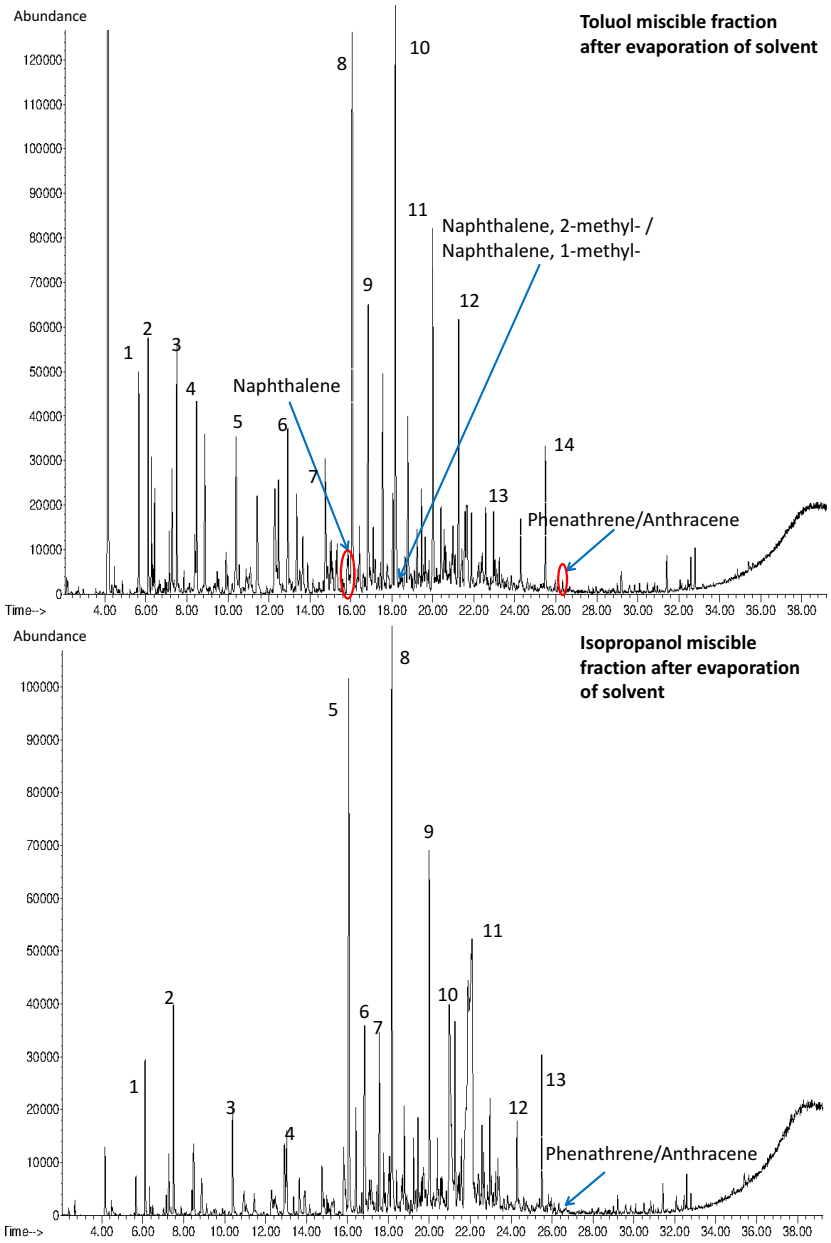

Figure 6.6: *GC-MS analysis of the toluol (top) and isopropanol (bottom) phases for heptane-washed wood pyrolysis experiments.*

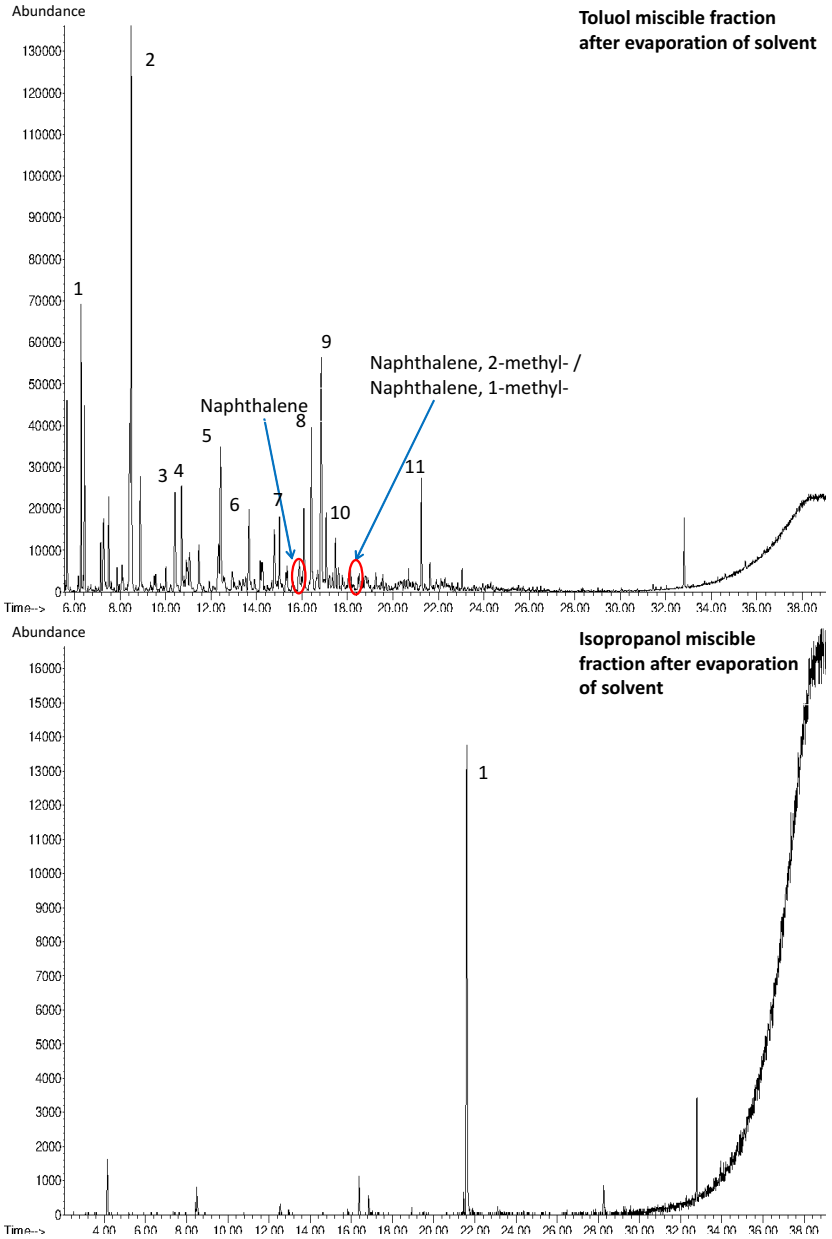

Figure 6.7: *GC-MS analysis of the toluol (top) and isopropanol (bottom) phases for holocellulose with low ash content pyrolysis experiments.*

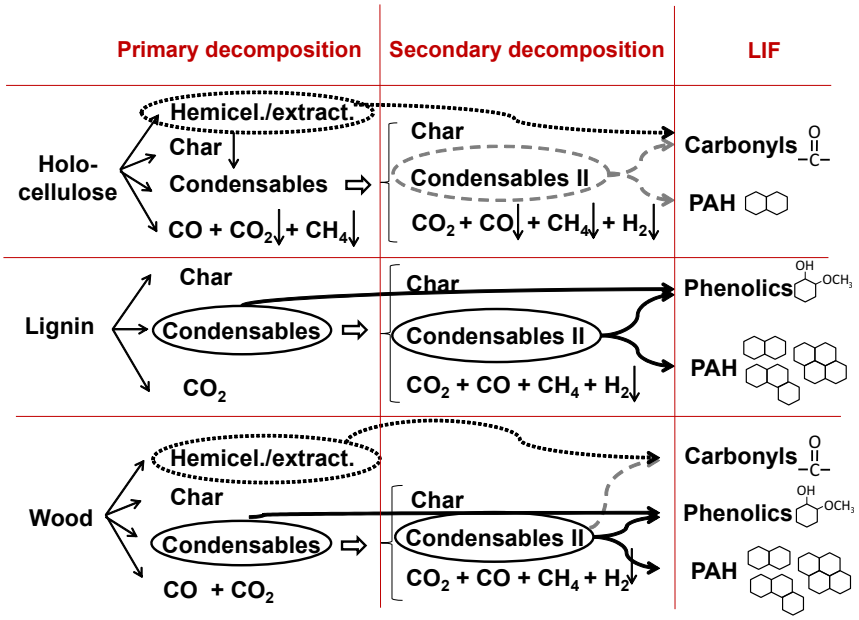

Figure 6.8: *Graphical conclusions. Possible reactions and source of compounds emitting fluorescence. Holocellulose (dashed lines), lignin (solid lines) and hemicellulose/extractives (dotted lines).*

with HCl and distilled water has shown that this signal does not come from extractives susceptible of solving in these two compounds. Future work is needed to precisely identify the source of this signal. Besides this, acid washing removes partially the alkali content in wood, reducing then the formation of PAHs, due to the catalyzing effect of the alkalis in these reactions. During most of the experiment the fluorescence signal is dominated by the fluorescence of species of lignin origin, i.e., aromatic compounds of one (phenolics) and several (PAH) rings. The fluorescence at lower temperatures is dominated by primary aromatic products of lignin (phenolics) and small PAHs. At higher temperatures the proportion of PAH species, obtained from secondary reactions, increases and PAH species with more rings are produced, as for pure lignin. A small contribution from holocellulose is also present.

Chapter 7

Biochar

7.1 Introduction

According to the definition given by Lehmann et al. [143], biochar is a carbon-rich product produced by thermal decomposition of biomass (organic material such as agricultural, forestry and animal residues), at moderate temperatures (< 700 °C), in a closed container and with little or no air/O_2 availability. This process definition matches also the definition of pyrolysis for charcoal production, however, the difference between biochar and charcoal is that biochar is produced not as a solid fuel but "to be applied to soil, with the objective of improving soil fertility, carbon (C) storage and filtration of percolating soil water" [143].

As it has been pointed out in Section 1, the up-scaling of bioenergy systems requires, among others, a sustainable and efficient land management in order to be considered a renewable energy source, to protect biodiversity, as well as water and soil quality. Besides, GHG emissions reduction in comparison with the use of fossil fuels has to be ensured. As an example and according to a recent study published by Schulze et al. [144], if 20% of current global primary energy supply was to be produced by forest biomass, 60% of the global increment in woody biomass would be necessary just for bioenergy production, leading to a reduction of biomass CO_2 pools, depletion of soil fertility and therefore increase in the need of fertilization, provoking increase of GHG emissions among other. This would also increase the price of wood for other industrial applications, leading to an over exploitation of the biomass, including relatively nutrient-rich biomass residues (slash) and root stocks. As a result, further depletion of soil nutrients and cations stock as well as organic matter would be induced. The same situation would happen if all the agricultural residues were used for bioenergy purposes [144]. While the nutrients can be further supplied by fertilizers, despite their negative effect on emissions, maintenance or improvement of soil fertility, structural stability or water holding capacity requires recirculation of organic matter to the soil [145]. It is in this

case where biochar application to the soil would constitute a possible contribution to the global solution that bioenergy production shortcomings require.

However, before any systematic application of biochar in the European Union should be considered, several aspects need to be clarified, including definition of quality standards, soil performance and complete assessment of long-term risks, especially for human health and soil biodiversity [146]. Once these knowledge gaps are fulfilled, a clear and solid legislative framework needs to be developed to regulate biochar use, respecting also intra-international laws and regulations. This is not an easy task due to the fact that biochar is a technology with implications in various EU policy areas, including environment protection, waste management, agricultural policy, climate change policy, development aid, research policy, industry and energy [146].

Therefore, a first step towards its application is to define what biochar is (including the final product, the conversion process and the used starting material) and to fully understand the interaction of biochar with soil. This could be encompassed in three main lines. Firstly it is necessary to identify which biochar properties have the potential capacity of improving soil quality and to understand which is the mechanism behind. For example, the increase of soil fertility could be related to an increase in nutrients availability due to an enhancement of the cation exchange capacity (CEC) of soil - associated to the high CEC of biochar - [147], liming effect - related to the higher pH of biochar in comparison with soil in acidic soils - [147], increase in soil organic carbon or improvement of structural stability, water holding capacity or aeration - related to biochar porosity - [148]. Secondly, it is necessary to assess the potential of biochar to include toxics which may contaminate not only the soil but also the underground water and under which conditions the biochar can release those contaminants [147]. In the same way, biochar may also have the capacity of removing soil contaminants. In this aspect biochar needs to fulfill the environment, soil and water protection regulations at local and international level. Thirdly, it is necessary to know the stability of biochar once applied to soil, that is to say, how many years would it take to release all the carbon stored if it is going to be used as carbon sink [149].

The next step would be to co-relate the desired biochar properties, according to its expected function in soil (nutrients carrier, carbon sequestration, soil amendment, etc.), with the production conditions and feedstock to be used. The production process has to ensure also environmental sustainability and economic viability [41]. Finally, instructions about biochar application, i.e., which kind of biochar needs to be applied where and how are necessary [150]. Once this is achieved, biochar certification should be possible and, consequently, the development of a regulation framework for biochar application.

Great efforts have been already done to address the aforementioned issues. A good example is the development of two voluntary initiatives: the International Biochar

Initiative (IBI) [151] and the European Biochar Certificate (EBC) [41], whose objective is to develop industrial standards through the establishment of parameters to define biochar quality and production criteria, as well as the required analytical methods (unified methodology) to address them. In fact, Switzerland became in 2013 the first country in Europe where certified biochar use in agriculture was oficially approved, being this approval supported on strict quality and sustainability regulations developed based on the European Biochar Certificate [49]. The same happened afterward for Austria, also under the certification of the European Biochar Certificate [152].

However the situation in other European countries is different since the use of biochar for soil amendment purposes is not forbidden, but as previously said, a regulation for its sustainable application does not exist either and the aforementioned aspects have to be further addressed. Therefore, it is the task of the scientific community to provide a clear definition of what biochar is, as well as quality parameters regarding production, properties and performance, in order to help the decision makers to establish exact rules for assessment of biochar reliability and usability [150]. That is why in the last years several research projects have been sponsored by the European Union on the topic. Some examples are:

- Interreg IVB North Sea Region "Biochar: climate saving soils" [153], with the main objectives of establishing transnational strategy for biochar production and application and communicating with and educating people about biochar, including authorities, producers and end-users.
- EuroChar, focused on the development of technologies for long-term carbon sequestration.
- Refertil and Fertiplus [154, 155], centered in recycling organic waste as compost and biochar for fertilizing purposes, so that the use of mineral fertilizers and chemicals can be reduced in agriculture. While Refertil deals with the development of technologies at industrial scale for safe and economic nutrient recovery processes, as well as with the revision of the Fertilizer Regulation for inclusion of biochar as organic fertilizer and soil additive; Fertiplus deals with the development of new technologies for conversion of urban and farm organic waste into biochar.

Besides the research institutions involved in these projects, many other scientific groups from different fields (agronomy, soil science, thermochemical and biochemical conversion of biomass, etc.) work nowadays on biochar production, characterization and application. This leads to the problem that current biochar investigation in Europe is very fragmented and unnecessarily repeated [9]. Together with this, and due to the

lack of specific norms and analytical procedures for biochar characterization when it stepped into the scientific community, many analytical techniques and methods (developed initially for soil, biomass, coal, etc.) coexist with the same final characterization purposes, leading to a very high degree of difficulty or even impossibility to compare results, reducing therefore the chances of gaining further knowledge.

To try to solve these drawbacks, a networking project started in 2012, the EU COST Action TD1107 'Biochar as option for sustainable resource management', funded by COST (intergovernmental framework for European Cooperation in Science and Technology) [9]. The ultimate goal of this project is to bring together researchers, stakeholders and potential users of biochar from EU and candidate countries, so that meaningful advances in understanding and optimizing biochar production and performance can be achieved and directly implemented, in order to move towards a regulated environment for efficient and beneficial biochar application [9].

The core of this Cost Action is divided in four groups, as it is shown in Figure 7.1, which address the aforementioned critical issued regarding biochar use. During the realization of the present work, the author collaborated with the first working group, focused on the relationship between biochar production parameters, material properties and generalization of effects after soil application [9]. In particular, the contribution of the author was located in the area of Method Standardization 7.1, consisting in the participation in a Ring Trial, where three unknown biochars had to be characterized following the methods usually applied in each lab. The objective was to identify the different analytical methodologies applied for biochar characterization, as well as the possible sources of results disagreement among labs in order to be able to develop standard analytical methods for biochar characterization. The knowledge gained during this project, in particular for biochar production (best practice), biochar characterization (developed and standardized methodology) and biochar perfomance would be used as groundwork for further development of the European Biochar Certificate.

7.2 Biochar origin and production

The application of charred or partially charred organic matter to soil for amendment purposes has been done for hundreds or even thousands of years. According to a review on the origin of biochar management and research done by Lehmann and Joseph [143], benefits of charcoal application on increasing and quickening vegetation (Trimble in 1851 [156]), absorbing and retaining water, gases and solutions in the soil (Morley in 1927 and 1929 [157,158]) and improving soil chemistry (Tyron in 1948 [159]) have been already investigated and reported during the last two centuries. However, the scientific attention developed in the last years on biochar has greatly surpassed these earlier

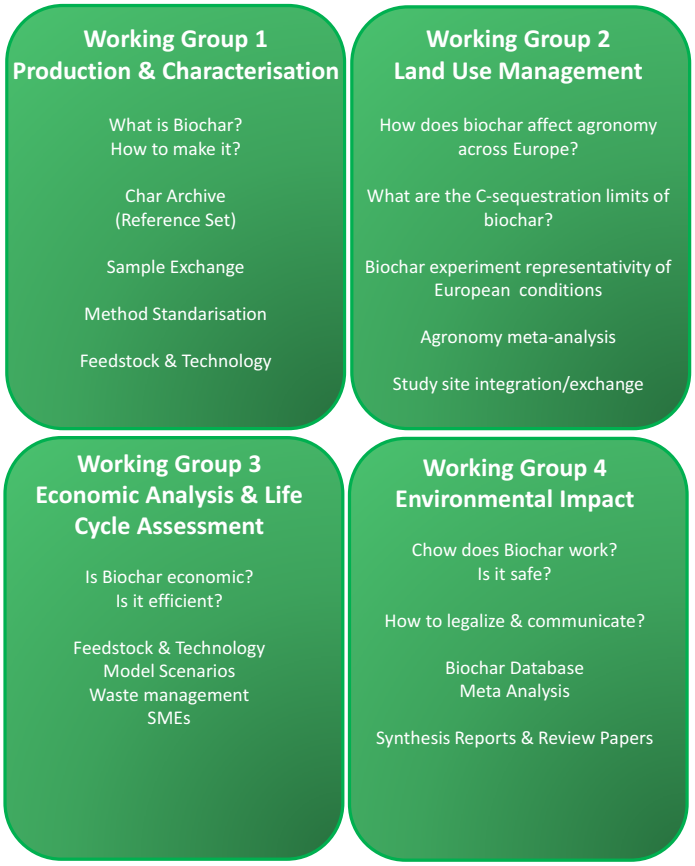

Figure 7.1: *Structure of the Cost Action [9].*

activities. The origin of the current interest lies on the finding that the higher levels of soil organic matter content and sustained fertility (higher water-holding capacity, nutrient-holding capacity, pH and nutrients content, such as N, P, Ca, K) in Amazonian Dark Earths (known as Terra Preta do Indio), in comparison to surrounding soils, is due to the application (intentionally or unintentionally) of charred organic matter and other organic and inorganic matter to the soil [160]. This could show the development of man-made soils from surrounding poor soils, i.e., the potential existence of soil management practices based on application of charred organic matter in ancient Amerindian civilizations [143]. At the same time, the high radiocarbon age (more than 2000 years in some cases) reported for this black carbon supports the affirmation of its high stability in soil [160]. Both phenomena combined with the current needs of reducing greenhouse gas emissions (carbon sequestration) and developing sustainable soil management, including quality and productivity, explain the great interest that biochar application raises nowadays.

It is in this context when the term biochar began to be used [161], to differentiate the use of charred organic matter for soil amendment from charcoal, i.e, the use of charred organic matter as solid fuel, for metallurgic purposes, for chemicals production, etc. However, this early definition did not include the application of biochar for mitigation of greenhouse emissions (carbon sequestration), as addressed in Section 7.1, included for example later on in [143].

Despite this differentiation in terminology, the production technology has been traditionally the same for both purposes, that is to say, carbonization with a low presence of oxygen so that partial combustion would take place to provide the necessary heat in order to sustain the globally endothermic process of pyrolysis. In the early ages, this conversion process was performed in kilns such as pit or mound kilns. With time, these kilns evolved to concrete, brick or metal kilns where a better control of the process (air supply and therefore temperature) was possible so that higher process efficiency with better product quality would be achieved [162]. These processes are though not appropriate nowadays due to the high pollution and low efficiency that characterize them, since all the vapors would be emitted to the environment without further utilization or post-processing. As it has been commented in Section 7.1, biochar production needs to be environmentally and economically sustainable. This implies (a) sustainable biomass use (fast growing plants, plant residues from certified forestry management, agricultural residues and organic wastes from urban areas [150]), (b) clean and efficient conversion technology, i.e., a technology which is able to deal with the high heterogeneity of biomass materials included in the previous definition (including high ash and moisture content), providing a high conversion efficiency and fulfilling the emissions regulations and (c) the whole process has to ensure a zero or negative C emission and be economically viable. This is why recently the European Biochar Certificate introduced a new

definition of biochar "biochar is a heterogeneous substance rich in aromatic carbon and minerals. It is produced by pyrolysis of sustainably obtained biomass under controlled conditions with clean technology and it is used for any purpose that does not involve its rapid mineralization to CO_2 and preserves its capacity to become eventually a soil amendment" [41]. This definition includes other applications of biochar besides soil amendment and carbon sequestration, i.e., considers biochar as a basic material for synthesis of new products for the bio-based economy [150] and specifically establish pyrolysis as the technology for biochar production.

However, besides conventional pyrolysis, there are other conversion technologies available which are being investigated for biochar production. These technologies offer some advances for the processing of some biomass types in comparison with conventional pyrolysis and are listed below.

- **Flash carbonization**: this is a process developed at the University of Hawaii under the leadership of Prof. Antal. In this process air is used to pressurize the vessel where the packed bed of biomass is placed, with typical pressures of 1-2 MPa. A flash fire is ignited from the bottom of the packed bed and air is supplied to the top. Typical reaction times are around 30 min with maximum temperatures of 600 °C [163]. According to the description of the process is a type of pressurized oxidative pyrolysis. It allows higher fixed-carbon yields, increasing therefore the efficiency conversion and C sequestration in the solid product.
- **Gasification**: the objective of this process is the production of a gas product. However, there is always a solid residue which can be considered also for biochar applications.
- **Fast pyrolysis**: as for gasification, the objective of this process is the production of a liquid bio-fuel, but the solid bio-product can be used for biochar application.
- **Hydrothermal carbonization**: this process is carried out in the presence of subcritical, liquid water and it can be also called hydrous pyrolysis. Typically the process temperature is kept below 250 °C and pressures can go up to 20 bar. The advantage of this process is that it can process wet biomass with relatively high solid yields without the need of drying before the converion process [164]. The solid product of this process is also often called hydrochar, which will be the name used in this document from now on.

7.3 Physical and chemical properties

As it has been explained in Section 7.1 one of the key issues for biochar development is to understand the relations between biochar properties, its performance in soil and

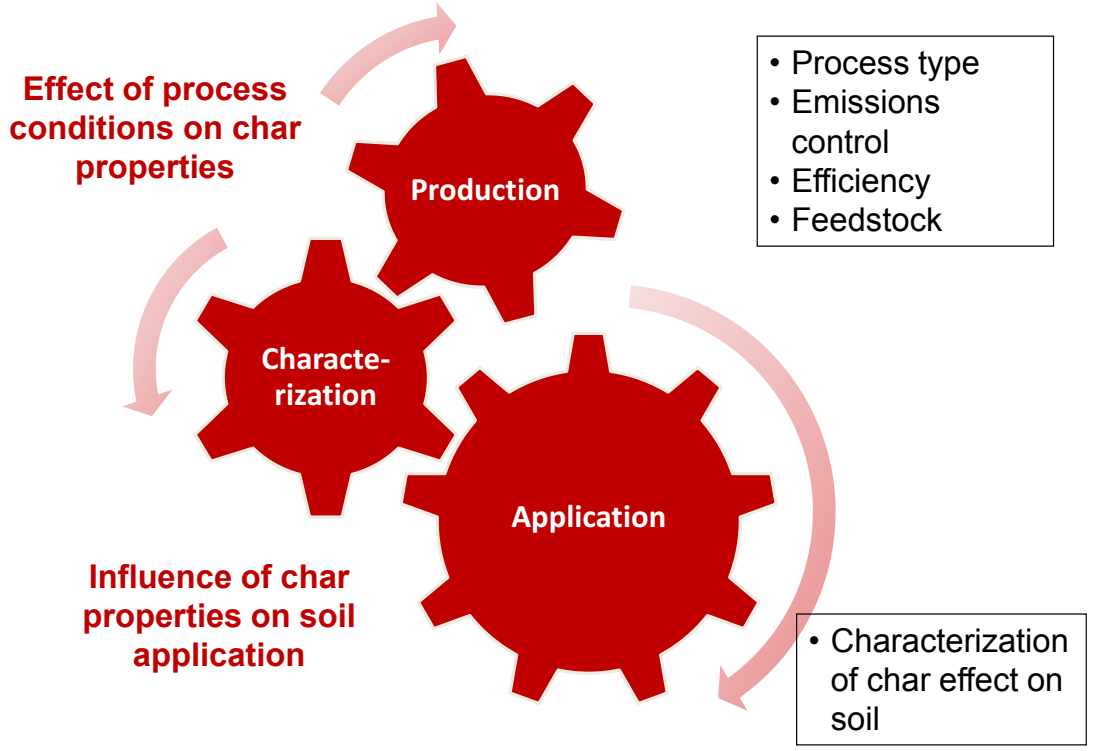

Figure 7.2: *Scheme summarizing the objectives of this work with respect to biochar characterization.*

its production conditions, including initial feedstock. The objective of this work is to contribute to this understanding by characterizing several physical and chemical properties of biochar produced with slow pyrolysis at different conditions. This is shown in Figure 7.2.

The first step is to identify which are the potential functions of biochar in soil and determine the necessary biochar properties that need to be characterized in order to address them. Therefore, in the following sections, a short review on biochar potential impacts on soil and properties determining them, as well as dynamics of these properties with biochar production conditions is presented.

7.3.1 Biochar physical properties: structure evolution

Regarding improvement of physical soil properties, the application of biochar may contribute to a change in "the bulk surface area, pore size distribution (PSD), density and packing" and therefore, potentially influence "soil response to water, aggregation, workability during soil preparation, swelling-shrinking dynamics and permeability", as highlighted by Downie et al. in [148]. Besides, biochar physical properties may also

influence other chemical, biological and nutrient functions in soil. For example, with higher specific surface area, the availability of sites for cation retention and exchange may be higher, enhancing therefore the cation exchange capacity (CEC) and reducing the possibility of leaching [147, 148]. This topic will be further addressed in Section 7.3.2.

The physical and structural properties of biochar are highly dependent on the initial feedstock and the process conditions since the structure of starting material tend to remain in the final solid product, but reducing its contribution with increasing severity in the conversion process [165]. In this way, the natural honeycomb-like macroporosity (typical of the biological capillary structure) of the biomass raw material allows the release of volatiles when low heating rates are employed, and therefore big morphological changes do not take place [165, 166]. As the conversion process evolves (increase in charring degree), the initial biomass macromolecular structure (amorphous hemicellulose, crystalline cellulose and amorphous lignin [10]) evolves firstly to an amorphous char which can give place, at higher temperatures, to the formation and evolution (in size and order degree) of turbostratic crystallites, together with a significant evolution of the porous structure, as it is reported by Keiluweit et al. in [10] and shown in Figure 7.3, also taken from [10]. These turbostratic crystallites consist of flat sheets of highly conjugated aromatic structures (graphite-like) of higher density than amorphous char and cross-linked in a random manner [148]. It must be noted at this point that despite many authors in literature refer to these crystallites as turbostratic, experts in the carbon materials field assess that this term is not correctly used here due to the fact that it is thought these layers to be randomly orientated relative to each other and not in a parallel disposition with a specific sequence [167]. The interstices produced by the cross-linkage of these crystallites, together with voids in the hexagonal planes and the presence of heteroatoms in the sheets edges (forming O-containing functional groups which may prevent a closer rearrangement of the sheets) are the main sources for further development of char porosity, mainly microporosity [10, 148] during conversion process. At higher temperatures also pores which were blocked with condensed volatiles at lower temperatures, can become available due to further volatilization of these compounds.

When high heating rates are employed, melting of the cell structure leads to lower biochar structure complexity, accompanied by the development of mostly macropores [148, 165, 166]. The same could also happen with high ash content feedstock due to fusion, swelling or sintering phenomena [148].

Despite the fact that porosity and surface area increase with increasing maximum conversion temperature (HTT), due to the release of volatiles and the progressive development of crystalline structures at expenses of the amorphous C matrix (Fig. 7.3, [10]), it has been also widely reported in literature that this ascendent trend has a top in tem-

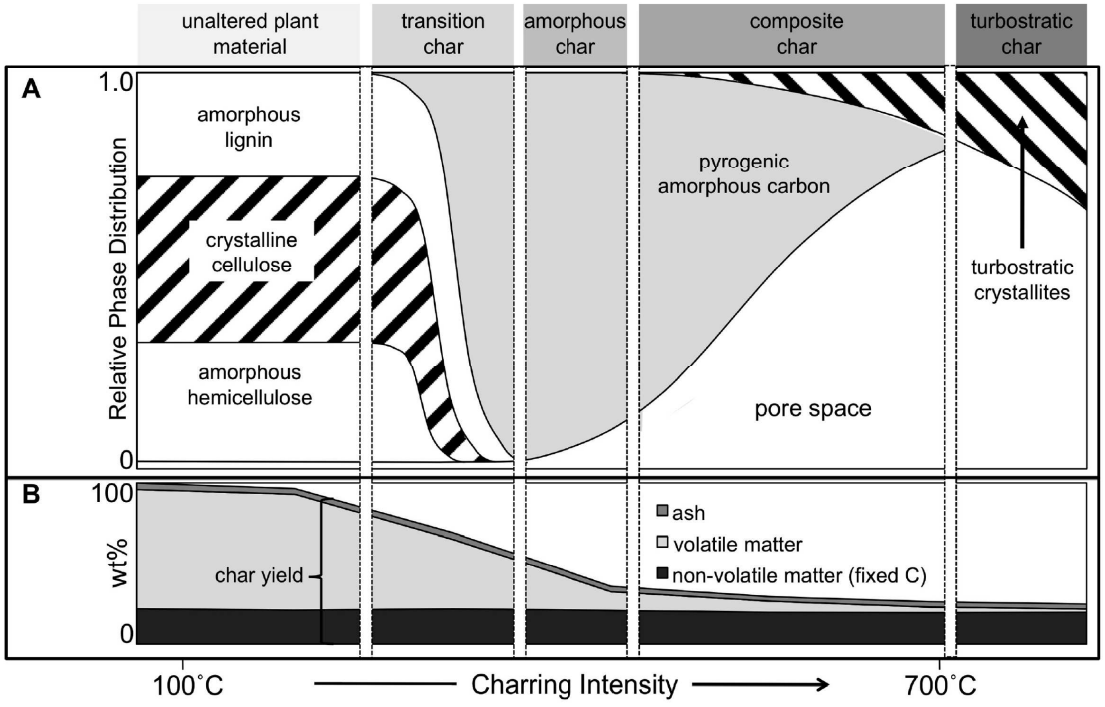

Figure 7.3: *Structure evolution of biomass-derived char with charring intensity. Figure taken from [10].*

perature, after which the surface area and porosity decrease [166, 168–170], parallel to an increase in solid density. This maximum in temperature ranges mostly between 600 °C and 900 °C, depending on the feedstock and conversion conditions. Several interpretations have been given in literature for this behavior. For example, Guo et al. [170] attribute this reduction in surface area to "sintering effect (after reaching post-softening and swelling temperatures) accompanied by shrinkage of the particle and realignment of the char structure provoking narrowing or closing of pores". Other authors support also the theory that pores shrinkage at high temperatures due to the fact that gradual thermal transformation of the carbon structure is taken place, as it is the case of Pulido-Novicio et al. [168] or Brown et al. [169], who talks about "microstructural rearrangement" at high temperatures. A different perspective has been given, on the other hand, by authors such as Guerrero et al. [166], who attribute this behavior not only to the previously mentioned increase in structural ordering but also to micropore coalescence. This phenomenon of pore fusion has been reported also by other authors, such as Zhang et al. [171], during physical activation of char with CO_2, i.e., further burn off of C to increase microporous surface area, assessing that when this treatment is too severe (for example too high retention time) micropores may collapse giving place to bigger pores. If this was the case for decreasing surface area at high temperatures, this would be accompanied by an increase in total pore volume (bigger pores), however several authors reported a decrease also in total porosity [168, 170] parallel to the decrease in surface area. The effect of pressure in char structure development must be also taken into account. Cetin et al. [165] investigated the effect of pressure (1, 5, 10 and 20 bars) at high heating rates (up to 500 °C/s) for pine (low ash content), eucalyptus (low ash content) and bagasse (high ash content), observing a slightly decrease in surface area with higher pressures, as well as the development of larger cavities with thinner walls and bigger particle size due to particle clusters formation because of the melting.

It is clear that a deep understanding of the porous structure development during thermochemical conversion is very difficult and depends strongly on the raw material composition and structure (for example, different proportions of hemicellulose, cellulose and lignin lead to different reactivities for pyrolysis process and therefore different degree of structure development with the process conditions; or higher ash content can contribute to structure melting and therefore development of bigger pores instead of micropores) and on the history of the conversion process (high heating rates lead to structure melting and development of mostly macropores, as well as high pressures do, while high final conversion temperatures may lead to higher ordering degree and therefore shrinkage or sealing of micropores or micropores collapse, which may not affect high heating rate produced biochars [169]). Besides, only one characterization method, such as for example N_2 adsorption (combined with BET model) is not enough to characterize the pore structure of such complex materials for two main reasons: on

one hand is not enough to address the "pore structure history" and secondly, it is necessary to know which type of pores are present in order to determine the possible function of this biochar in soil. For example, micropores are good for enhancing cation exchange capacity and therefore nutrients cycling and availability, mesopores are good for liquid adsorption, increasing the water holding capacity and macropores contribute to aeration, hydrology and can serve also as habitats for microorganisms [148].

Hence, in this work, a deeper characterization of the porous structure of several materials (low and high ash content) obtained with different process conditions will be performed, using N_2 adsorption combined with different mathematical methods to evaluate the pore size distribution.

7.3.2 Biochar chemical properties: biochar chemical composition and surface functional groups

Regarding biochar chemical properties, they can be encompassed in two main groups: biochar chemical composition and biochar surface functional groups.

Biochar chemical composition is of high significance because it gives information about the aromaticity and maturation degree of biochar and therefore its expected stability in soil [149, 172, 173]; the potential that this biochar may have to provide nutrients [147], as well as to contribute to soil contamination, depending upon its content in heavy metals [147].

In previous sections, definitions of biochar regarding production process as well as potential use and legal situation have been given. However, no further explanation about what biochar is or should be, from a chemical point of view, has been provided. This is difficult to assess due to the complexity and variety of conversion conditions as well as feedstock composition and post-processes that can be employed, leading to the fact that "biochar is not a single chemical entity and should be seen as a part of a black C continuum", as introduced by Spokas [172]. The defining property, which has already been partially introduced when describing physical structure evolution, is: "the organic portion of biochar has a high C content, which mainly comprises so called aromatic compounds characterized by rings of six C atoms linked together without oxygen (O) or hydrogen (H), the otherwise more abundant atoms in living organic matter", as defined by Lehmann and Joseph in [143]. The question here is which is the degree of aromaticity or maturation of this structure, i.e. to which extent these aromatic clusters (more stable) should evolve in number, size and order at expenses of the amorphous C (more labile compounds) in order to be considered biochar and not just partially charred organic matter. This is important because the degree of aromaticity could have a direct impact on the stability of char against decomposition in soil [174, 175]

and hence give information about the durability and capacity of this char to storage C in the soil. This issue is usually correlated to the biochar organic atomic ratios H/C and O/C, represented in the Van Krevelen diagrams [175, 176]. For example, it has been proposed by Knicker et al. [173] that H/C ratios can be used to deduce information about the chemical bonds in the solid matrix. In this way, while a H/C ratio of 1.3 could suggest that most C is directly bonded to a H or connected through an OH group; ratios between 0.4 and 0.6 may indicate that every second to third C is connected to a H [173]. To further correlate the changes in molecular structure with H/C and O/C ratios, combination with other analytical techniques is required. For example Baldock et al. [177] used solid-state ^{13}C nuclear magnetic resonance (NMR) spectroscopy and diffuse reflectance infrared Fourier transform spectroscopy (DRITF) to address the chemical changes in structure during heating up of Pinus resinosa wood from 150 to 350 °C in a muffle oven (not completely inert,i.e., some oxygen was present). They observed a decrease in H/C and O/C ratios when conversion temperature increased from 150 to 300 °C. However, up to 350 °C, the O/C ratio further decreased whilst the H/C increased, indicating a change in the pathway reaction for the mass loss. The main reaction pathway suggested to explain the loss in H and O was dehydration, accompanied, by loss of CO_2 and CO (decarboxylation [176]) at higher temperatures. Regarding the chemical structure, up to 150 °C the same signals were observed as for raw wood, i.e., O-alkyl and di-O-alkyl characteristic from cellulose, acetate and carboxyl groups from hemicellulose and methoxyl, aryl and O-aryl C associated to lignin. At 250 °C significant changes were already observed, becoming the contributions from aryl C and O-aryl C (furan-like structures coming from cellulose) dominant, while O-alkyl and di-O-alkyl C signals decreased. From the DRIFT results, at temperatures $>$ 200 °C decreases in the O-H and C-H groups intensities were observed, consistent with the dehydration reaction hypothesis and suggesting that a decrease in H/C ratio is indicative of the formation of structures containing unsaturated carbons, such as aromatic rings. With higher temperatures, up to 350 °C, progressive increase in aryl C was noted, as well as progressive loss of C=O bonds relative to C=C, consistent with the further decrease in O/C ratios. Similar studies were performed by other groups as it is the case of Knicker et al. [173], registering also the likely transformation of protonated aromatic C typical of lignins to condensed aromatic structures (dehydrogenation [176]) and relating H/C ratios to possible cluster sizes.

From this results, complemented also by what has been reported in [175] for other biomass such as grass, it can be concluded that biochars produced at temperatures higher than 350 °C, although presenting a dominant aromatic structure accompanied by low H/C ratios, still show characteristics of original plant material, such as O-alkyl C. Hence, their chemical composition would be still highly dependent on the production processes and initial composition of the feedstock. On the contrary, biochars produced

above 500 °C would be dominated by aryl C, with minor contributions of O-aryl C and small proportions of carbonyl, O-alkyl and alkyl C. This has to be taken into consideration regarding stability of biochar in soil, since these labile compounds, as well as small aromatic clusters are more prone to be oxidized by lignin degrading organisms [173].

Therefore, the next step would be to correlate the biochar chemical structure with the stability in soil. Of course, this stability would not depend only on the biochar itself, but also on the type of soil, microorganisms, water dynamics, climatology, erosion, soil use, mineral content, etc. [149]. Together with all these possible variables, and as it has been stated by Spokas in a recent review about biochar stability in soil [172], the lack of standards in stability research, i.e., the high variety of laboratory methods used to address this property, including analytical quantification, incubation conditions (need for accounting of biotic and abiotic degradation) or length of the study, difficult the attempts of unifying results on stability, ranging from decades to millennia and, hence, to develop an accurate predictor for biochar stability in soil environment [172].

Although production temperature has been often used as deterministic property for biochar stability [172, 177], high influence of parent material and process conditions on chemical structure for biochars obtained at temperatures lower than 500 - 600 °C [177] advices against it. On the contrary, O/C ratios account not only for the conversion degree of biochar (O/C decreases with increasing HTT [96, 175, 177] due to release of volatile matter) but it also takes into account post processing conditions (for example possible surface oxidation when cooled down with water or in absence of inert atmosphere), the effect of the storage time due to abiotic degradation, the presence of volatile and non-volatile fractions in the biochar and the number and composition of surface functional groups, which increase biochar reactivity [172]. This is consistent with the better relation between biochar stability in soil and O/C ratios than with other possible predictors as temperature and volatile matter content as reported in the studies evaluated by Spokas [172], suggesting besides that an O/C ratio smaller than 0.2 could account for a half-life of 1000 years.

Taking into account such results, Schimmelpfennig et al. proposed in 2012 [176] the use of H/C and O/C together with the black carbon (BC) concentrations as parameters to determine the desirable biochar properties for soil amendment, in order to ensure a good quality for environmental management. In particular, the values should be H/C < 0.6 and O/C < 0.4 and BC $> 15\%$ based on C. Also based on that, the European Biochar Cetificate (EBC) [41] defined that biochar should have a H/C ratio lower than 0.7 and a O/C lower than 0.4. Other than that, partially charred biomass should not be considered biochar due to lack of fulfillment of quality standards.

Regarding the direct nutrient value of biochar, determined by the biochar nutrients total content and their availability (nitrogen (N), phosphorus (P), potassium (K),...) [147],

it depends in the first place on the parent material, and secondly on the conversion conditions, since the release dynamics of each one of these elements, as well as their chemical form (influencing their availability) are dependent on these parameters, mainly temperature [147]. Despite of the total content of N, mineral N (ammonium-N and nitrate-N) tends to be very low, as reported in [147] for several biochars. In organic substrates (soil, compost, etc), the ratio C/N is often used as an indicator of their ability to mineralize and release inorganic N. A C/N ratio of 20 is used as a critical limit above which immobilization of N by microorganisms may occur, becoming not available for plants " [147]. However it is not clearly understood yet if that would be the case for biochars too. P availability is highly dependent on feedstock and process conditions. For example, as it has been reviewed by Chan and Xu in [147], P availability may vary in three orders of magnitude for different biochar types, presenting the highest availability those produced from poultry manure and the lowest those coming from plants. K availability is typically high [147].

With respect to biochar surface chemical structure, although its composition is included already in the chemical composition of biochar, its origin, structure, evolution and, above all, characterization of its behavior regarding biochar functions in soil is highly important and requires further understanding, i.e., potential contribution to total pH, capacity to retain and exchange cations or anions, electrical charge, hydrophobicity, etc. Besides, in this category are included the species adsorbed on the char surface and produced during thermochemical conversion, such as PAHs or dioxines, which have the potential to contaminate the soil.

Biochar contribution to nutrients enhanced availability in soil can be, not only due to direct nutrients supply, as previously introduced, but may be also attributed to a more efficient nutrients management, i.e., nutrients dynamics, due to increase in nutrients retention, while maintaining its availability for plants and therefore reducing its leaching [178]. This is specially evident when biochar is applied together with a fertilizer, as it has been reported by Chan et al. [179], with a substantial improvement of N fertilizer-use efficiency and hence a reduction also of soil and water contamination due to minerals leaching. Two could be the main possible mechanisms behind this behavior. On one hand, Chan et al. [179] attributed it mostly to improvement of soil physical properties, mainly water-holding capacity and reduction of soil strength, while Lehmann et al. [178] concluded that this enhancement in nutrients retention in an exchangeable plant-available form is related to "adsorption (electrostatic) to an exchange complex created by charcoal addition". This adsorption capacity is related to the high surface charge density and surface area properties of biochar [147,180], leading to a high cation exchange capacity (CEC) and increasing therefore this property in soil [180]. Some studies have also reported that biochar is able to adsorb phosphate (which is an anion) in a significant manner, therefore potential anion exchange capacity

in soil should be also considered [181]. Besides increasing cation exchange capacity and improving soil physical properties, other positive effects of biochar application regarding fertilization and related to its surface include the inmobilization of compounds harmful for plants development, as it is the case of exchangeable (Al) in acidic soils; or the adsorption of organic compounds that could inhibit nitrification and ammonification or lead to higher N inmobilization [182].

As it has been previously introduced, the biochar potential cation exchange capacity is dependent upon its surface characteristics, in particular, the net negative charge determined by the presence of functional groups [180,183] and the environment pH [184], as well as the total surface area, due to availability of adsorption sites [180]. These functional groups are developed due to breaking down of biomass macromolecules during thermochemical conversion. In low-temperature biochars higher amount of acid-basic surface functional groups are found [147], which are released at higher temperatures as volatiles, as well as carbonized in a more aromatic structure, as previously explained. Ash content in biochars also influences the chemical surface properties, particularly in low temperature biochars with higher likelihood to be dissolved [147]. However, the effect of temperature on cation exchange capacity is not clear. Gaskin et al. [185] reported a decrease in CEC for biochars produced from poultry litter, pine wood chips and peanut hulls as the production temperature increases from 400 to 500 °C. Mukherjee et al. [184] showed also a decrease in CEC with increasing production temperature from 250 to 650 °C for oak and pine biochars for the pH range from 1.5 to 7. However, using grass as feedstock, biochars produced at 650 °C showed higher CEC than biochars produced at 400 °C for pH $>$ 4. Lehmann et al. [181] reported an increase in CEC for woody biochars when production temperature increased up to 500 °C, followed by a reduction in CEC in the temperature range of 500 - 600 °C and again an increase in CEC for temperatures $>$ 600 °C. The CEC is also highly dependent on the pH at which is determined [184, 186], therefore this must be taken into account when applying in soils. With low pH, the CEC is very low, but increases with increasing pH [184]. It has been also shown that further oxidation of biochar surface, for example due to aging effects once applied in soil, increased significantly the surface negative charge, while decreased the positive surface area (high in fresh biochars), decreasing therefore the point of zero net charge (PZNC), i.e. the pH at which positive and negative surface charge are equal [186]. The increase in CEC with aging has been attributed to the formation of oxygenated functional groups on char surface, such as carboxylic groups [183].

However, not all the biochar effects are good in soil. Negative impacts have been also reported, mainly due to decrease in efficiency regarding some micronutrients, due to its alkaline nature or due to N inmobilization [147] or due to the introduction of contaminants or toxic elements for plants.

As it can be seen, understanding the behavior and possible impacts of biochar in soil is a complex matter where many variables influence from both sides, biochar production and properties, as well as soil, plants and environment conditions. Evidence of the positive potential impact of biochar in the long term for soil and environment are still needed. In the same way, further understanding of the relation between production conditions and material, biochar properties and its influence on soils are required.

In this work, further understanding of the effect of production conditions and initial feedstock on several physical and chemical properties of biochar will be investigated.

As previously said, much attention must be paid when experimental results are compared, since analytical methodology is very different and many times the methods and sample preparation are not correctly described, leading to the impossibility of comparing results.

7.4 Biochar characterization

Biochar characterization has been performed in collaboration with other research groups. Therefore it will be clarified which method development and measurement has been performed at the Technische Universität Berlin (EVUR) and which one externally.

7.4.1 Biochar characterization performed at the TU Berlin

Porous structure characterization

Characterization of biochar porous structure has been carried out at the Technische Universität Berlin. Part of the development of this method, as well as part of the samples characterization have been performed in the framework of the master thesis from Alberto Rueda Garcia [187], of which I am coordinator.

The specific surface area (SSA) is considered as a main characterizing parameter of biochar (as reported by the European Biochar Certificate [41] and the International Biochar Initiative [151]), however, without knowing the pore size distribution, the simple value of surface area might mislead the interpretation of the properties and functionality of biochar. For example, the low or medium SSA of a biochar can be due both to high macroporosity with low microporosity or to mesoporosity with e.g. collapsed micropores. This would make a significant difference in the application of the biochar, since micropores and mesopores would contribute more to the adsorption of nutrients and to increase the soil-water retention [148], while macropores would have other possible functions more related to aeration, hydrology or life or microorganisms

[148]. According to the IUPAC classification, micropores are pores with size (typically in diameter) $\leq$2 nm. Mesopores range between 2 - 50 nm and macropores are bigger than 50 nm in diameter.

There are different analytical techniques to characterize a porous solid, such as gas adsorption, radiation scattering, pycnometry, calorimetric determinations, intrusion,... [188]. In the present study gas adsorption will be the analytical technique applied, using N_2 as adsorptive/adsorbate. This is the most widely used and therefore established technique for characterization of porous structure, more specifically for micropores and mesopores.

According to the IUPAC, adsorption is defined as "an increase in the concentration of a dissolved substance at the interface of a condensed and a liquid phase due to the operation of surface forces. Adsorption can also occur at the interface of a condensed and a gaseous phase" [189]. Consequently, gas adsorption always takes place, to some extent, when a clean solid surface (adsorbent) is exposed to a gas (adsorptive). The amount of gas adsorbed (adsorbate) depends upon the temperature, the absolute pressure and the potential interaction between the gas molecules and the surface [190]. Depending on the strength of these interactions, gas adsorption can be divided in physical and chemical adsorption. According to Rouquerol et al. [191], in chemical adsorption (chemisorption), chemical bonding takes place between the gas (or liquid depending on the type of adsorption) molecules and reactive parts (active sites) of the surface, being usually an activation energy involved, and with a chemisorption energy similar to the energy variation in a comparable chemical reaction. Chemical adsorption is necessarily confined to one layer adsorption, due to the chemical nature of the bonding, and it may be referred to as irreversible, meaning that if the adsorbed molecule undergoes chemical reaction cannot be recovered by desorption [191]. Although chemical adsorption is used to characterize the reactive surface area (active sites) of porous materials such as catalysts, it does not allow the characterization of pore volume and therefore pore size distribution. Hence, in the present work, physical adsorption is the one applied. In this type of adsorption, the interaction forces are the van der Waals forces, of the same kind as those present in vapor condensation and deviation from ideal behavior in real gases, as highlighted by Rouquerol et al. in [191]. Physical adsorption is always exothermic and the energy involved is usually low. With high partial pressures it generally takes place as a multilayer phenomenon [191], which allows also pore filling, enabling pore volume measurements. In opposition to chemical adsorption, physical adsorption is a reversible process where equilibrium is reached fast [190], except in small pores due to diffusion limitations.

The basic step in porous structure characterization with gas adsorption is the determination of the adsorption isotherm. This curve is obtained by plotting the amount of gas adsorbed versus pressure at a constant temperature (the measurement temper-

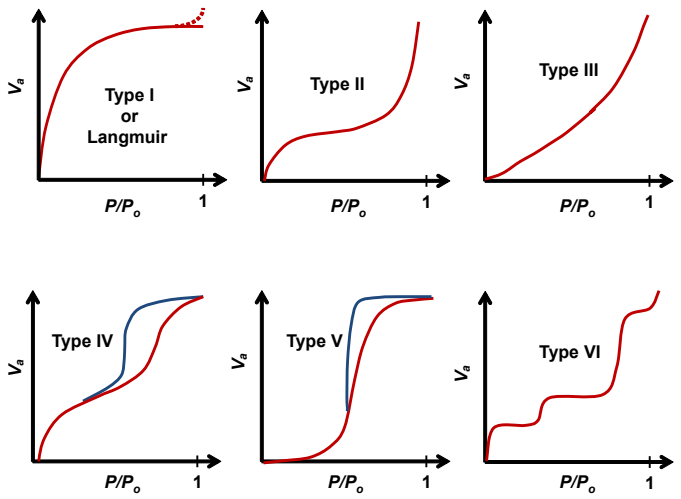

Figure 7.4: *Classification of isotherms according to the IUPAC [11].*

ature) [190]. The IUPAC recommended a classification of these physical adsorption isotherms [11], based on an earlier review by Brunauer et al. [192]. Six are the possible shapes of the adsorption isotherm according to this recommendation, as it is shown in Fig. 7.4, each of one reflecting some unique property. In these graphics, V_a is the gas volume adsorbed and P/P_o is the partial pressure, where P is the absolute pressure in the device and P_o the saturation pressure of the adsorbate at the measurement temperature. The used gas sorption analyzer is a NOVA 2000 series model from Quantachrome, with two degassing stations and two analytical stations. The software used to control the device and analyze the results is called NovaWin, also provided by Quantachrome.

As explained in [11, 190], isotherms type I are characteristic of microporous materials, with a pore size not larger than a few times the diameter of the adsorbate molecule. Type II isotherms are typical of non-porous or macroporous materials. Type III is for materials with weak interactions adsorbent-adsorbate. Type IV occurs for mesoporous materials, being the hysteresis an indication of capillary condensation. Type V is for materials also with weak interaction with the adsorbate but containing mesopores. Type VI presents layered adsorption on a uniform non-porous surface.

Taking this into account, the shape of the adsorption and desorption isotherms provides the initial information about the porous structure of the biochars under study.

The next step would be the application of several mathematical models to the adsorption and desorption isotherms to gain information about the total surface area, total pore volume, as well as pore surface and volume related to each pore size.

Sample pretreatment

Before performing the N_2 adsorption measurements, the sample needs to be pretreated. The first point of discussion is whether the sample should me milled, crushed or analyzed as it is produced. The reason for milling the samples is based on the presence of pore diffusion limitation when the porous structure is mostly formed by micropores, specially small ones. In these conditions, bottle necks may be formed which slow down the movement of the molecules into the pores. Consequently, part of the surface will not be covered by N_2 and thermodynamical equilibrium will not be reached. This is still worsened by the low temperature at which this measurement needs to be performed, 77 K. If the sample is milled, part or the totality of these bottle necks may be broken, reducing this effect. Therefore, thermodynamical equilibrium should be reached and the measured surface area should be more reliable describing the real one. However, when milling the sample, if the particle size is too small, external surface area, i.e., the pore surface due to particles agglomeration, may contribute in a significant way to the total surface area, leading also to false surface area determination. To avoid this, the particle size of the sample should be kept at least two orders of magnitude bigger than the maximum size of the pores expected to be measured. For example, if pores up to 100 nm in diameter are expected, the minimum size of the particle should be bigger than 10 μm.

In the present work, due to strong presence of diffusion limitations and therefore low repeatability in the results, it has been decided, based on the experimental results, that the sample should be milled and the surface area should be referred to as maximum surface area measured in the specified conditions.

The sample needs also to be degassed before the adsorption measurements are performed. This is due to the fact that other molecules present in the environment will be adsorbed at the surface, such as water, carbon dioxide, oxygen, etc. When looked into the literature, or in the DIN norms, typical degassing times are quite large, usually around 12 hours or more, and the temperature used is dependent upon the material. In the present work, however, it has been determined, based on the experimental results, that degassing in vacuum of 3 hours is enough to clean the surface of these chars, or in other words, longer times do not lead to bigger measured surface areas. The temperature used for degassing in the present work is 150 °C. This is based also on experimental results obtained at different conditions, leading to the conclusion that samples produced in pyrolysis above 300 °C should be degassed at 150 °C and samples produced below that temperature would be degassed at 120 °C. More severe conditions could lead to irreversible damage of the sample.

Once the adsorption isotherm is obtained, several models are applied to gain information on the surface area, pore volume and pore size distribution. Those are:

BET and Langmuir models

The BET model is the most employed method nowadays for determination of the total specific surface area. It supposes an extension of the Langmuir theory [193]. Langmuir, in his adsorption theory, tried to quantitatively determine the molecules adsorbed on a solid plane surface, considering that this adsorption would be "true adsorption", which he defined as follows: "in cases of true adsorption this layer [adsorbed layer] will usually be not more than one molecule deep, for as soon as the surface becomes covered by a single layer the surface forces are chemically saturated" [193]. He also defined the forces involved in the adsorption phenomenon as chemical forces, indicating that he was referring to chemical adsorption. In this work, he proposed first a simple adsorption theory which then extended to more complex cases. In this first adsorption theory, he assumed that all the potential adsorption sites were equal, having then the same adsorption energy, and that each one of these sites could only hold one adsorbed molecule. Besides, based on the concept of true adsorption, he assumed that the forces acting between two adsorbed layers would be much weaker than the forces between the solid surface and the first adsorbed layer, leading to the fact that the rate of evaporation from the second layer would be much greater than that from the first layer and, therefore, the molecules adsorbed on the second layer would be negligible in comparison to the first layer. Besides, he considered the range of low pressures, i.e., pressures far below the saturation pressure to avoid capillary condensation. In these conditions, taken moreover into account that thermodynamically equilibrium would have been reached, the surface covered by adsorbed molecules would be described as [193]:

$$\Theta = \frac{[\alpha\mu]}{[1 + \alpha\mu]} \tag{7.1}$$

where Θ is the surface fraction covered by adsorbed molecules, α is the fraction of molecules striking the surface which will condense and μ represents the number of gram molecules of gas striking the surface.

This theory may be then appropriate to describe chemical adsorption or physical adsorption in case of isotherms Type I with very small pores (see Fig. 7.4), i.e., when the porous structure is completely microporous and, therefore, there is no possibility of several layers adsorption. However it cannot describe other types of isotherms, where a convex-shape curve appears at the highest pressure range. This behavior has been attributed by Brunauer, Emmett and Teller [194] to multimolecular adsorption, induced mostly by the same forces that produce condensation, rather than by condensation in capillaries of molecular dimensions. This multilayer adsorption would be enhanced by the higher probability that a gas molecule would strike and be adsorbed on an adsorbed molecule due to the higher pressures and therefore concentration of the gas [190]. With these considerations, Brunauer, Emmett and Teller developed a theory describing the

multimolecular layer adsorption similar to Langmuir derivation for unimolecular layers, i.e., the BET model [194] of the form:

$$\frac{P}{v(P_o - P)} = \frac{1}{v_m C} + \frac{C-1}{v_m C}\frac{P}{P_o} \tag{7.2}$$

where P_o is the saturation pressure of the gas, P is the absolute pressure at each step, v_m is the volume of gas adsorbed in the first layer when it is completely covered and C is a constant related to the heat of adsorption on the first layer and therefore an indication of the magnitude of solid/gas interactions. From the value of $v_m C$ the surface area can be determined, assuming a value of the cross-section of the molecule. The assumptions on which this theory is built are that the heat of adsorption in the first layer is independent of the number of gas molecules already adsorbed on the first layer, and that the heat of adsorption in the second and upper layers is equal to the heat of liquefaction and, therefore, constant for all the layers, as any other constant involved. Besides, Equation 7.2 implies that an infinite number of layers can be adsorbed on the solid surface. Braunet, Emmet and Teller developed in the same work [194] a description for the isotherm in case that the number of possible adsorbed layers would be limited, for example due to small pore sizes, however, this second equation is not usually applied.

Despite the widely extended use of the BET theory for total specific surface area determination, it has been also source of severe criticism. This lays mainly on the assumptions which this theory relies on. In general the BET may fail in the range of very low relatives pressures, (below 0.05) due to the assumption of an energetically homogeneous surface [190]. Another point of criticism is the assumption that the heat of adsorption for the second and upper layers is equal to the heat of liquefaction. This contributes to the failure at partial pressures above 0.35 [190]. However, in the partial pressure range of 0.05 - 0.35, close to complete coverage of the first layer, the BET theory is generally valid for most of the isotherms [190].

However, for microporous materials the BET model does not present linearity in this region, being necessary to shift the partial pressures range to lower pressures.

Total pore volume

The determination of the total pore volume with gas adsorption is based on the Gurvich rule [195], i.e., the fact that "at saturation the liquid volume of different adsorbates, when measured on porous adsorbents, is essentially constant and it is independent of the adsorbate" [190]. This indicates that at saturation pressure, that is to say, when the partial pressure is close to 1 in the adsorption isotherm determination, the pores are filled with liquid adsorbate. Based on that, the total pore volume can be determined knowing the adsorbed gas quantity and the properties of the adsorbate [190].

V-t method and BJH method

In the V-t method, the isotherm of the material to be analyzed is compared with an standard Type II isotherm [196] for determination of the micropore volume and surface area, based on the t-curve, which is the statistical thickness (t) plotted versus the relative pressure P/P_o. This t-curve can be defined by the de Boer equation as 7.3:

$$t(Angstrom) = (\frac{13.99}{log\frac{P}{P_o} + 0.034})^{(\frac{1}{2})} \tag{7.3}$$

assuming hexagonal close packing, i.e., the thickness of one molecular layer of nitrogen is 3.54 (Angstrom). This statistical thickness is then used to evaluate the analysis isotherm as a t-curve, by plotting the volume of adsorbed gas versus t [190]. Depending on the shape of the isotherm and consequently the t-plot, several analysis can be made as explained by Lowell et al. [190]. For example, if the sample presents mostly microporosity, when the t-plot is represented, the linear part of the t-plot (in the high statistical thickness region) would show a positive intercept with the adsorbed volume axis. This positive intercept would be equivalent to the micropore volume, and the slope of the straight line would be proportional to the external surface area.

The BJH method has been developed by Barrett, Joyner and Halenda [197] and it is applied to characterize the pore size distribution for pores bigger than 3 nm. It is based on the assumption that at a partial pressure close to 1 the pores are filled with liquid nitrogen. As summarized in [198], in each pore, a physically adsorbed layer of thickness t would enclose an inner capillary with radius r_k, from which evaporation would take place, as the partial pressure decreases. The total pore radius would be then $r = r_k + t$. As the desorption proceeds, the volume desorbed in each partial pressure step corresponds to the volume of condensate desorbed from the next larger size pores together with volume desorbed from the physically adsorbed layer left from the pores with bigger size. A deeper explanation on the algorithm for the application of this method can be found in [198].

DFT method

The application of the density functional theory (DFT) for calculating the pore size distribution in porous materials from the adsorption isotherm has been proposed for the first time by Seaton et al. in 1989 [199]. According to a recent review on the topic performed by Landers et al. [200], this approach provides, as they introduced, "a more reasoned and versatile approach to calculating the pore structure parameters compared to conventional methods based on the Kelvin equation", based on its "rigorous theoretical basis that covers the whole region of micro- and mesopores" [200]. As the next step, the non-local density functional theory (NLDFT) evolved, firstly developed for

slit geometries in activated carbons, concluded into a library of computational methods, taking into account several pore structures and morphologies potentially present in typical adsorbent materials [200]. Those computational methods include besides assessment of physical phenomena related to geometries of specific pore structures. As an step forwards appeared the advanced quenched solid density functional theory (QSDFT), which takes also into account the roughness and heterogeneity of the pore wall surfaces [200]. All these computational models are included as library in the software from the Quantachome Instrument, for several adsorbates and pores geometry. These models are compared to the experimental data from the adsorption isotherm and the model which best fits the experimental results is the considered one for analysis of the pore structure. In the present work, for all the samples, the model QSDFT for slit/cylindrical pores was the applied.

Proximate and elemental analysis

Proximate and elemental analysis of the biochar samples have been performed at the Technische Universität Berlin.

Proximate analysis, i.e., volatiles and ash content have been determined following the DIN norms DIN 51719 and DIN 51720 respectively. Fixed carbon content is then determined as 100% - (volatiles(%,db) + ash(%,db)). Briefly, for volatiles determination the char sample is kept during 7 min in the oven at 900 °C in close crucibles and for ash determination the char is introduced in the oven in open crucibles with the following temperature program: starting with ambient temperature, the temperature is raised to 500 °C in 30 min, and then up to 815 °C in 45 min and held at this temperature for 60 minutes. Organic elemental composition (CHNS) has been characterized in a Vario EL elemental analyzer. Oxygen content is determined then as 100%-(ash%+C%+H%+N%+S%). Inorganic elemental content is characterized in an ICP-OES (Inductively Coupled Plasma Optical Emission Spectrometry) after digestion in a microwave (Multiwave 3000 Anton Paar).

The procedure is the following: after drying the sample at 106 °C for 90 min, and milling it, it is digested in the microwave. For that, approximately 4 mg of sample is mixed with 5 ml HNO_3 and 2 ml H_2O_2 in sealed vessels of 50 ml. In the microwave, the sample is subjected to a power of 500 W, reached after 25 min, and held for 50 min. The temperature reached by the sample must overcome 200 °C and the maximum pressure that can be reached is 60 bar. After that, the sample obtained from the microwaved is diluted up to 50 ml with distilled water and then introduced in the ICP-OES for further measurement.

Electrical conductivity and pH

To measure the pH and electrical conductivity, the sample is mixed with distilled water and the measurements are taken while stirring. Several concentrations have been tried. The first concentration is the one suggested by Pulido-Novicio et al. [168], i.e., 1 g of char in 20 ml of distilled water. On the other hand, the norm DIN ISO 10390 suggests a volumetric relation 1:5 solute solvent. If 5 ml of sample is taken, it should be dissolved in 25 ml water. However, 5 ml of sample is dependent on the bulk density, and therefore on the particle size, density of the sample and packing. This leads to the situation that for 5 ml the sample mass ranges between 0.5 g up to 2 g. Consequently, two measurements were performed: 1 g in 25 ml water and 5 ml sample in 25 ml water. For pH the results are very similar in all the cases. Therefore the results reported here are correspondent to 1 g in 20 ml water. The pH is measured with a pH-electrode Sen Tix HW, attached to a pH meter WTH pH 340 and the electrical conductivity is measured with an electrical conductivity meter, model WTW KLE 1/T.

Surface functional groups. Boehm titration

As it has been previously outlined, characterization of surface chemical structure is of high significance since it has a direct impact on pH, capacity to retain and exchange cations or anions, electrical charge, hydrophobicity, etc. However, qualitative and quantitative determination of this property is not an easy task, due to the high heterogeneity in composition and lack of a standard and reliable method, above all, to quantify the surface functional groups.

According to Amonette and Joseph [201], "operational determination of acidic and basic functional groups on biochars can be performed by Boehm titration". However, this methods would not work appropriately if significant amounts of tar or mineral surfaces are present [201].

Other alternative methods that have been used to examine surface chemistry of biochar include diffuse reflectance infrared Fourier transform spectroscopy (FTIR), X-ray photoelectron spectroscopy (XPS), energy dispersive X-ray spectroscopy (EDX) or near-edge X-ray absorption fine structure (NEXAFS) spectroscopy [202]. However, these methods are not able to provide a reliable quantification of the surface functional groups, if any at all, being more appropriate for qualitative evolution characterization.

In the present work, the Boehm titration method is the one applied, including pretreatment of the biochar samples to reduce the effect of possible tar adsorbed on the solid surface, as well as inorganic species. This method has been developed in 1964 by Boehm and his colleagues [203], with the aim of characterizing the surface oxides in carbon. The idea behind this method is that the oxygen-containing functional groups

on the biochar surface have different acidities and therefore can be neutralized with bases of different strengths [204]. The acidic groups to be determined are carboxylic, phenolic and lactonic groups.

The development of this method, as well as the characterization of some biochar samples according to it, have been partially performed during the master thesis of Alba Yebra Dominguez (in submission) of which I am coordinator. The experimental procedure applied is the one carefully described by Goertzen et al. [204], including a sample pretreament proposed by Tsechansky and Graber [205]. Due to the presence of inorganic basic and acidic components, which can be condensed on the biochar surface but not be part of the biochar structure, false results from the Boehm titration could be obtained because of the solubilization of these components in the Boehm basic solutions. Consequently they should be removed prior titration. This washing is performed first with HCL (0.05M) and NaOH (0.05 M) during 24 h each to remove basic and acidic species repectively. After this, a final washing with HCL is performed to protonate the acidic species on the char surface again. After each washing and before the next one, the biochar is washed with deionized water until a conductivity lower than 10μS/cm is reached. The final step is the degassing using N_2 and finally the sample can be titrated with the different bases.

7.4.2 Biochar characterization performed externally

Char wettability

Determination of char wettability has been carried out by Dr. Gerardo Ojeda (with current affiliation Universidad Nacional de Colombia) and Prof. Jörg Bachmann (with current affiliation Institute of Soil Science, Leibniz University of Hannover), as result of a common collaboration. The methodology applied can be found in [206]. Briefly, a glass tube 6 cm high with 0.9 cm of internal diameter is filled with the different biochar samples up to a height of 3 cm. Then the tube is attached to a high precision scale. Below the tube, a glass filled with water or hexane is placed and carefully risen until it touches the bottom part of the tube. Water/hexane capillary absorption is measured by registering the weight increase in the biochar column during 200 s.

Contaminants: polyaromatic hydrocarbons (PAHs) content

The determination of PAHs in biochar has been performed by Alessandro G. Rombola, with the supervision of Prof. Fabbri at the University of Bologna, as result of a common collaboration. The method applied for characterization of the 16 USEPA (United States Environmental Protection Agency) PAHs is described in [207]. Briefly, the biochar

samples were Soxhlet extracted with an acetone/cyclohexane (1:1) solvent mixture and then the PAHs were analyzed in a GC-MS.

Stability

This characterization has been performed by Alessandro G. Rombola with the supervision of Prof. Fabbri, at the University of Bologna, as result of a common collaboration.

In this case, the stability of biochar has been evaluated by characterizing to which extent the biochars had been charred in the pyrolysis process. That is to say, the biochars samples were subjected again to an analytical pyrolysis process, up to a temperature of 900 °C and the species emitted were analyzed in a GC-MS. The technique is called Py-GC-MS. In this way, depending on the quantity and nature of the labile species, it can be determined how recalcitrant the biochar is. The method applied in described in [208].

Chapter 8

Results, discussion and conclusions of biochar characterization

8.1 Elemental and proximate characterization

Biochar elemental and proximate characterization is included in the description of biochar chemical structure, as explained in Section 7.3.2.

In Fig. 8.1, the Van Krevelen diagram, i.e., the representation of H/C molar ratio versus O/C molar ratio is presented for numerous biochars produced from several raw materials under different pyrolytic conditions. As it has been aforementioned, this diagram is often used to illustrate the degree of maturity and aromaticity of biochar [175].

It is observed that higher conversion temperatures lead to a decrease in both molar ratios due to the carbonization process and consequent progressive loss of volatiles, mainly through dehydration, decarboxylation, decarbonylation and demethylation reactions, leading to a more condensed solid structure, with higher aromatization degree. However, these results show that biochar chemical composition depends not only on the conversion conditions, but also on the initial feedstock composition, having a significant impact on final biochar chemical properties. This is illustrated with the results of corn digestate (CD) versus those for pine and beech wood or cellulose. With the same process conditions, corn digestate biochars show significantly lower hydrogen (H) content and higher oxygen (O) content. This indicates that reactions involving H loss, such as demethylation, should occur to a higher extent than those leading to O release. Looking at the composition of the raw material, corn digestate presents a very similar H/C ratio (dry ash free basis, daf) to wood and a slightly lower O/C ratio. However, the main difference between them is the ash content. While wood has an ash content below 1% (wt, db), the content of corn digestate goes up to around 20% (wt, db).

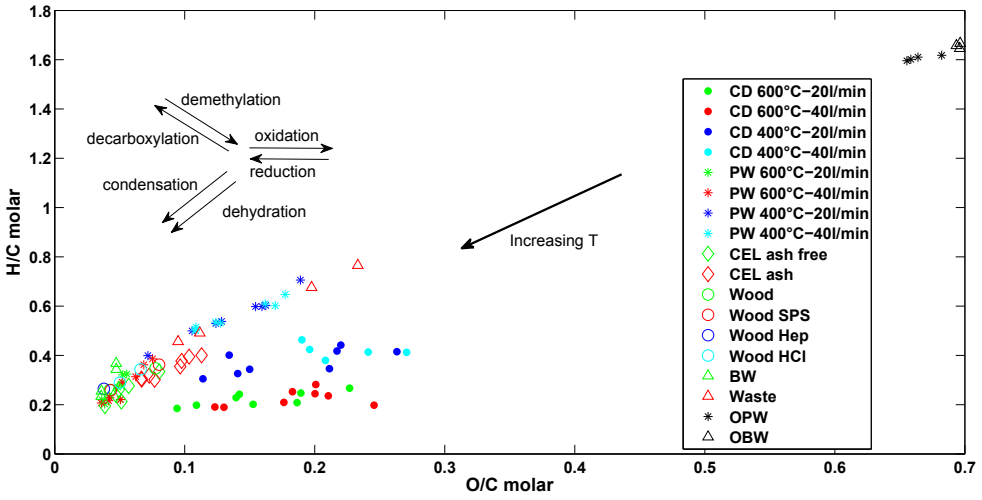

Figure 8.1: *Van Krevelen diagram for biochars produced from different raw materials and process conditions, as specified in Section 4.2. The molar ratios are given in dry ash free basis (%wt, daf).*

.

This difference in ash could be the main reason lying under the reported differences in elemental composition, enhancing H loss reactions.

According to the definition given by the European Biochar Certificate (EBC) [41], almost all chars (except waste derived biochar with the lower charring degree) reported in this Section could be considered biochars, since H/C is lower than 0.7 and O/C ratio is lower than 0.4. Going further, and according to a recent review from Spokas [172] on char stability, those biochars with an O/C content lower than 0.2 could "provide, at minimum, a 1000-year biochar half-life". Those would be all biochars produced from wood and cellulose and most of those produced from corn digestate and waste with the most severe conditions.

In Fig. 8.2 the H/C and O/C ratios are plotted versus the volatiles (%wt, daf) content in biochar. It is noteworthy to highlight the linear behavior of O/C ratio as a function of volatiles content. From this linear behavior, it could be withdrawn that volatiles content could be also used to assess biochar stability. In this case, biochar with a volatiles content (%wt, daf) lower than 35 %, or in other words, a fixed carbon content (%wt, daf) higher than 65%, could ensure an acceptable stability in soil. The advantage of using volatiles instead of the O/C ratio is that is easier and cheaper to determine. However, this tool has to be used carefully, since the determination method may strongly influence the result. According to Spokas [172] and Zimmerman [209], volatiles content could be also a good indicator of biochars produced in the same pyrolysis unit or process.

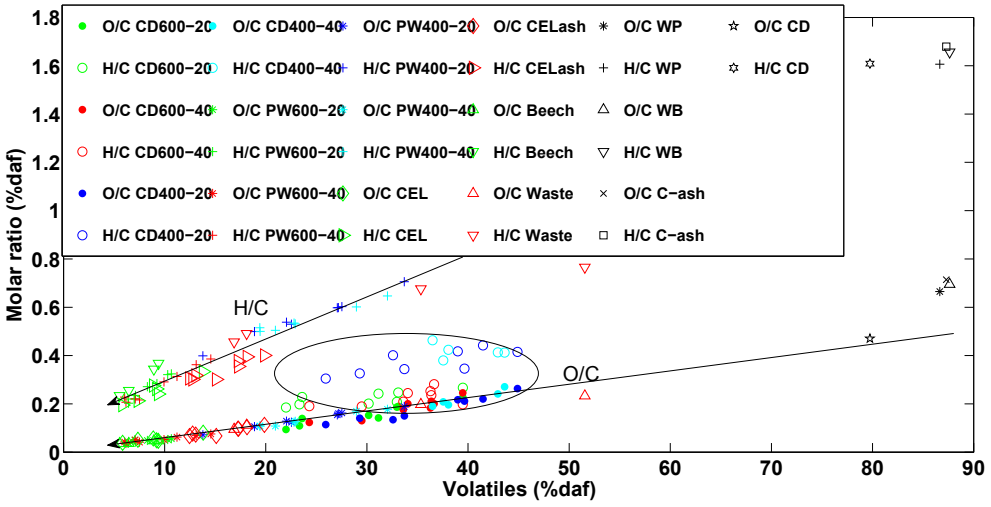

Figure 8.2: *H/C and O/C ratios plotted versus volatiles content in biochar, given in dry ash free basis (daf) for several biochars produced under different pyrolytic conditions and using several raw materials, as specified in Section 4.2.*

8.2 pH

Biochars can possess both acidic or alkaline character and this property is of high relevance for its application in soil, since it determines not only its potential liming effect, but it also has an influence on other properties, such as the cation exchange capacity or the water holding capacity. It has been reported in literature that pH may be dependent on both, the surface chemistry and the ash content. In this way, Pulido-Novicio et al. [168] affirms that acidic and basic properties in woody chars could be attributed to the presence of acidic and basic surface groups. However, Nguyen and Lehmann [210], when analyzing the effect of black carbon oxidation (during incubation) on pH, reported that the lack of correlation between C loss and pH could be due to two different phenomena, the increase of carboxyl groups, with high acidity, or the dissolution of mineral matter in high ash-containing biomass. Carrier et al. [211], based on previous investigations, affirm also that pH (together with cation exchange capacity and electrical conductivity) depends on the content and the composition of the mineral fraction.

These both influences are further confirmed in the present study. In Fig. 8.3 (top) pH is plotted versus the volatiles content of the biochar in dry ash free basis (% daf). Three different regions can be observed. The black points correspond to corn digestate biochars, which, as it can be seen, present higher pH than woody biochars, having similar volatiles content. However, a trend can be observed in the behavior pH - volatiles also for this material, i.e., the lower the volatiles content, the higher the pH. It must be clarified that all the corn digestate biochar samples present quite similar

ash content, ranging from 38% in dry basis to 46%. Therefore, this difference in ash content could probably not explain the variation in 3 points in the pH value.

In the middle region, in green, blue and pink, are the pH values for biochar samples coming from woody biomass and cellulose. It is observed that the relation between pH and volatiles content is quite linear. Noteworthy to mention is, however, the fact that the pH of cellulose with ash is slightly above the mean values of pH for wood and cellulose biochars, with similar volatiles content. Besides, biochars produced from wood, with and without washing, show significantly different values. By washing the wood with HCl, previous to the pyrolysis conversion process, the ash content is removed (final ash content value of 0.01 %wt in dry basis) and consequently the produced biochar has lower pH.

The third region is for biochar produced from cellulose and bio-waste, with a significantly lower degree of conversion. In these biochars the pH is completely acidic, possibly due to the surface functional groups, both quantity and nature, as shown in Fig. 8.4.

Fig. 8.3 shows the pH plotted versus ash content for the same samples. The two regions between low and high content biomass is clear, however it is also noteworthy to mention that the biochars with the highest carbonization degree from low ash content biomass present similar pH values to biochars with the lowest cabonization degree from high ash content biomass.

These results indicate that both phenomena, that is to say, influence of surface acidity and ash content are coupled regarding the pH behavior of biochars, or in other words, that pH is dependent on feedstock and carbonization degree.

8.3 Surface functional groups

In Fig. 8.4, information about the acidic functional groups present on the biochar surface is presented. These results have been obtained as explained in Section 7.4.1, i.e., by performing the Boehm titration. This method gives information about three main acidic functionalities present on biochar surface: caboxylic, phenolic and lactonic groups. The content of each of these functional groups has been then compared with volatiles content, O/C and H/C ratios and pH. The biochars selected for these analysis include pine wood, corn digestate, cellulose and bio-waste biochars, to have a wide representation of feedstock and conversion conditions. In the first graphic of Fig. 8.4, the comparison of these functional groups with volatiles (%wt, daf) is presented. It can be seen that content of total and phenolic & lactonic acidic groups shows a linear behavior with respect to the volatiles content for all biochars, except high ash content

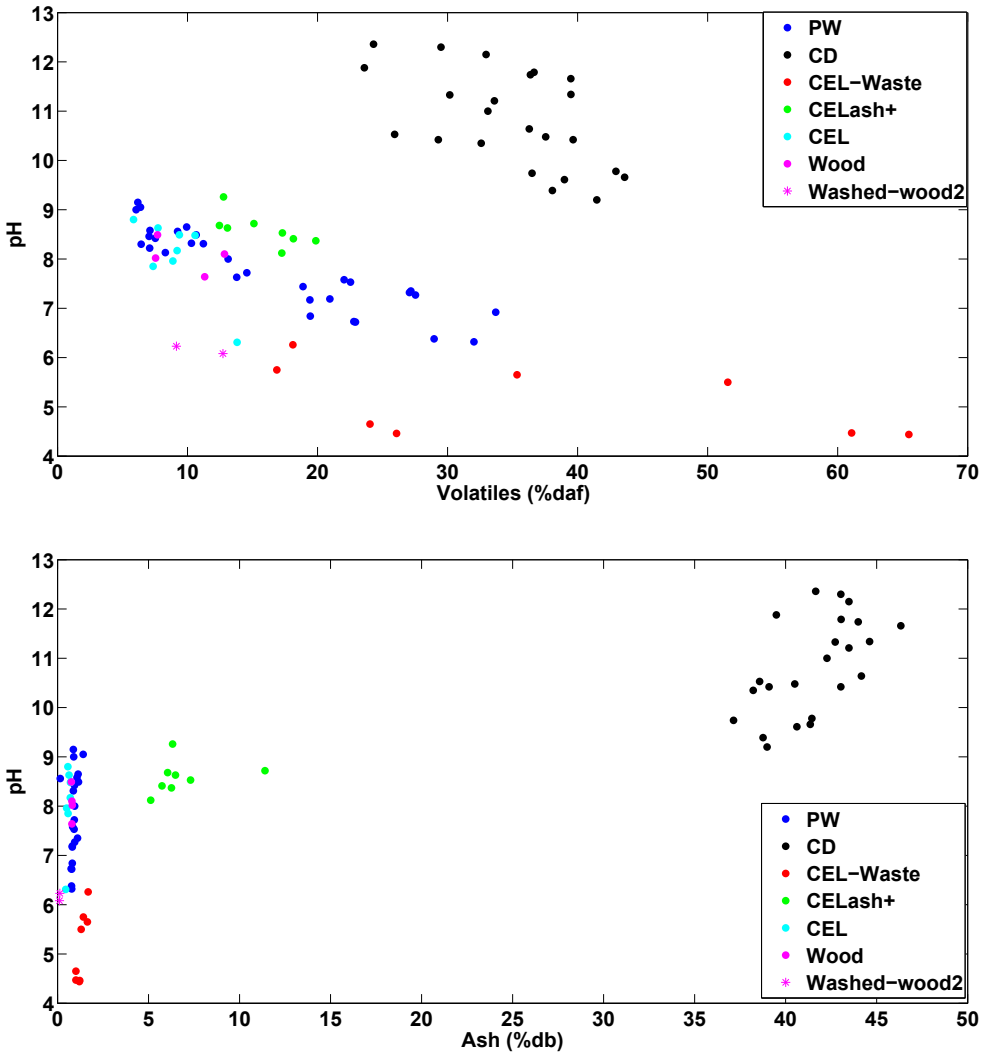

Figure 8.3: *Top: pH vs. volatiles content in dry ash free basis (%daf). Bottom: pH vs. ash content is dry basis (%db).*

biochar, i.e., corn digestate biochars. The first explanation for this behavior is that the acidic groups are expressed with respect to biochar mass in dry basis. Therefore, the biochars with high ash content will present necessarily less total functional groups, since the organic part is considerably lower than for biochars with low ash content. For carboxylic groups, the content is very low for all biochars, independently of the volatiles content. The same results are observed when compared with O/C ratio, since the relation between O/C and volatiles content is also linear, as reported in Section 8.1.

Interestingly enough is the fact that, when these surface acidic groups are compared with H/C ratios, a quite linear relation is obtained, independently of the ash content. Looking back at Fig. 8.2, the H/C ratio was lower for corn digestate biochars than for woody biochars with the same volatiles content. This could be due to two main reasons. The low H/C ratio reported by corn digestate biochars could be due to an enhancement in H release reactions, such as demethylation, due to the high ash content; or it could be that the measured volatiles content in corn digestate volatiles was not totally organic, but also a significant inorganic fraction would be also present, due to the high inorganic content of this feedstock. As consequence of the second possibility, the H/C ratio of corn digestate biochars would be actually higher for the same (organic) volatiles content than it is currently reported and, at the same time, it could be a better representation of the organic fraction of the biochar. Coming back to the surface functional groups, if these groups were represented with respect to the organic part of the biochar, for the same H/C ratio, higher content of acidic groups would be present in high ash content biochars.

The last graphic in Fig. 8.4 shows the comparison of these groups with pH. It is observed that there is a clear relation between the increase in pH and the decrease in total acidity of the biochar surface. With higher pH, the total acidity decreases, as well as the carboxylic functional groups for both feedstocks.

8.4 Porosity characterization

In this Section, the evolution of biochars porosity is evaluated. As it has been already introduced in Section 7.3.1, as the charring intensity increases, the release of volatiles and the development of crystalline structures [10] leads to an increase of porosity and, consequently, biochar internal surface area. This is shown in Fig. 8.5, where evolution of the internal surface area is plotted versus the biochars volatiles content (expressed in %wt, daf). The lower the volatiles content, the higher the internal specific surface area, determined in this case with the BET method.

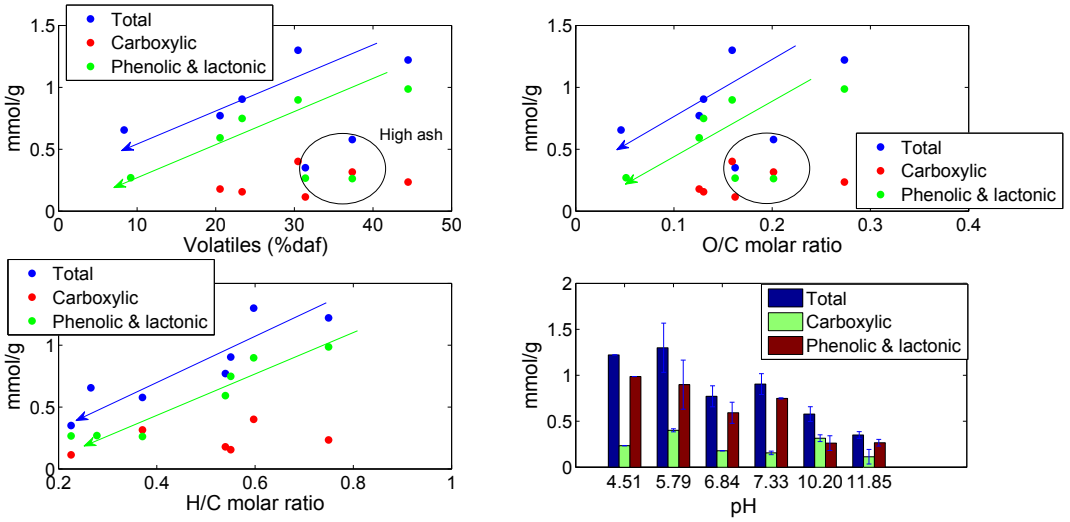

Figure 8.4: *Acidic functional groups present on the biochar surface determined with the Boehm titration method.*

It has been also introduced in Section 7.3.1 that this porosity should be mainly microporosity, attributed to interstices in the evolving graphite-like structure. This is shown for example in Fig. 8.6 (top), where representative isotherms from pine wood biochars are plotted. According to the introduction to this methodology given in Section 7.4.1, the shape of the adsorption isotherms from pine wood biochars produced at 600 °C (reference position) resembles the one of Type I isotherm (Fig. 7.4), indicating that the porosity in this material is mostly due to the presence of micropores. On the contrary, biochars produced at 400 °C show a very low capacity of adsorbing N_2, indicating that, at this temperature, the evolution of porous structure has not been significantly triggered yet.

Similar isotherm shapes have been shown for example by Carrier et al. [211] and Guo and Lua [170] for oak wood biochar (460 °C) and oil palm stones (600 - 800 °C) respectively, although the specific surface area values (BET method) reported by Guo and Lua are lower than those obtained in this work, even at higher conversion temperatures, probably due to the higher ash content.

This leads to the next question: what is then happening to corn digestate biochars? Why do they have such low capacity to adsorb N_2 (Fig. 8.6, bottom), i.e., low specific surface area, even when they have been produced at temperatures as high as 600 °C? To explain this, two effects need to be taken into account. In the first place, it has been shown that corn digestate biochars have an average ash content around 40 %wt in dry basis, therefore, an important fraction of the mass being analyzed corresponds to inorganic compounds. Secondly, these compounds could clog or block the access to micropores [212], limiting therefore the access of N_2 to the pores, but also avoiding volatiles to be released from the pores during conversion. This could be in agreement

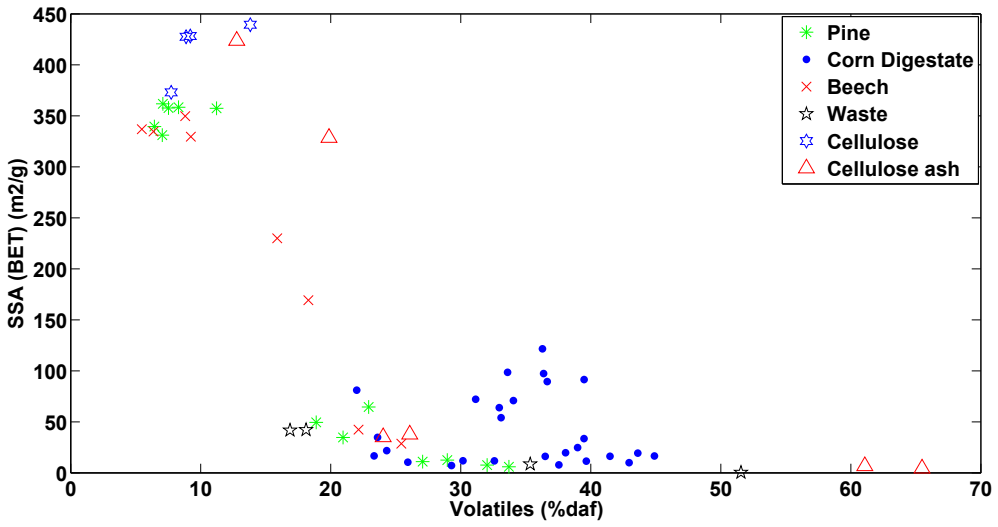

Figure 8.5: *Specific surface area determined with the BET method (based on N_2 adsorption) plotted versus the volatiles content in %wt dry ash free basis (daf) for several biochars produced under different pyrolytic conditions.*

with the higher volatiles content (%wt, daf) of corn digestate biochars, in comparison to woody biochars, for the same conversion temperatures.

However, to get a deeper and quantitative knowledge of the pore size distribution, further analysis of the adsorption and/or desorption isotherms needs to be carried out, applying different models, already introduced in Section 7.4.1.

The models applied here, besides BET for total specific surface area characterization and the determination of the N_2 adsorbed up to a partial pressure of 0.99 for total pore volume analysis, are: the density functional theory model (DFT), in particular the QSDFT model applied to the adsorption isotherm (considering that the pores are slit/cylindrical), for determination of total specific surface area, total pore volume, microporosity (surface area and volume) and mesoporosity, up to 30 nm in pore size (surface area and volume); the V-t model for determination of microporosity (surface area and volume) and surface area attributed to pores bigger than 2 nm; and the BJH method for characterization of pores bigger than 3 nm (surface area and volume). The results are summarized in Tables 8.1 and 8.2. Besides, in Fig. 8.7 (top) the total specific surface area and surface area distribution (pores smaller and bigger than 2 nm, according to the DFT method) for all the samples under consideration are compared. The same is done for volume in Fig. 8.7 (bottom).

As it can be seen, total specific surface area values of around 400 m^2/g are reported for pine wood biochars, produced at 600 °C, decreasing to below 10 m^2/g for samples produced at 400 °C. In the case of corn digestate biochars, the surface area values can go up to around 100 m^27g for biochars produced at 600 °C, with a flushing flow of 40

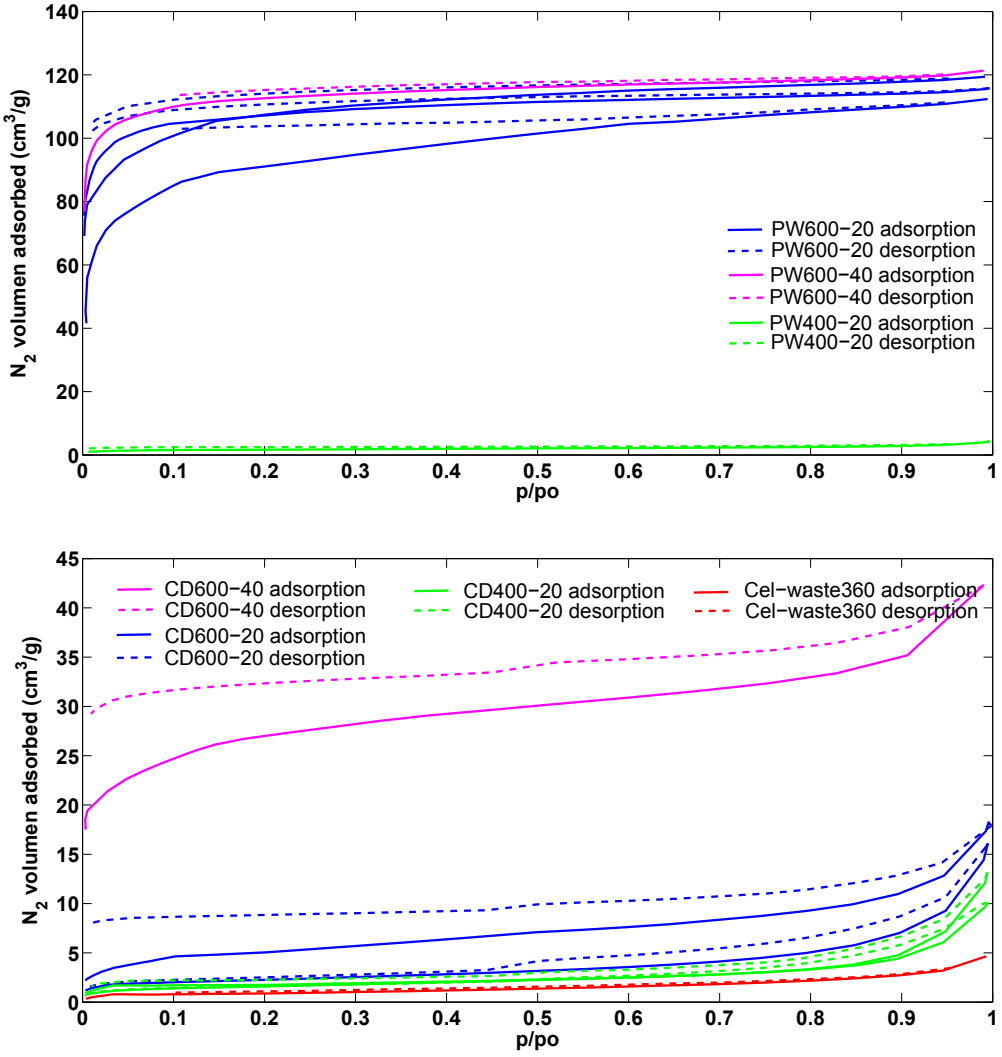

Figure 8.6: *Top: adsorption and desorption isotherms for pine wood biochar. Bottom: adsorption and desorption isotherms for corn digestate biochar and cellulose-waste biochar. For each case, the solid line corresponds to the adsorption isotherm while the dashed line to the desorption isotherm.*

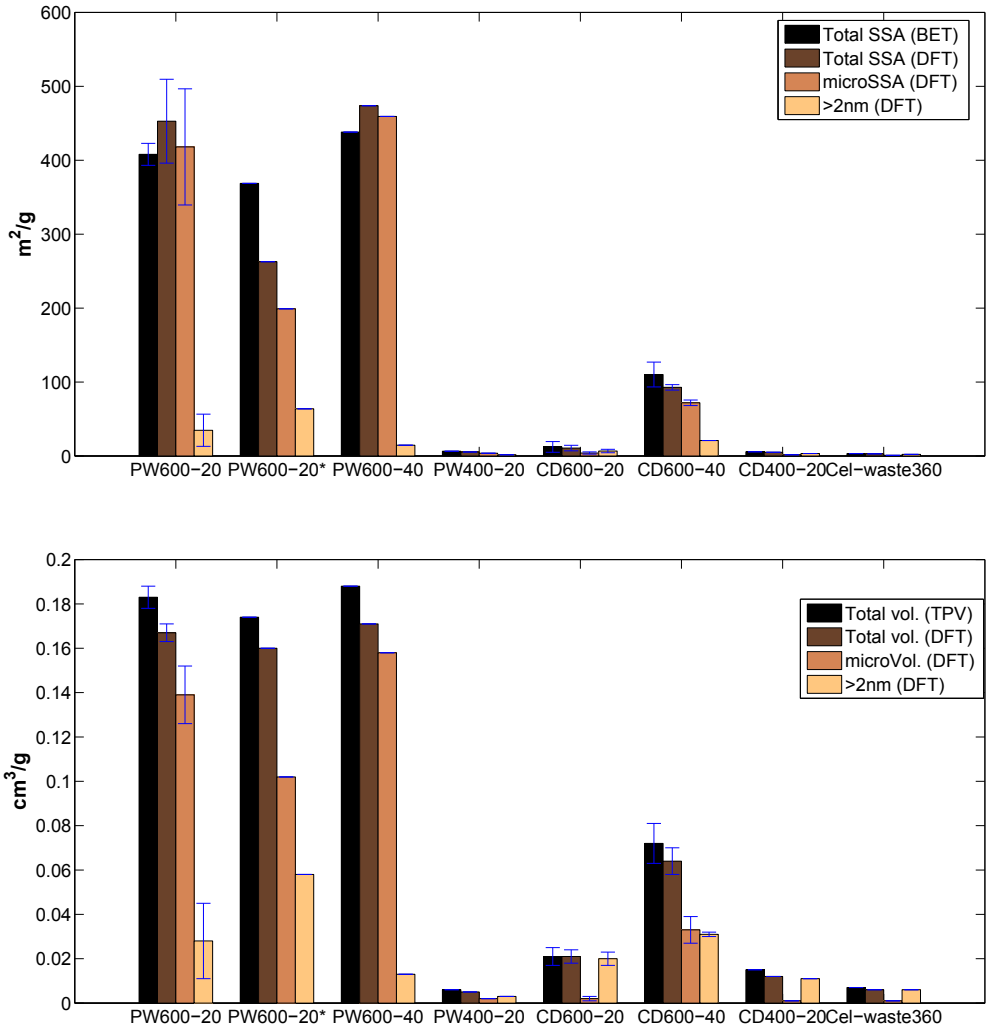

Figure 8.7: *Top: total specific surface area according to the BET and the DFT models and pore size distribution (surface area) according to the DFT model. Bottom: total pore volume determined at a partial pressure of 0.99 and according to the DFT model and pore size distribution (volume) according to the DFT model. *Sample with significant diffusion limitation.*

l/min, while for the rest of the samples the values would remain below 20 m^2/g. The major contribution to the surface area and volume for woody biochars produced at 600 °C is provided by the presence of micropores, as qualitatively explained with the evaluation of the adsorption isotherms. However, in the case of corn digestate biochars, mesopores have a much more significant contribution to the total pore volume. Therefore, inorganics would not only reduce the presence of micropores through potential blocking, but could also enhance the development of mesopores. As far as the author is aware of, this enhancement of mesopores in biochar due to the presence of inorganics has not been previously reported in literature.

Finally, it is important to highlight a phenomenon caused by the biochar porosity and enhanced by the measurement conditions (77 K), which can have a very significant

impact on the final results: diffusion limitation. This is easily observable in Fig. 8.6 for all the isotherms except PW600-40 and some of the corn digestate biochars. The fact that the desorption isotherm does not come back to the adsorption isotherm (the same quantity of N_2 adsorbed is then desorbed) might be an indication of the presence of this phenomenon. To further support this, three different samples of PW600-20 were plotted in Fig. 8.6 (top). It can be seen that the adsorption behavior also differs significantly among them. Besides, the lower the adsorption in the low pressure range (smaller pores are filled) is, the further the desorption isotherm remains with respect to the adsorption isotherm. Another indication would be that for the three samples, the final N_2 volume adsorbed is quite similar, i.e., for those samples which present the highest diffusion limitation in the low pressure range, once the N_2 concentration is increased, this limitation may be partially overcome. This leads to a change in the shape of the curve, which then conducts to false results once the models are applied. This is why in Tables 8.1 and 8.2 the values for each repetition (a, b and c) are shown, instead of giving averages and standard deviations. In this way, it can be seen besides that not all the models have the same sensibility to this phenomenon, being the DFT model the most problematic, since it analyzes the whole adsorption isotherm and not only a specific range.

It is not possible to avoid this phenomenon, since it is related to the biochar porous structure and to the measurement temperature, however it should be always evaluated and reported. Therefore, any result reported with those models is relative and it must be compared to other models and related to the measurement conditions and the type of char being analyzed. As far as the author is aware of, this problematic has not been previously addressed in literature for biochar characterization.

Interestingly enough is the fact that pine wood biochar produced at 600 °C with the highest flushing flow (40 l/min) does not present this diffusion limitation and, at the same time, shows higher N_2 adsorption in the low pressure range. This could indicate that with higher flushing rate this problematic could be partially avoided or, in other words, this limitation could be related to deposition of volatiles, partially clogging the smallest pores, or to the formation of secondary char, due to the higher volatiles concentration and retention time with lower flushing rates.

In the case of corn digestate, biochars produced at 600 °C with a N_2 flushing rate of 40 l/min present also higher porosity than those produced with 20 l/min, but the transport limitation seems to be still significant.

This will be further investigated in the future, using another gas which reduces the diffusion limitations, CO_2, since the measurements are done at 0 °C.

The sample from cellulose and waste presents the lowest porosity due to the lower conversion temperature.

(m^2/g)	**SSA**	**SSA**	**μSSA**	**μSSA**	**>2nm**	**>2nm**	**>3nm**
Method	BET	DFT	V-t	DFT	V-t	DFT	BJH
PW600-20 a	397.50	412.74	360.06	362.61	37.44	50.13	11.21
PW600-20 b	418.58	493.04	387.43	473.69	31.16	19.35	8.08
PW600-20 c	338.80	262.79	263.61	199.01	75.19	63.78	29.46
PW600-40	438.11	473.77	412.38	459.29	25.73	14.48	8.81
PW400-20	6.36	5.36	3.25	3.74	3.10	1.62	1.42
CD600-20 a	7.88	8.07	1.19	3.20	6.69	4.87	7.82
CD600-20 b	20.59	14.93	5.24	5.66	15.35	9.27	7.41
CD600-20 c	8.19	8.84	0.75	3.11	4.45	5.74	8.63
CD600-40 a	98.26	95.41	78.63	74.53	19.64	20.88	8.30
CD600-40 b	122.06	90.20	90	69.21	32.27	20.98	11.24
CD400-20	5.64	4.93	0.80	1.65	4.84	3.28	3.03
Cel-waste	3.15	2.92	0	0.79	3.15	2.14	2.21

Table 8.1: *Total specific surface area according to the BET method, total specific surface area according to the DFT method and surface area distribution in microporosity (< 2 nm) and porous bigger than 2 nm according to the methods V-t, DFT and BJH.*

(cm^3/g)	**TPV**	**TPV**	**μvol**	**μvol**	**>2nm**	**>3nm**
Method		DFT	V-t	DFT	DFT	BJH
PW600-20 a	0.186	0.170	0.153	0.130	0.040	0.018
PW600-20 b	0.179	0.164	0.153	0.148	0.016	0.013
PW600-20 c	0.174	0.160	0.109	0.102	0.058	0.038
PW600-40	0.188	0.171	0.164	0.158	0.013	0.014
PW400-20	0.006	0.005	0.001	0.002	0.003	0.004
CD600-20 a	0.022	0.018	0.001	0.001	0.017	0.024
CD600-20 b	0.017	0.022	0.001	0.003	0.019	0.022
CD600-20 c	0.025	0.024	0	0.001	0.023	0.025
CD600-40 a	0.066	0.059	0.034	0.029	0.030	0.025
CD600-40 b	0.078	0.068	0.035	0.037	0.031	0.033
CD400-20	0.015	0.012	0	0.001	0.011	0.014
Cel-waste	0.007	0.006	0	0	0.006	0.007

Table 8.2: *Total pore volume measured at a partial pressure of 0.99, total pore volume according to the DFT method and pore volume distribution in microporosity (< 2 nm) and porous bigger than 2 nm according to the methods V-t, DFT and BJH.*

8.5 Biochar wettability and contact angle

As it has been already introduced in section 7.4.2, the determination of char wettability has been performed by Dr. Gerardo Ojeda and Prof. Jörg Bachmann, as result of a common collaboration. However, the interpretation of these results and correlation to other biochar properties and production conditions is topic of the present work.

In Fig. 8.8 the water absorption behavior of several biochars samples is shown. On the left, those for corn digestate and cellulose and, on the right, the behavior for woody biochars. Corn digestate biochars produced at different pyrolytic conditions show a similar pattern regarding water absorption, with higher capacity as the conversion process severity increases, leading to an increase in porosity and reduction in surface functional groups. Woody biochars present two completely different behaviors. While chars produced at the highest severity (600 °C, 40 l/min) show similar patterns to those from corn digestate biochar (although with slightly lower capacity of absorbing water), those produced at lower temperatures do not show almost capacity to absorb water, reaching an asymptotic behavior after the first seconds. Cellulosic biochar shows similar behavior as woody biochars produced at mild conditions. These behaviors are directly related to biochar hydrophobicity.

When water is substituted by hexane, corn digestate biochars still show similar absorption capacity in comparison with water, however the capacity of absorbing hexane by pine wood biochars is much higher than the one for water. If both absorption curves are compared, the contact angle can be determined. For that, the slope of each water and hexane curve is evaluated in intervals of approximately 10 s and compared with each other. The contact angles obtained are shown in Table 8.3. As it can be seen, pine wood biochars present contact angles close to 90°, except PW600-40, which is an indication of higher potential hydrophobicity [213], while corn digestate biochars present lower contact angles. From these results it can be concluded that biochars are mostly hydrophobic. However, it has been also shown that after one year in soil, they loose part of this hydrophobicity [213].

8.6 PAHs content

When biochar is applied to soil, it can also have negative impacts, among others, due to the contaminants introduced in the soil. These contaminants may be heavy metals or organic compounds, such as polycyclic aromatic hydrocarbons (PAHs) or dioxines. In this Section the presence of PAHs in several biochar samples is evaluated.

As previously reported in Section 7.4.2, these measurements have been performed at the University of Bologna by Alessandro G. Rombola and Prof. Fabbri, as result of

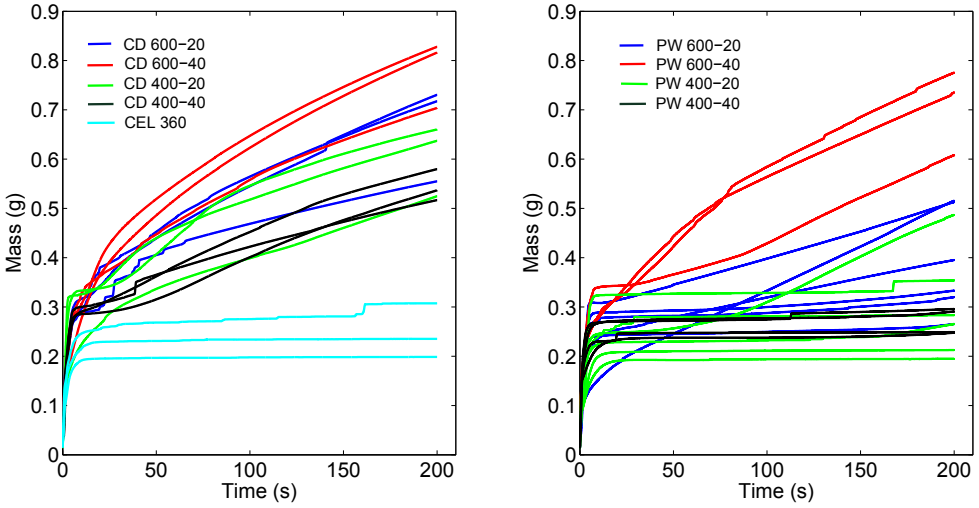

Figure 8.8: *Water absorption behavior over a period of 200 s for several biochar samples: corn digestate and cellulose biochars on the left and pine wood biochars on the right.*

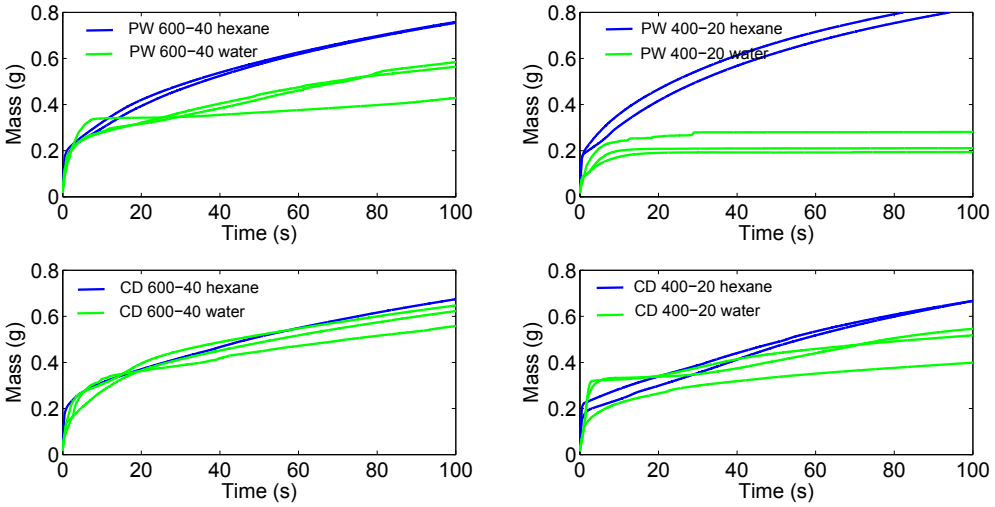

Figure 8.9: *Comparison between hexane absorption and water absorption for several biochars.*

t(s)	**PW600-40**	**CD600-40**	**PW600-20**	**PW400-40**	**CD400-40**	**CEL360**
2-10	73.7°	66.2°	77.2°	81.4°	70.1°	84.1°
10-20	83.1°	57.1°	89.3°	88.8°	88.3°	89.2°
20-30	81.3°	66.8°	89.8°	89.8°	89.4°	89.9°
30-40	79.5°	73.1°	89.8°	89.9°	88.8°	89.9°
40-50	77.7°	74.9°	89.9°	90.0°	88.4°	90.0°
50-60	77.3°	73.8°	89.8°	89.9°	88.0°	89.9°
60-70	77.0°	73.6°	89.7°	89.9°	87.5°	89.9°
70-80	74.7°	74.0°	89.7°	89.9°	87.1°	89.9°

Table 8.3: *Contact angle from several biochar obtained from comparison of water absorption velocity for water and hexane during 100 s.*

a common collaboration. However, the evaluation and correlation with other biochar properties characterized in the present work, as well as with the production conditions, is a topic of the present work. Part of these results, in particular PW600-20 (ID), PW400-20 (ID), CD600-20 (EU), CD400-20 (EU), BW600-20 (ID) and BW340-50 (ID), will be published in a paper with the title "Biochar stability characterization by hydropyrolysis and pyrolysis-GC/MS" (in preparation for submission), in which I will be co-author. In this paper, the stability of these biochar samples, determined according to two different methods, is compared, and the results of PAHs content are included for further characterization of the sample. In the present work, these results are also included to have a better comparison of biochar PAHs content behavior, according to physical distribution inside the reactor bed. That is to say, they belong to the same experiments as the rest of the results presented in this thesis, but taken from different parts of the bed.

According to the European Biochar Certificate [41], the biochar PAH content, which is defined as the sum of the EPA (US Energy Protection Agency) 16 priority pollutants, must be under 12 mg/kg for basic grade biochar and below 4 mg/kg for premium grade biochar.

If the results shown in Chapter 5 and 6 are considered, PAHs can be produced during pyrolysis, even at temperatures as low as 400 °C, due to secondary reactions inside the solid matrix. They are not definitely one of the main products of pyrolysis at such temperatures (for example Fagernäs et al. [100] reported yields ranging from 0.1 - 0.4 %wt of the tar yield in slow pyrolysis, at a final pyrolysis temperature of 500 °C), but their presence in biochar may be high enough to advise against its use in soil.

This PAHs content in the char is dependent on the process conditions, mainly maximum temperature reached in the process, feedstock and mass transport limitations due to potential enhancement of heterogeneous secondary reactions. For example, as reported

in Chapter 6, the emission of PAHs (detected in the vapor phase) for pine wood chips starts when the temperatures inside the solid bed ranges between 300 - 350 °C (Fig. 6.3, f)); being at those temperatures 2-ring aromatic compounds the main species. This is in good agreement with the results shown in Fig. 8.10 and 8.11, where it is already observable that at 340 °C PAHs species are present in the biochar from beech wood, being naphthalene the most significant species. At higher temperatures (400 °C for biochar coming from pine wood), the presence of PAHs increases, for two main reasons: more volatiles are produced, which can further react in the solid matrix and, at those temperatures, these secondary reactions could be also enhanced. However, when the temperature further increases to 600 °C the presence of PAHs decreases significantly. At those temperatures almost no more volatiles, which can further react, are being produced and the temperatures are also high enough to evaporate a good part of the PAHs still present in the solid matrix.

In both Fig. 8.10 and 8.11 results are shown for bottom (ID, ED) and top (EU, IU) of the reactor bed. It can be seen that for pine wood the PAHs content is always higher at the bottom of the reactor. This is due to the fact that the temperatures are always lower in this position, as consequence of the heat transport phenomena behavior inside the reactor. For the experiment at 400 °C (this temperature is measured in the reference position at 10 cm from the bottom of the reactor), the lowest of the maximum reached temperatures (at the end of the experiment) was 360 °C (temperature measured at the inlet of the bed). Therefore, the temperatures correspondent to the sample bottom would be between 360-400 °C. On the other hand, the average temperature of the gas phase above the bed is 575 °C. Consequently, the sample correspondent to the top of the reactor would have a minimum temperature of 400 °C and could go up to a maximum temperature of 575 °C. At those temperatures, the evaporation of volatiles from the sample is already significant and that could explain the lower content. For 600 °C the temperature correspondent to the sample from the bottom of the reactor would range between 580 - 600 °C, while the temperature in the gas phase is 700 °C, so the temperature for the top sample could range from 600 °C up to a maximum possible temperature of 700 °C. Evaporation could explain the low content in PAHs of the sample at the top of the reactor.

With respect to beech wood, the values at the top and bottom of the reactor are similar for both temperatures 340 and 600 °C, being at 600 °C the PAHs total content for the bottom of the reactor very similar to the ones of pine wood biochar produced in similar conditions. This is due to the fact that the temperatures are similar. At the top of the reactor, however, the PAHs content is higher in the case of beech wood samples. This could be explained by the fact that the temperature of the gas phase in the beech wood experiments at 600 °C is 630 °C. At that temperature, less PAHs could be evaporated in comparison with pine wood (maximum possible temperature of 700 °C). Besides, the

particle size is bigger in the case of the beech wood samples, enhancing therefore mass transport limitations. For the experiment of 340 °C, the axial temperature gradient is 10 °C, hence the similarity in temperatures would explain the similarity in PAHs content.

For corn digestate, however, the trend is the opposite, being the PAHs content always higher at the top of the reactor. In both cases the temperatures were also higher at the top than at the bottom of the reactor, suggesting that the pyrolysis mechanism behind the formation of PAHs is different in this case and it is shifted to higher temperatures. It must be taken also into account that the ash content in the corn digestate biochar is very high, with values around 40 %wt in dry basis. Since the volatiles are produced in the organic phase, to compare the total PAHs in the same basis for corn digestate and wood biochars (volatiles % wt,daf), the PAHs content in the case of corn digestate should be multiplied by an approximate factor of 1.7. This leads to higher PAHs concentration in corn digestate than in pine or beech wood for all the cases, except bottom reactor at 400 °C in pine wood. This different behavior in the PAHs content could be explained by the ash content and the nature of this ash.

To know more about these PAHs, in Fig. 8.11 the quantitative characterization is presented. It is of high interest the variations in composition, above all for samples coming from pine wood and from corn digestate. The most significant result is the fact that in biochar from pine wood at 400 °C, the main PAH species is phenanthrene followed by other species such as fluoranthene and pyrene. This means that even at those low temperatures, 3- and 4-ring aromatic compounds are being produced. At higher temperatures, naphthalene is the main species, at it is for beech wood. The fact that at 340 °C the presence of bigger PAHs for beech wood is very reduced could be explained by the still too low temperatures for the formation of these compounds. In the case of corn digestate, naphthalene is for all the conditions the most abundant PAH, with a significant difference over the other species. This reaffirms the different mechanisms in formation of such species for both types of biomass.

Regarding to the application of biochar to soil, while in almost all the cases a basic grade biochar is obtained, it can be concluded that for a high quality biochar temperatures close to 600 °C must be reached.

8.7 Stability

The pyrolysis-GC-MS analysis presented in the this Section have been performed at the University of Bologna by Alessandro G. Rombola and Prof. Fabbri, as previously explained, as result of a common collaboration. These results will be published in a

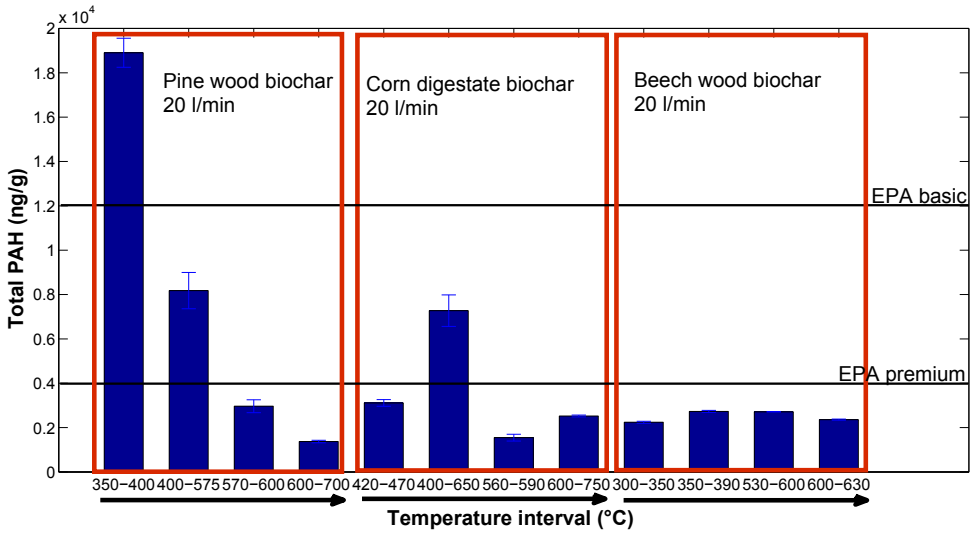

Figure 8.10: *Total PAHs content for biochar samples produced at different conditions from three different feedstocks. For each case, samples from the top and the bottom of the reactor are analyzed.*

paper with the title "Biochar stability characterization by hydropyrolysis and pyrolysis-GC-MS" (in preparation for submission), in which I will be co-author. In this paper, these two techniques to address biochar stability are compared, being the samples produced during the present work under investigation. These results will appear also in the PhD thesis of Alessandro G. Rombola (University of Bologna), since he develops an accumulative thesis (with journal publications). However, in this thesis, the objective is to relate the biochar stability with other biochar properties evaluated during the present work, as well as with the biochar feedstock and production conditions, and not to compare two techniques to address biochar stability.

As it has been previously said in Section 7.3.2 and 8.1, stability in soil is a very important property of biochar, since it determines its oxidation capacity and therefore its changes in surface properties but, above all, its capacity to retain carbon in soil. Studies to address stability in soil are not easy to perform, since they have to be carried out in a relatively short amount of time (several months to a couple of years) but give information about biochar evolution in hundreds of years. This is why so many studies are available, with different methodology and wide variety of results, as it has been reported by Spokas [172] in a review about the topic. However, results seem to indicate that it is possible to correlate the stability of biochar in soil with, at least, the O/C molar ratio [172]. In this way, biochars with a O/C molar ratio < 0.2 seems to account for a half life of at least 1000 years in soil. This has been analyzed for the biochars evaluated in the present work in Section 8.1. However, to get further in the correlation of this potential stability of biochar with its composition and structure, pyrolysis-GC-MS measurements have been included, where these biochars are further pyrolyzed up to 900 °C and the species produced are characterized with a GC-MS.

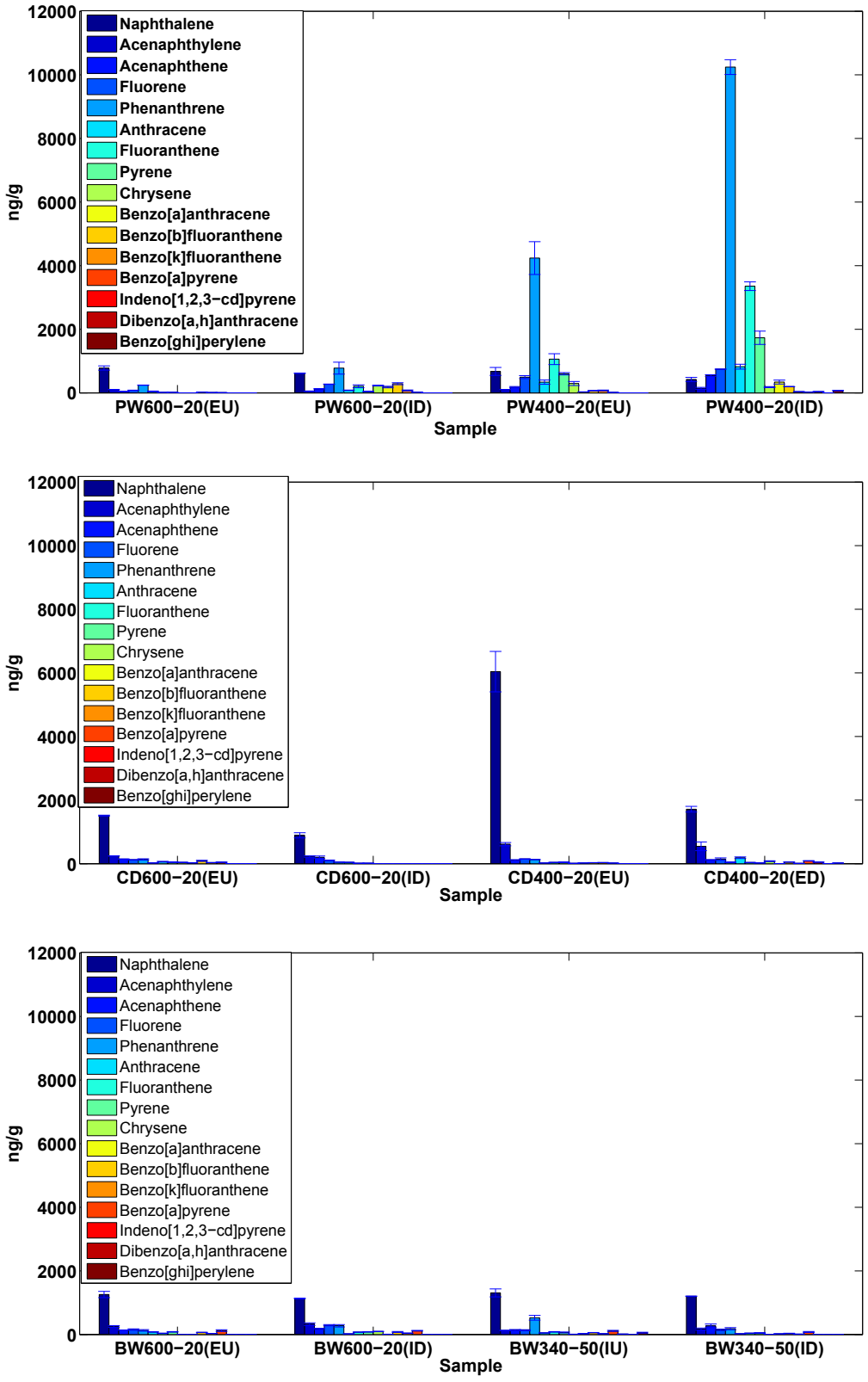

Figure 8.11: *PAHs species present in biochar produced from pine wood (top), corn digestate (middle) and beech wood (bottom) at different conditions.*

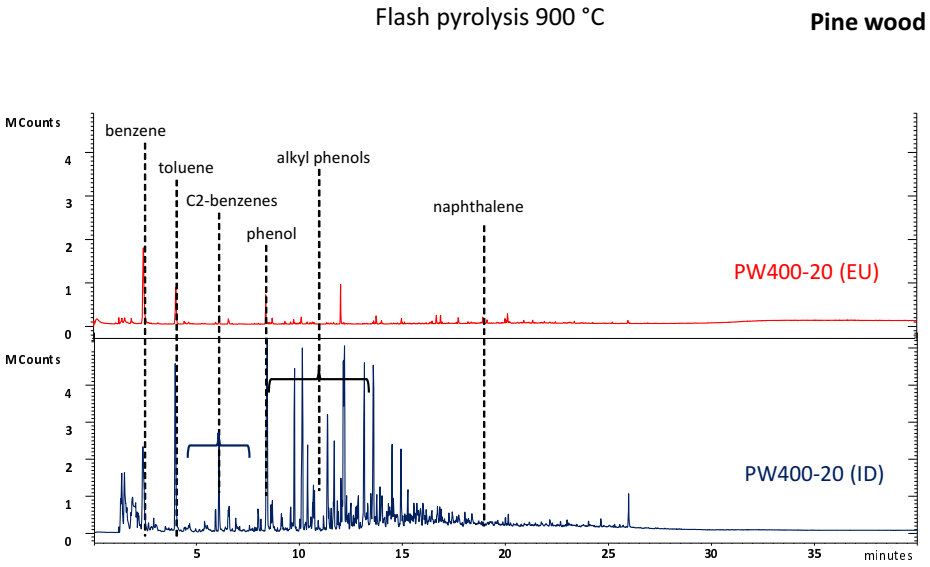

Figure 8.12: *Py-GC-MS analysis of pine wood biochar samples produced until a temperature of 400 °C (reference position). The samples are taken from the top and bottom of the reactor.*

Fig. 8.12 shows the results for biochars from pine wood produced at 400 °C from both positions inside the reactor, top (EU) and bottom (ID). These samples have a volatiles content of 13.78 %wt and 33.7 %wt in dry ash free basis, O/C molar ratios of 0.07 and 0.19 respectively and H/C molar ratios of 0.40 and 0.71. Those data are in accordance with the pyrograms, i.e., the volatile matter still present in the biochar sample is significantly higher in the case of PW400-20 (ID) and that would explain the release of those labile compounds, i.e. mostly alkyl phenols; while the pyrogram coming from the PW400-20 (EU) is quite clean, indicating a higher degree of carbonization already in the sample and, therefore, significantly lower lability of the biochar, also consistent with the O/C ratio of 0.07.

Fig. 8.13 shows the pyrograms for the four biochar samples produced from corn digestate, at both, 600 and 400 °C. The first thing that should be remembered here is that these samples have a quite high ash content, around 40 %wt, consequently, in order to compare these quantitative values with the ones from pine or beech wood, they should be multiplied by a factor of approximately 1.7. This is why the pyrograms seem more stable and clean, because they are represented with respect to the whole biomass sample, not only with respect to the organic phase. Nevertheless, both samples show already a high aromatization degree. This is also consistent with the results for H/C molar ratios shown in Fig. 8.2, where for similar volatiles content, the H/C

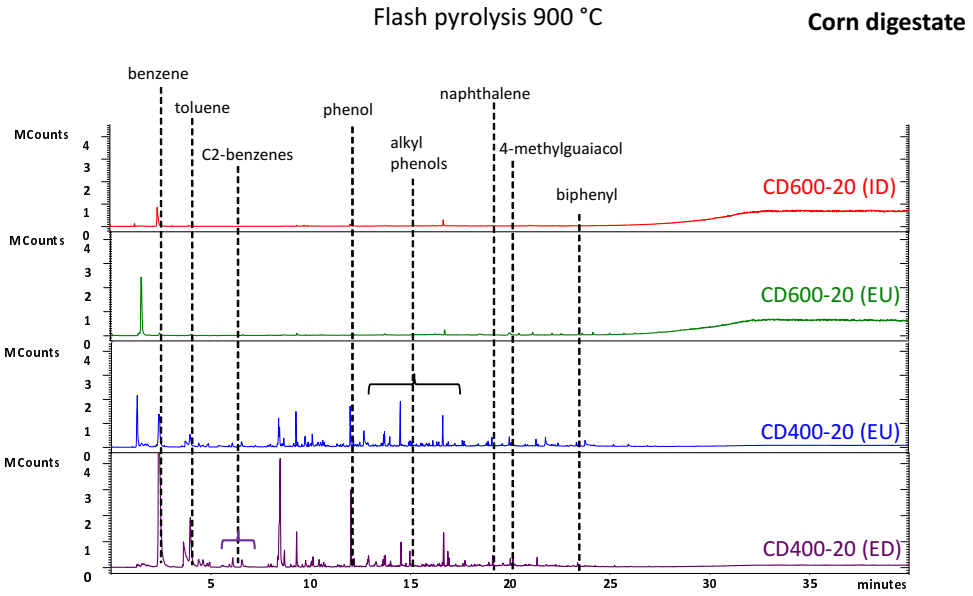

Figure 8.13: *Py-GC-MS analysis of corn digestate biochar samples produced until a temperature of 600 and 400 °C (reference position). The samples are taken from the top and bottom of the reactor.*

ratios were lower in the case of corn digestate than for any other sample, while the O/C ratios were in accordance with the other results. Therefore, with biomass with high ash content, less severity in the process is required to reach higher stability due to the inorganic phase. The question that may arise here is: where are then going all those volatiles detected for corn digestate biochar samples, since the pyrograms are so clean? This could indicate that a significant part of the volatiles content measured for corn digestate is not organic and, therefore, cannot detected in the Py-GC-MS, but inorganic, such as carbonates. These results would support then the explanation presented in Section 8.3 for the lower H/C ratios of corn digestate biochars, with the same volatiles content (%wt, daf), in comparison to woody biochars.

Fig. 8.14 shows the pyrograms for beech wood. It is interesting to notice that for the pyrograms at low temperatures, i.e., 340 °C for beech wood, despite the fact that they are dirty, i.e., still a lot of species are still released, showing a high degree of lability, these species are different in comparison with the pyrogram from pine wood biochar, with higher presence of compounds such as methyl-syringol, biphenyl or naphthalene, while in the case of pine wood biochar at lower temperatures, the main compounds are alkyl phenols. At 600 °C the pyrogram is almost clean, consistent with the volatiles content on 5.80 %wt, daf basis and the O/C and H/C ratios of 0.04 and 0.17 respectively.

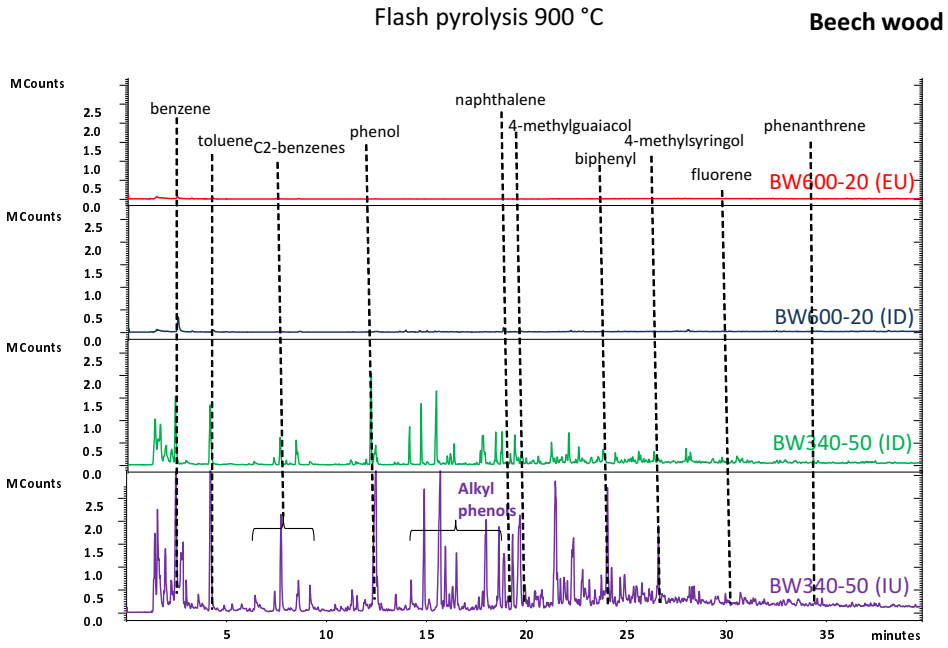

Figure 8.14: *Py-GC-MS analysis of beech wood biochar samples produced until a temperature of 600 and 340 °C (reference position). The samples are taken from the top and bottom of the reactor.*

8.8 Conclusions

Biochar samples were produced using several raw materials (agricultural residues, biowaste, wood and cellulose) at different pyrolysis conditions, with the objective of having an array of samples able to simulate a wide range of potentially produced and marketed biochars nowadays.

Several properties of these biochars have been characterized. These could be divided in primary characterization, i.e., minimum set of properties that need to be addressed to determine that the sample is indeed biochar and not only partially charred organic matter; and advanced characterization, that is to say, those properties that give more information about the physical and chemical structure of biochar and can work as a relation link between primary characterization (related to the feedstock and pyrolysis conditions) and biochar application. Primary characterization would include H/C and O/C ratios, volatiles, and ash content while advanced characterization would encompassed pH, surface functional groups and porosity distribution. Finally another set of properties, which could be defined as application-related properties, have been evaluated, including potential PAH toxicity, stability and wettability.

The combination of production conditions, primary and advance characterization provides knowledge about how to produce biochar, and the application-related properties describes its possible behavior in soil. This information could be then used as feedback in the production process, so that biochar would be "engineered" for different sets of requirements regarding its application in soil.

Regarding primary characterization, it has been shown that O/C ratios present a linear behavior with respect to volatiles content (%wt, daf), independently of the pyrolyis conditions and feedstock, for a wide range of biochars. While in the case of H/C ratios, corn digestate presents different behavior (for all pyrolyis conditions) with respect to other biochars. This could be attributed to different pyrolysis pathways due to the high ash content of corn digestate, enhancing aromatization in the biochar. But it could be also related to a high inorganic fraction in the volatiles content. In this case, the low H/C ratio could be potentially correlated to a lower organic fraction of the volatiles. Consequently, the behavior of the H/C ratio in corn digestate biochars would be more similar to the one for woody biochars. Py-GC-MS results of the corn digestate biochars are quite clean, i.e., almost no labile species are released. That is related to the high ash content of these biochars, but could also support the idea of a relevant inorganic fraction in the volatiles content, since they would not be detected by the Py-GC-MS, when further pyrolyzed up to 900 °C.

In the case of pH, it shows a clear dependence on both, process severity, and therefore carbonization degree (represented with the volatiles content), and initial feedstock, distinguishing between low and high ash content feedstock. Values ranging from 4 to almost 13 were obtained. A good correlation has been also observed between biochar pH and biochar surface functional groups: the lower the acidic functional groups content, the higher the pH.

Porous structure varies greatly among biochars. While woody biochars produced at 600 °C present typically micropore structure with total specific surface areas around 400 m^2/g; in chars produced from corn digestate this microporosity is not present in most cases. Woody biochars produced at 400 °C present also micropores, but much less developed than higher temperature woody biochars, i.e., microporosity must be still developed through volatiles release, to open the pores, and further solid aromatization. The explanation for the lack of microporosity in corn digestate biochars is attributed to the high inorganics content which could potentially block the pores. It has been also shown that higher N_2 sweeping flow during the pyrolysis process, leading to a lower retention time and concentration of volatiles in contact with the solid matrix, enhance microporosity development (from below 20 m^2/g up to 100 m^2/g for corn digestate biochars produced at 600 °C with 20 and 40 l/min flow respectively). This indicates that micropores blocking is related to volatiles which, due to the high concentration and retention time, may further react to form secondary char or condense in the pores. The

fact that this phenomenon is also that significant in corn digestate biochars, suggests that pore blocking is also related to volatiles. High ash content enhances, moreover, mesoporosity development. Besides pore size characterization, assessment of diffusion limitations during the measurement and relation to the production conditions has been performed. These transport limitations lead to false results interpretation if not taking into account and make the results only significant from a relative perspective, rather than provide absolute values. As far as the author is aware of, the influence of flow rate, the development of mesoporosity due to high ash content and the assessment of transport limitations are here reported for the first time in the field of biochar.

Both pH and porous structure seem to have an impact on char wettability. The more acidic the biochar surface, the lower the capacity to absorb water. Besides, the higher the diffusion limitations inside the biochar sample, the lower the capacity to absorb water. However, microporosity does not seem to play a role in this case, since the biochars with no microporosity absorb the same quantitiy of water as those with microporosity. With the same production conditions, corn digestate biochars show significantly lower hydrophobicity (lower contact angle) than woody biochars. This seems to indicate that pH and surface functionality are the determining properties, having basic biochars better wettability.

Finally, regarding the presence of PAHs, it has been shown that at temperatures as low as 340 °C, PAHs are already produced. Then, for temperatures around 400 °C, the maximum quantity of PAHs is detected in the biochar sample, overcoming the maximum level of admitted PAHs content for pine wood biochar. At higher temperatures, the PAHs content is reduced again, due to vaporization of these species from the solid matrix. At temperatures above 550 °C, premium quality biochar, regarding PAHs content, can be produced. The composition of these species is also completely different depending on the feedstock, while naphthalene is the main species in corn digestate biochar, phenanthrene and fluoranthene are the main species in pine wood biochars at low temperature. This seems to indicate different formation pathways of these compounds, depending on the feedstock composition.

Knowledge gained on detailed pyrolysis mechanisms, specially with respect to the presence of secondary reactions, has been also key to understand the results obtained for biochar characterization.

In Fig. 8.15 this conclusions are also summarized. Biochar should be produced at temperatures above 550 °C, independently of the initial feedstock, to guarantee the quality criteria of H/C and O/C ratios and PAHs content. N_2 flow during the pyrolysis process would significantly enhance microporosity evolution. If biochar is produced with the final goal of increasing water holding capacity, biochars with relatively high ash content should be preferred, since they present lower hydrophobicity. This characteristic would

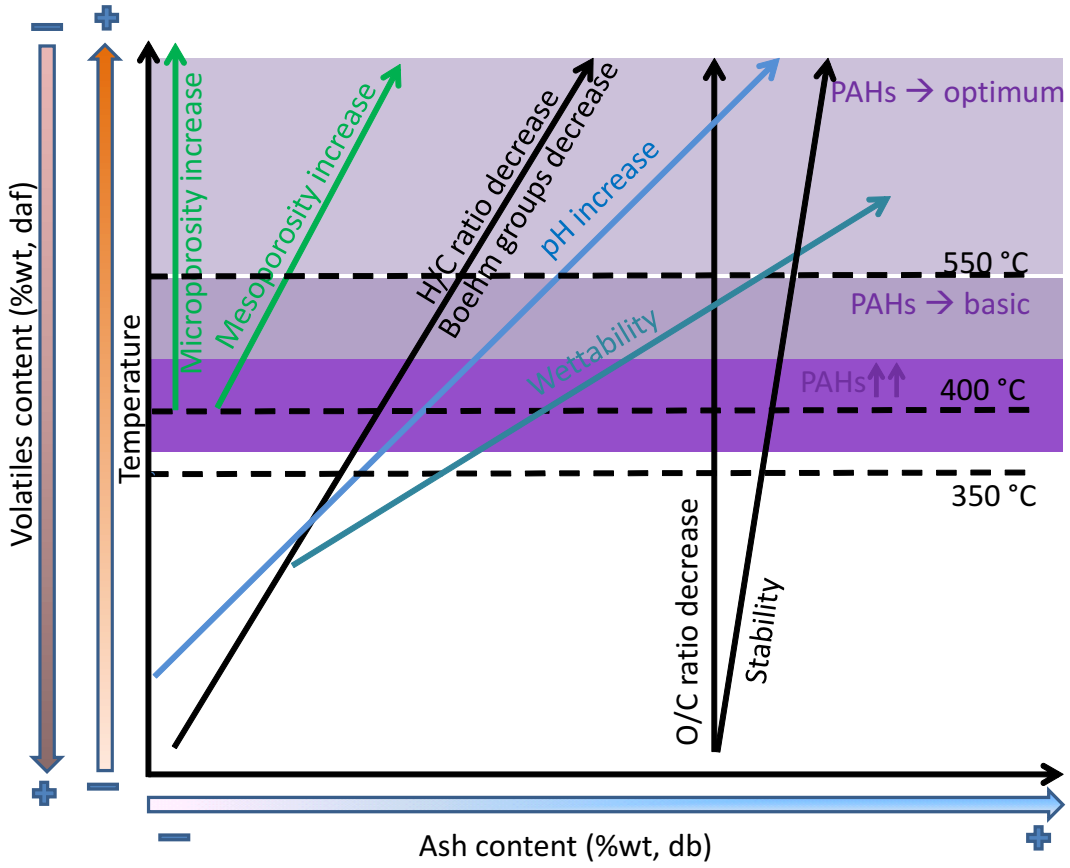

Figure 8.15: *Conclusions from biochar characterization*

also affect to other properties related to water dynamics. These conclusions can be applied to "engineer" appropriate biochars with respect to soil demands and certification requirements, as well as to improve biochar certification.

Chapter 9

Summary

Two were the main objectives of this thesis: to get a deeper understanding of slow pyrolysis conversion of lignocellulosic materials in conditions similar to the ones present at industrial scale, by contributing to the development of detailed pyrolysis mechanisms, with focus on heterogeneous secondary reactions and the pathways leading to the formation of polyaromatic hydrocarbons (PAHs); and to evaluate this process as a potential way of producing biochar for soil amendment and carbon sequestration.

To this end, a technical-scale fixed-bed reactor was built to perform on-line characterization of the transitory evolution of the pyrolysis process through temperatures and permanent gas composition characterization, as well as LIF spectroscopic analysis of species potentially able to emit fluorescence under the measurement conditions applied in this work.

Besides, several characterization techniques were developed to address biochar properties and behavior in order to correlate process conditions with biochar properties and its potential applications. When needed, external collaborations were established to address both, validity of some characterization techniques or to let new biochar properties be analyzed.

Regarding on-line pyrolysis characterization, the major contribution of this work was the detection of heterogeneous secondary reactions, enhanced by larger residence time of produced volatiles in contact with the solid matrix, resulting in the production of PAHs. With the combination of both techniques, GC-TCD and LIF spectroscopy, it was possible to discriminate between primary pyrolysis and secondary reactions of primary volatiles, with this second stage characterized by the enhancement of CH_4 and PAHs production including 2-, 3- and 4-ring aromatic compounds. Increase in volatiles concentration and residence time in contact with the solid matrix led to increase in gas yields at the expense of liquid yields. The exothermic character of these secondary reactions was also addressed. As far as the author is aware of, it is the first time that LIF spectroscopy has been applied to qualitatively follow the emission of PAHs during

slow pyrolysis in a technical-scale reactor, as a pathway to address the presence and enhancement of heterogeneous secondary reactions.

To further understand the origin of these observations, further investigation on the pyrolysis mechanism of lignocellulosic materials was performed. For that, holocellulose and lignin, the main macromolecules present in lignocellulosic materials, were considered, as well as wood and washed wood, where alkali and other metals content is reduced. Based on the experimental results, a pyrolysis mechanism was proposed. Briefly, hollocellulose would be the major source of volatiles products. Primary holocellulose decomposition would produce small char yields, CO, small quantities of CO_2 and CH_4. Secondary reactions of primary volatiles would lead to increased char yields and significant release of CO_2. With the release of CO_2, 2-ring aromatic compounds (PAH) such as naphthalene, would be also produced, according to the LIF spectroscopic analysis. Other species containing carbonyl structures would also contribute to the total fluorescence signal. Lignin would be the major contributor to char yields, as well as to PAHs species. During primary devolatilization, mainly 1-ring aromatic compounds (phenolics), together with 2-ring aromatic compounds (PAHs), would be released. In this zone CO_2 would be also formed. At higher temperatures, heterogeneous secondary reactions would become significant, being coincident with the onset in the emission of CH_4, CO and H_2, and giving place to a shift in the fluorescence spectra to longer wavelengths due to the formation of PAHs with three and four rings. For pine wood, fluorescence signal presented two stages: an early one, at low temperatures, attributed to the release of species with carbonyl functional groups present in extractives or hemicellulose. This signal would be observed also occasionally in holocellulose. And a second stage attributed to the formation of PAHs. Wood pretreatment with HCl and distilled water or heptane, as organic solvent, showed that the early fluorescence signal does not come from extractives susceptible of dissolving in these substances. However, it was observed that this washing had a direct impact on the LIF signal correspondent to PAHs emission, being reduced. This would be related to the fact that this washing removed partially the alkali and other metals content in wood, which are known to enhance secondary reactions. Future work is needed to precisely identify the source of the early fluorescence signal. The results regarding PAHs emissions, qualitatively detected by LIF spectroscopy, were further confirmed by GC-MS analysis. This knowledge on pyrolysis conversion has been crucial to understand biochar responses to process conditions.

Regarding biochar production and characterization, the first step was the development of several characterization techniques to address biochar properties. Of special significance was the development and knowledge achieved in porosity characterization. In this field, the author took part in the EU COST Action TD1107 'Biochar as option for sustainable resource management', as previously explained. With respect to the

results presented here, it has been shown that temperatures above 550 °C in the production process are required to fulfill most of the biochar quality criteria described in the European Biochar Certificate. Besides, the utilization of N_2 during the production process would increase significantly biochar quality, regarding microporosity evolution and char wettability. It has been also shown that pH value in biochar correlates with both, acidic surface functional groups and ash content, and it seems to be the most determining parameter in biochar wettability. At the same time, ash content in biochars hinders microporosity development while enhancing mesopore formation. With respect to potential toxicty of biochar in soil due to PAHs content, it has been also shown that with production temperatures above 550 °C, premium quality biochar is guaranteed. As far as the author is aware of, the relations between flushing flow and biochar microporosity, as well as between biochar ash content and mesoporosity development, have been characterized for the first time in the present work. These conclusions can be applied to "engineer" appropriate biochars with respect to soil demands and certification requirements, as well as to improve biochar certification.

9.1 Future work

Further investigation on the effect of process conditions on products yields and compositions, including further quantitative characterization, is required, due to the fraction of volatiles that can neither be measured on-line nor condensed with the current equipment. To complete this, experiments will be performed in the near future in an external institution where a FTIR will be attached to the reactor for on-line characterization of light volatiles. Besides, information about the water yields is required, as well as on the elemental balances of the process.

These experimental results will be used for validation of a mathematical model previously developed in this research group [15].

Further development in the LIF system, firstly to avoid self-absorption due to high volatiles concentrations, and secondly to be able to reach semi-quantitative values, is required.

Regarding biochar, further investigation with alternative adsorptive species which present lower diffusion limitation, for example CO_2, will be performed to gain more knowledge on the biochar porous structure. Further investigation on the surface functionalities, specially regarding cation exchange capacity (CEC) will be also performed.

Publications

Part of the contents of the present thesis have been already published in the following peer-reviewed papers:

1. A. Dieguez-Alonso, A. Anca-Couce, N. Zobel, F. Behrendt (2015). Understanding the primary and secondary slow pyrolysis mechanisms of holocellulose, lignin and wood with laser-induced fluorescence, Fuel, 153, 102-109.

2. A. Dieguez-Alonso, A. Anca-Couce, N. Zobel, (2013). On-line tar characterization from pyrolysis of wood particles in a technical-scale fixed-bed reactor by applying Laser-Induced Fluorescence (LIF), Journal of Analytical and Applied Pyrolysis, 102 (2013) 33-46.

Bibliography

[1] I. Obernberger, G. Thek, Combustion and gasification of solid biomass for heat and power production in europe - state-of-the-art and relevant future developments, in: Proceedings of the 8th European Conference on Industrial Furnaces and Boilers, April 2008, Vilamoura, Portugal.

[2] U. Henriksen, J. Ahrenfeldt, T. K. Jensen, B. Gobel, J. D. Bentzen, C. Hindsgaul, L. H. Sorensen, The Design, construction and operation of a 75 kW two-stage gasifier, Energy 31 (10-11) (2006) 1542–1553. doi:10.1016/j.energy.2005.05.031.

[3] Wellons Fei Corp, Manufacturer of Wood Heat Systems and Wood Boiler Equipment, Website, Online available at: http://www.wellonsfei.ca/. Last accessed 08.05.2015.

[4] N. Zobel, A. Anca-Couce, Slow pyrolysis of wood particles: Characterization of volatiles by Laser-Induced Fluorescence, Proceedings of the Combustion Institute 34 (2013) 2355 – 2362. doi:10.1016/j.proci.2012.06.130.

[5] M. Asmadi, H. Kawamoto, S. Saka, Thermal reactivities of catechols/pyrogallols and cresols/xylenols as lignin pyrolysis intermediates, Journal of Analytical and Applied Pyrolysis 92 (1) (2011) 76–87. doi:10.1016/j.jaap.2011.04.012.

[6] R. Sun, Analysis of gas-phase polycyclic aromatic hydrocarbon mixtures by laser-induced fluorescence, Ph.D. thesis, Technische Universität Berlin, ISBN: 978-3-938720-81-3 (2010).

[7] F. Cignoli, G. Zizak, S. Benecchi, D. Tencalla, Atlas of Fluorescence Spectra of Aromatic Hydrocarbons. Vol. I, Tech. rep., Istituto Tecnolgie dei Materiali e dei Processi Energetici (TeMPE), CNR, Milano, Italy (2004).

[8] M. de Joannon, R. Ragucci, A. Cavaliere, A. Ciajolo, Identification of oxygenated compounds in combustion systems, Chemosphere 42 (5-7) (2001) 843

– 851, Proceedings of the 6th Intl Congress on Toxic combustion . doi:10.1016/S0045-6535(00)00259-9.

[9] European Biochar Research Network. Biochar as option for sustainable resource management, Website, Online available at: http://cost.european-biochar.org. Last accessed 27.11.2015.

[10] M. Keiluweit, P. S. Nico, M. Johnson, M. G.and Kleber, Dynamic Molecular Structure of Plant Biomass-Derived Black Carbon (Biochar), Environ. Sci. Technol. 44 (4) (2010) 1247–1253. doi:10.1021/es9031419.

[11] K. S. W. Sing, D. H. Everett, R. A. W. Haul, L. Moscou, R. A. Pierotti, J. Rouquerol, T. Siemieniewska, Reporting physisorption data for gas/solid systems with special reference to the determination of surface area and porosity, Pure and Applied Chemistry 57 (4) (1985) 603–619. doi:10.1351/pac198557040603.

[12] European Commission, Climate Action, 2020 climate & energy package, Website, Online available at: http://ec.europa.eu/clima/policies/strategies/2020. Last accessed 05.10.2015.

[13] European Commission, Climate Action, 2050 low-carbon economy, Website, Online available at: http://ec.europa.eu/clima/policies/strategies/2050. Last accessed 05.10.2015.

[14] Directive 2009/28/EC of the European Parliament and of the Council of 23 April 2009 on the promotion of the use of energy from renewable sources and amending and subsequently repealing Directives 2001/77/EC and 2003/30/EC, The European Parliament and the Council of the European Union, [2009] O.J. L 140/16.

[15] A. Anca-Couce, Multi-scale approach to describe fixed-bed thermo-chemical processes of biomass, Ph.D. thesis, Technische Universität Berlin, ISBN: 978-3-943685-28-2 (2012).

[16] M. Kaltschmitt, H. Hartmann, H. Hofbauer (Eds.), Energie aus Biomasse. Grundlagen, Techniken und Verfahren, Springer-Verlag Berlin Heidelberg, 2009, ISBN: 978-3-540-85095-3.

[17] P. Basu, Biomass Gasification and Pyrolyis. Practical Design, Elsevier Inc., 2010, ISBN: 978-0-12-374988-8.

[18] European Commission, Commission staff working document. State of play on the sustainability of solid and gaseous biomass used for electricity, heating and cooling in the EU, SWD (2014) 259 final, 28 July 2014.

[19] Sjaak van Loo and Jaap Koppejan (Ed.), The Handbook of Biomass Combustion & Co-firing, Earthescan in the UK and USA, 2010, ISBN:978-1-84971-104-3.

[20] I. Obernberger, The present state and future development of industrial biomass combustion for heat and power generation, in: ASME-ATI-UIT 2010, Conference on Thermal and Environmental Issues in Energy Systems, 16-19 May 2010, Sorrento, Italy.

[21] I.E.A. Bioenergy, Potential Contribution of Bioenergy to the World´s Future Energy Demand, IEA Bioenergy. ExCo: 2007:02.Online available at: http://www.ieabioenergy.com/publications/potential-contribution-of-bioenergy-to-the-worlds-future-energy-demand/. Last accessed 08.10.2015.

[22] T. Nussbaumer, Overview on Technologies for Biomass Combustion and Emission Levels of Particulate Matter, prepared for Swiss Federal Office for the Environment (FOEN) as a contribution to the Expert Group on Techno-Economic Issues (EGTEI) under the Convention on Long-Range Transboundary Air Pollution (CLRTAP), Tech. rep., Verenum. Ingenieurbüro für Verfahrens-, Energie- und Umwelttechnik (June 2010).

[23] H. Jüntgen, K. H. Heek, Kohlevergasung. Grundlage und technische Anwendung, Verlag Karl Thiemig, 1981, ISBN: 3521061361.

[24] J. Brandin, M. Tuner, I. Odenbrand, Small Scale Gasification: Gas Engine CHP for Biofuels, Linnaeus University, Växjö, 2011, ISBN: 978-91-86983-07-9 .

[25] H. Knoef (Ed.), Handbook Biomass Gasification, Second Edition, BTG Biomass Technology Group BV, The Netherlands, 2012, ISBN: 978-90-819385-0-1.

[26] I. Ridjan, B. V. Mathiesen, D. Connolly, A review of biomass gasification technologies in Denmark and Sweden, Tech. rep., Department of Development and Planning, Aalborg University, ISBN: 978-87-91404-54-2 (2013).

[27] ECN, MILENA Biomass Gasification process, Website, Online available at: http://www.milenatechnology.com. Last accessed 26.04.2015.

[28] Göteborg Energi, Gobigas, Website, Online available at: http://gobigas.goteborgenergi.se/English_version/The_plant. Last accessed 13.04.2015.

[29] Bioliq. Biomass to Liquid Karlsruhe, The bioliq Process, Website, Online available at: http://www.bioliq.de/english/55.php. Last accessed 10.10.2015.

[30] C. DiBlasi, Combustion and gasification rates of lignocellulosic chars, Progress in Energy and Combustion Science 35 (2) (2009) 121 – 140. doi:10.1016/j.pecs.2008.08.001.

[31] B. B. Uzun, N. Sarioglu, Rapid and catalytic pyrolysis of corn stalks, Fuel Processing Technology 90 (5) (2009) 705 – 716. doi:10.1016/j.fuproc.2009.01.012.

[32] M. Asadullah, M. Rahman, M. Ali, M. Rahman, M. Motin, M. Sultan, M. Alam, Production of bio-oil from fixed bed pyrolysis of bagasse, Fuel 86 (16) (2007) 2514 – 2520. doi:10.1016/j.fuel.2007.02.007.

[33] C. Branca, P. Giudicianni, C. DiBlasi, GC/MS Characterization of Liquids Generated from Low-Temperature Pyrolysis of Wood, Ind. Eng. Chem. Res. 42 (14) (2003) 3190–3202. doi:10.1021/ie030066d.

[34] I.E.A. Bioenergy, Task 34 - Pyrolysis, Website, Online avilable at: http://www.pyne.co.uk. Last accessed 13.04.2015.

[35] European Biomass Industry Association (EUBIA), Pyrolysis, Website, Online available at: http://www.eubia.org/index.php/about-biomass/. Last accessed 26.05.2015.

[36] BTG, Biomass Technology Group, Fast Pyrolysis, Website, Online available at: http://www.btgworld.com/en/rtd/technologies/fast-pyrolysis. Last accessed 12.10.2015.

[37] Empyro, Energy & Materials from Pyrolysis, Website, Online available at: http://www.empyroproject.eu/. Last accessed 12.10.2015.

[38] I.E.A. Bioenergy, Task 34 - Pyrolysis, Country Report - Finland, Online available at: http://www.pyne.co.uk/?_id=122. Last accessed 12.10.2015 (November 2014).

[39] European Biofuels, Technolgy Platform, Bio-oil (via pyrolysis / thermochemical conversion) and Tall Oil for production of advanced biofuels, Website, Online available at: http://www.biofuelstp.eu/bio-oil.html. Last accessed 15.12.2015.

[40] EBC Foundation/Certificate. EBC certified producers, Website, Online available at: http://www.european-biochar.org/en/producer. Last accessed 26.10.2015.

[41] European Biochar Foundation (EBC), Arbaz, Switzerland. EBC (2012) "European Biochar Certificate - Guidelines for a Sustainable Production of Biochar", Website, Online available at: http://www.european-biochar.org/en/download%20the%20certificate. Last accessed 08.06.2015.

[42] Carbon Terra GmbH, Website, Online available at: http://www.carbon-terra.eu/de. Last accessed 26.10.2015.

[43] Pyreg GmbH, Unternehmen Klimaschutz, Online available at: www.pyreg.de. Last accessed 26.10.2015.

[44] Swiss Biochar GmbH, Website, Online available at: www.swiss-biochar.com. Last accessed 09.06.2015.

[45] Verora GmbH, Ressourcenschonende Naturezeugnisse, Website, Online available at: http://www.verora.ch. Last accessed 26.10.2015.

[46] Sonnenerde, Online avilable at: www.sonnenerde.at. Last accessed 09.06.2015.

[47] Lixhe Compost SA, Website, Online available at: http://lixhe-compost.gandi.ws. On the 26.10.2015 the website was still under construction.

[48] Fetzer Rohstoffe + Recycling GmBH, Website, Online available at: www.fetzerohstoffe.de. On the 26.10.2015 the website was still under construction.

[49] H. P. Schmidt, Pflanzenkohle, eine Schlüsseltechnologie zur Schließung der Stoffkreisläufe, Ithakajournal. Winbau Ökologie Klimafarming 1|2012 (2012) 75–79.

[50] International Biochar Initiative (IBI). Biochar companies and organizations (compiled september 2012 by Erich Knight), Website, Online available at: http://www.biochar-international.org/company_list. Last accessed: 26.10.2015.

[51] Regenis, BioEnergieTechnologie. Regenerative Energie Wirtschaftssysteme GmbH, Website, Online available at: www.rewenergy.de. Last accessed 26.10.2015.

[52] BlackCarbon A/S, Black Carbon. A Biochar Technology, Website, Online available at: http://www.blackcarbon.dk. Last accessed 25.10.2015.

[53] Biomacon GmbH, Website, Online available under: www.biomacon.com. Last accessed 07.06.2015.

[54] Splainex, Website, Online available at: http://www.splainex.com/. Last accessed 26.10.2015.

[55] A. Dieguez-Alonso, A. Anca-Couce, N. Zobel, On-line tar characterization from pyrolysis of wood particles in a technical-scale fixed-bed reactor by applying Laser-Induced Fluorescence (LIF) , Journal of Analytical and Applied Pyrolysis 102 (0) (2013) 33 – 46. doi:10.1016/j.jaap.2013.04.005.

[56] A. Dieguez-Alonso, A. Anca-Couce, N. Zobel, F. Behrendt, Understanding the primary and secondary slow pyrolysis mechanisms of holocellulose, lignin and wood with laser-induced fluorescence, Fuel 153 (2015) 102–109. doi:10.1016/j.fuel.2015.02.097.

[57] J. E. White, W. J. Catallo, B. L. Legendre, Biomass pyrolysis kinetics: A comparative critical review with relevant agricultural residue case studies, Journal of Analytical and Applied Pyrolysis 91 (1) (2011) 1 – 33. doi:10.1016/j.jaap.2011.01.004.

[58] S. Sensöz, M. Can, Pyrolysis of Pine (Pinus Brutia Ten.) Chips: 1. Effect of Pyrolysis Temperature and Heating Rate on the Product Yields, Energy Sources 24 (4) (2002) 347–355. doi:10.1080/00908310252888727.

[59] K. Raveendran, A. Ganesh, K. C. Khilar, Pyrolysis characteristics of biomass and biomass components, Fuel 75 (8) (1996) 987 – 998. doi:10.1016/0016-2361(96)00030-0.

[60] C. Di Blasi, Kinetic and Heat Transfer Control in the Slow and Flash Pyrolysis of Solids, Ind. Eng. Chem. Res. 35 (1) (1996) 37–46. doi:10.1021/ie950243d.

[61] A. Anca-Couce, N. Zobel, H. A. Jakobsen, Multi-scale modeling of fixed-bed thermo-chemical processes of biomass with the representative particle model: Application to pyrolysis, Fuel 103 (0) (2012) 773–782. doi:10.1016/j.fuel.2012.05.063.

[62] B. Peters, E. Schröder, C. Bruch, Measurements and particle resolved modelling of the thermo- and fluid dynamics of a packed bed, Journal of Analytical and Applied Pyrolysis 70 (2) (2003) 211–231. doi:10.1016/S0165-2370(02)00133-X.

[63] M. Antal, M. Gronli, The art, science, and technology of charcoal production, Industrial & Engineering Chemistry Research 42 (8) (2003) 1619–1640. doi:10.1021/ie0207919.

[64] I. Milosavljevic, V. Oja, E. M. Suuberg, Thermal effects in cellulose pyrolysis: Relationship to char formation processes, Industrial Engineering Chemistry Research 35 (3) (1996) 653–662. doi:10.1021/ie9504381.

[65] A. Anca-Couce, R. Mehrabian, R. Scharler, I. Obernberger, Kinetic scheme of biomass pyrolysis considering secondary charring reactions, Energy Conversion and Management 87 (0) (2014) 687 – 696. doi:10.1016/j.enconman.2014.07.061.

[66] C. D. Blasi, C. Branca, F. Masotta, E. D. Biase, Experimental Analysis of Reaction Heat Effects during Beech Wood Pyrolysis, Energy & Fuels 27 (5) (2013) 2665–2674. doi:10.1021/ef4001709.

[67] J. Rath, M. G. Wolfinger, G. Steiner, G. Krammer, F. Barontini, V. Cozzani, Heat of wood pyrolysis, Fuel 82 (1) (2003) 81–91. doi:10.1016/S0016-2361(02)00138-2.

[68] A. Galwey, Is the science of thermal analysis kinetics based on solid foundations? a literature appraisal, Thermochimica Acta 413 (1-2) (2004) 139–183. doi:10.1016/j.tca.2003.10.013.

[69] E. Ranzi, A. Cuoci, T. Faravelli, A. Frassoldati, G. Migliavacca, S. Pierucci, S. Sommariva, Chemical kinetics of Biomass Pyrolysis, Energy & Fuels 22 (6) (2008) 4292–4300. doi:10.1021/ef800551t.

[70] C. Di Blasi, Comparison of semi-global mechanisms for primary pyrolysis of lignocellulosic fuels, Journal of Analytical and Applied Pyrolysis 47 (1) (1998) 43 – 64. doi:10.1016/S0165-2370(98)00079-5.

[71] C. Di Blasi, Modeling chemical and physical processes of wood and biomass pyrolysis, Progress in Energy and Combustion Science 34 (1) (2008) 47 – 90. doi:10.1016/j.pecs.2006.12.001.

[72] R. J. Evans, T. A. Milne, Molecular characterization of the pyrolysis of biomass, Energy Fuels 1 (2) (1987) 123–137. doi:10.1021/ef00002a001.

[73] T. Hosoya, H. Kawamoto, S. Saka, Pyrolysis behaviors of wood and its constituent polymers at gasification temperature, Journal of Analytical and Applied Pyrolysis 78 (2) (2007) 328 – 336. doi:10.1016/j.jaap.2006.08.008.

[74] T. Fisher, M. Hajaligol, b. Waymack, D. Keellog, Pyrolysis behavior and kinetics of biomass derived materials, Journal of Analytical and Applied Pyrolysis 62 (2002) 331–349. doi:10.1016/S0165-2370(01)00129-2.

[75] M. Antal, G. Varhegyi, Cellulose pyrolysis kinetics: the current state of knowledge, Industrial & Engineering Chemistry Research 34 (3) (1995) 703–717. doi:10.1021/ie00042a001.

[76] G. Varhegyi, M. J. J. Antal, E. Jakab, P. Szaba, Kinetic modeling of biomass pyrolysis, Journal of Analytical and Applied Pyrolysis 42 (1) (1997) 73 – 87. doi:10.1016/S0165-2370(96)00971-0.

[77] M. G. Gronli, G. Varhegyi, C. Di Blasi, Thermogravimetric Analysis and Devolatilization Kinetics of Wood, Industrial & Engineering Chemistry Research 41 (17) (2002) 4201–4208. doi:10.1021/ie0201157.

[78] W.-C. R. Chan, M. Kelbon, K. B. B., Modelling and experimental verification of physical and chemical processes during pyrolysis of a large biomass particle, Fuel 64 (11) (1985) 1505 – 1513. doi:10.1016/0016-2361(85)90364-3.

[79] A. Broido, M. A. Nelson, Char Yield on Pyrolysis of Cellulose, Combustion and Flame 24 (1975) 263–268. doi:10.1016/0010-2180(75)90156-X.

[80] A. Broido, Kinetics of solid-phase cellulose pyrolysis, in: F. S. V. S. A. Tillman (Ed.), Thermal Uses and Properties of Carbohydrates and Lignins, Academic Press, 1976, pp. 19 – 36. doi:10.1016/B978-0-12-637750-7.50006-6.

[81] A. G. W. Bradbury, Y. Sakai, F. Shafizadeh, A kinetic model for pyrolysis of cellulose, Journal of Applied Polymer Science 23 (11) (1979) 3271–3280. doi:10.1002/app.1979.070231112.

[82] F. Shafizadeh, A. G. W. Bradbury, Thermal degradation of cellulose in air and nitrogen at low temperatures, Journal of Applied Polymer Science 23 (5) (1979) 1431–1442. doi:10.1002/app.1979.070230513.

[83] W. S. L. Mok, M. J. Antal, Effects of pressure on biomass pyrolysis. II. Heats of reaction of cellulose pyrolysis, Thermochimica Acta 68 (1983) 165 – 186. doi:10.1016/0040-6031(83)80222-6.

[84] J. Piskorz, D. S. A. G. Radlein, D. S. Scott, S. Czernik, Pretreatment of wood and cellulose for production of sugars by fast pyrolysis, Journal of Analytical and Applied Pyrolysis 16 (2) (1989) 127–142. doi:10.1016/0165-2370(89)85012-0.

[85] G. N. Richards, Glycolaldehyde from pyrolysis of cellulose, Journal of Analytical and Applied Pyrolysis 10 (3) (1987) 251 – 255. doi:10.1016/0165-2370(87)80006-2.

[86] G. Varhegyi, P. Szabo, W. S. L. Mok, M. J. Antal, Kinetics of the thermal decomposition of cellulose in sealed vessels at elevated pressures. Effects of the presence of water on the reaction mechanism, Journal of Analytical and Applied Pyrolysis 26 (3) (1993) 159 – 174. doi:10.1016/0165-2370(93)80064-7.

[87] V. Mamleev, S. Bourbigot, M. Le Bras, J. Yvon, The facts and hypotheses relating to the phenomenological model of cellulose pyrolysis: Interdependence of the steps, Journal of Analytical and Applied Pyrolysis 84 (1) (2009) 1 – 17. doi:10.1016/j.jaap.2008.10.014.

[88] T. R. Carlson, J. Jae, Y.-C. Lin, G. A. Tompsett, G. W. Huber, Catalytic fast pyrolysis of glucose with HZSM-5: The combined homogeneous and heterogeneous reactions, Journal of Catalysis 270 (1) (2010) 110 – 124. doi:10.1016/j.jcat.2009.12.013.

[89] C. Di Blasi, M. Lanzetta, Intrinsic kinetics of isothermal xylan degradation in inert atmosphere, Journal of Analytical and Applied Pyrolysis 40-41 (1997) 287 – 303. doi:10.1016/S0165-2370(97)00028-4.

[90] G. Varhegyi, M. J. Antal, T. Szekely, P. Szabo, Kinetics of the thermal decomposition of cellulose, hemicellulose, and sugarcane bagasse, Energy & Fuels 3 (3) (1989) 329–335. doi:10.1021/ef00015a012.

[91] C. A. Koufopanos, A. Lucchesi, G. Maschio, Kinetic modelling of the pyrolysis of biomass and biomass components, The Canadian Journal of Chemical Engineering 67 (1) (1989) 75–84. doi:10.1002/cjce.5450670111.

[92] D. Ferdous, A. K. Dalai, S. K. Bej, R. W. Thring, Pyrolysis of Lignins: Experimental and Kinetics Studies, Energy & Fuels 16 (6) (2002) 1405–1412. doi:10.1021/ef0200323.

[93] J. A. Caballero, R. Font, A. Marcilla, J. A. Conesa, New kinetic model for thermal decomposition of heterogeneous materials, Industrial & Engineering Chemistry Research 34 (3) (1995) 806–812. doi:10.1021/ie00042a012.

[94] H. Yang, R. Yan, H. Chen, D. H. Lee, C. Zheng, Characteristics of hemicellulose, cellulose and lignin pyrolysis, Fuel 86 (12-13) (2007) 1781–1788. doi:10.1016/j.fuel.2006.12.013.

[95] P. Fu, W. Yi, X. Bai, Z. Li, S. Hu, J. Xiang, Effect of temperature on gas composition and char structural features of pyrolyzed agricultural residues, Bioresource Technology 102 (17) (2011) 8211–8219. doi:10.1016/j.biortech.2011.05.083.

[96] Z. Wang, J. Cao, J. Wang, Pyrolytic characteristics of pine wood in a slowly heating and gas sweeping fixed-bed reactor, Journal of Analytical and Applied Pyrolysis 84 (2) (2009) 179–184. doi:10.1016/j.jaap.2009.02.001.

[97] T. Milne, R. Evans, N. Abatzoglou, Biomass Gasifier "Tars": Their Nature, Formation and Conversion, Tech. rep., National Renewable Energy Laboratory & Kemestrie, Inc., NREL/TP-570-25357 (1998).

[98] T. Hosoya, H. Kawamoto, S. Saka, Secondary reactions of lignin-derived primary tar components, Journal of Analytical and Applied Pyrolysis 83 (1) (2008) 78–87. doi:10.1016/j.jaap.2008.06.003.

[99] T. Hosoya, H. Kawamoto, S. Saka, Solid/liquid - and vapor - phase interactions between cellulose - and lignin - derived pyrolysis products, Journal of Analytical and Applied Pyrolysis 85 (2009) 237–246. doi:10.1016/j.jaap.2008.11.028.

[100] L. Fagernäs, E. Kuoppala, K. Tiilikkala, A. Oasmaa, Chemical Composition of Birch Wood Slow Pyrolysis Products, Energy Fuels 26 (2) (2012) 1275–1283. doi:10.1021/ef2018836.

[101] M. Hajaligol, B. Waymack, D. Kellogg, Low temperature formation of aromatic hydrocarbon from pyrolysis of cellulosic materials, Fuel 80 (12) (2001) 1799 – 1807. doi:10.1016/S0016-2361(01)00063-1.

[102] B. Scholze, D. Meier, Characterization of the water-insoluble fraction from pyrolysis oil (pyrolytic lignin). part i. py-gc/ms, ftir, and functional groups, Journal of Analytical and Applied Pyrolysis 60 (1) (2001) 41 – 54. doi:10.1016/S0165-2370(00)00110-8.

[103] L. J. Jandris, R. K. Force, Determination of the fluorescence properties of polynuclear aromatic hydrocarbons in the vapor phase and adsorbed on solid supports by laser-induced molecular fluorescence, Analytica Chimica Acta 175 (1985) 333 – 337. doi:10.1016/S0003-2670(00)82749-X.

[104] J. H. Richardson, M. Ando, Sub-part-per-trillion detection of polycyclic aromatic-hydrocarbons by laser-induced molecular fluorescence, Analytical Chemistry 49 (7) (1977) 955–959. doi:10.1021/ac50015a021.

[105] M. Prins, Z. Li, R. Bastiaans, J. van Oijen, M. Aldén, L. de Goey, Biomass pyrolysis in a heated-grid reactor: Visualization of carbon monoxide and formaldehyde using laser-induced fluorescence, Journal of Analytical and Applied Pyrolysis 92 (2) (2011) 280–286. doi:10.1016/j.jaap.2011.06.008.

[106] R. Sun, N. Zobel, Y. Neubauer, C. Cardenas Chavez, F. Behrendt, Analysis of gas-phase polycyclic aromatic hydrocarbon mixtures by laser-induced fluorescence, Optics and Lasers in Engineering 48 (12) (2010) 1231–1237. doi:10.1016/j.optlaseng.2010.06.009.

[107] D. A. Skoog, F. J. Holler, S. R. Crouch, Principles of Instrumental Analysis, Brooks/Cole, 2006, ISBN-10: 0495012017.

[108] Katharina Kohse-Höinghaus and Jay B. Jeffries (Ed.), Applied Combustion Diagnostics, Taylor & Francis,, 2002, ISBN: 9781560329138.

[109] F. Ossler, T. Metz, M. Aldén, Picosecond laser-induced fluorescence from gas-phase polycyclic aromatic hydrocarbons at elevated temperatures. I. Cell measurements, Applied Physics B: Lasers and Optics 72 (4) (2001) 465–478. doi:10.1007/s003400100519.

[110] A. Bruno, F. Ossler, C. de Lisio, P. Minutolo, N. Spinelli, A. D'Alessio, Detection of fluorescent nanoparticles in flame with femtosecond laser-induced fluorescence anisotropy, Optics Express 16 (8) (2008) 5623–5632. doi:10.1364/OE.16.005623.

[111] M. Sirignano, A. Collina, M. Commodo, P. Minutolo, A. D´Anna, Detection of aromatic hydrocarbons and incipient particles in an opposed-flow flame of ethylene by spectral and time-resolved laser induced emission spectroscopy, Combustion and Flame 159 (4) (2012) 1663 – 1669. doi:10.1016/j.combustflame.2011.11.005.

[112] C. Baumhakl, S. Karellas, Tar analysis from biomass gasification by means of online fluorescence spectroscopy, Optics and Lasers in Engineering 49 (7) (2011) 885–891. doi:10.1016/j.optlaseng.2011.02.015.

[113] C. Brackmann, M. Alden, P. Bengtsson, K. Davidsson, J. Pettersson, Optical and mass spectrometric study of the pyrolysis gas of wood particles, Applied Spectroscopy 57 (2) (2003) 216–222. doi:10.1366/000370203321535141.

[114] N. Zobel, A. Anca-Couce, Influence of intraparticle secondary heterogeneous reactions on the reaction enthalpy of wood pyrolysis, Journal of Analytical and Applied Pyrolysis (2015) –In Press. doi:10.1016/j.jaap.2015.08.019.

[115] Y. Wang, X. Li, D. Mourant, R. Gunawan, S. Zhang, C.-Z. Li, Formation of Aromatic Structures during the Pyrolysis of Bio-oil, Energy & Fuels 26 (1) (2012) 241–247. doi:10.1021/ef201155e.

[116] E. Schröder, Experiments on the pyrolysis of large beechwood particles in fixed beds, Journal of Analytical and Applied Pyrolysis 71 (2) (2004) 669–694. doi:10.1016/j.jaap.2003.09.004.

[117] R. M. Baldwin, K. A. Magrini-Bair, M. R. Nimlos, P. Pepiot, B. S. Donohoe, J. E. Hensley, S. D. Phillips, Current research on thermochemical conversion of biomass at the National Renewable Energy Laboratory, Applied Catalysis B: Environmental 115-116 (0) (2012) 320–329. doi:10.1016/j.apcatb.2011.10.033.

[118] J. Lakowicz, Principles of Fluorescence Spectroscopy, Springer Science+Business Media, LLC, 2006, ISBN: 978-0-387-46312-4.

[119] A. P. Schinkel, Zur Bildung und Degradation von Teeren aus der Pyrolyse nachwachsender Rohstoffe, Ph.D. thesis, Universitaet Kassel, ISBN online: 978-3-89958-709-4 (2008).

[120] D. Neves, H. Thunman, A. Matos, L. Tarelho, A. Gómez-Barea, Characterization and prediction of biomass pyrolysis products, Progress in Energy and Combustion Science 37 (5) (2011) 611–630. doi:10.1016/j.pecs.2011.01.001.

[121] P. Ahuja, S. Kumar, P. C. Singh, A model for primary and heterogeneous secondary reactions of wood pyrolysis, Chem. Eng. Technol. 19 (3) (1996) 272–282. doi:10.1002/ceat.270190312.

[122] M. L. Boroson, J. B. Howard, J. P. Longwell, W. A. Peters, Heterogeneous cracking of wood pyrolysis tars over fresh wood char surfaces, Energy Fuels 3 (6) (1989) 735–740. doi:10.1021/ef00018a014.

[123] H. Keller-Rudek, G. K. Moortgat, R. Sander, R. Sörensen, The MPI-Mainz UV/VIS spectral atlas of gaseous molecules of atmospheric interest, Earth Syst. Sci. Data 5 (2013) 365–373. doi:10.5194/essd-5-365-2013.

[124] M. Orain, P. Baranger, B. Rossow, F. Grisch, Fluorescence spectroscopy of naphthalene at high temperatures and pressures: implications for fuel-concentration measurements, Applied Physics B: Lasers ans Optics 102 (1) (2011) 163–172. doi:10.1007/s00340-010-4353-7.

[125] H. Grosch, Z. Sárossy, H. Egsgaard, A. Fateev, UV absorption cross-sections of phenol and naphthalene at temperatures up to 500 °C, Journal of Quantitative Spectroscopy and Radiative Transfer 156 (2015) 17 – 23. doi:10.1016/j.jqsrt.2015.01.021.

[126] L. R. Allain, D. N. Stratis, B. M. Cullum, J. Mobley, M. R. Hajaligol, T. Vo-Dinh, Real-time detection of PAH mixtures in the vapor phase at high temperatures, Journal of Analytical and Applied Pyrolysis 66 (1-2) (2003) 145–154. doi:10.1016/S0165-2370(02)00110-9.

[127] A. C. Somersall, J. E. Guillet, Photochemistry of Ketone Polymers. VIII. Fluorescence and Energy Transfer of Aliphatic and Poly(vinyl ketones), Macromolecules 5 (4) (1972) 410–415. doi:10.1021/ma60028a016.

[128] D. Hansen, E. Lee, Radiative and nonradiative transitions in the first excited singlet state of simple linear aldehydes, J. Chem. Phys. 63 (1975) 3272. doi:10.1063/1.431802.

[129] I. Duchesne, E. Hult, U. Molin, G. Daniel, T. Iversen, H. Lennholm, The influence of hemicellulose on fibril aggregation of kraft pulp fibres as revealed by fe-sem and cp/mas 13c-nmr, Cellulose 8 (2) (2001) 103–111. doi:10.1023/A:1016645809958.

[130] P. R. Patwardhan, R. C. Brown, B. H. Shanks, Product distribution from the fast pyrolysis of hemicellulose, ChemSusChem 4 (2011) 636–643. doi:10.1002/cssc.201000425.

[131] C. Di Blasi, G. Signorelli, G. Portoricco, Countercurrent Fixed-Bed Gasification of Biomass at Laboratory Scale, Ind. Eng. Chem. Res. 38 (7) (1999) 2571–2581. doi:10.1021/ie980753i.

[132] L. Aguiar, F. Márquez-Montesinos, A. Gonzalo, J. Sánchez, J. Arauzo, Influence of temperature and particle size on the fixed bed pyrolysis of orange peel residues, Journal of Analytical and Applied Pyrolysis 83 (1) (2008) 124–130. doi:10.1016/j.jaap.2008.06.009.

[133] A. Anca-Couce, N. Zobel, A. Berger, F. Behrendt, Smouldering of pine wood: Kinetics and reaction heats, Combustion and Flame 159 (4) (2012) 1708–1719. doi:10.1016/j.combustflame.2011.11.015.

[134] C. Ryu, V. N. Sharifi, J. Swithenbank, Waste pyrolysis and generation of storable char, International Journal of Energy Research 31 (2) (2007) 177–191. doi:10.1002/er.1241.

[135] E. Granada, P. Eguía, J. Vilan, J. Comesaña, R. Comesaña, FTIR quantitative analysis technique for gases. Application in a biomass thermochemical process, Renewable Energy 41 (0) (2012) 416–421. doi:10.1016/j.renene.2011.11.020.

[136] M. Boroson, J. Howard, J. Longwell, W. Peters, Product yields and kinetics from the vapor-phase cracking of wood pyrolysis tars, AIChE Journal 35 (1) (1989) 120–128. doi:10.1002/aic.690350113.

[137] P. Gilbert, C. Ryu, V. Sharifi, J. Swithenbank, Tar reduction in pyrolysis vapours from biomass over a hot char bed, Bioresource Technology 100 (23) (2009) 6045–6051. doi:10.1016/j.biortech.2009.06.041.

[138] V. Srinivasan, S. Adhikari, S. A. Chattanathan, S. Park, Catalytic Pyrolysis of Torrefied Biomass for Hydrocarbons Production, Energy Fuels 26 (12) (2012) 7347–7353. doi:10.1021/ef301469t.

[139] J. Ahrenfeldt, H. Egsgaard, W. Stelte, T. Thomsen, U. B. Henriksen, The influence of partial oxidation mechanisms on tar destruction in TwoStage biomass gasification, Fuel 112 (0) (2013) 662–680. doi:10.1016/j.fuel.2012.09.048.

[140] S. Xin, H. Yang, Y. Chen, X. Wang, X. Chen, ssessment of pyrolysis polygeneration of biomass based on major components: Product characterization and elucidation of degradation pathways, Fuel 113 (0) (2013) 266 – 273. doi:10.1016/j.fuel.2013.05.061.

[141] D. Shen, S. Gu, A. Bridgwater, The thermal performance of the polysaccharides extracted from hardwood: Cellulose and hemicellulose, Carbohydrate Polymers 82 (1) (2010) 39 – 45. doi:10.1016/j.carbpol.2010.04.018.

[142] M. Milhe, L. van de Steene, M. Haube, J. M. Commandre, W.-F. Fassinou, G. Flamant, Autothermal and allothermal pyrolysis in a continuous fixed bed reactor, Journal of Analytical and Applied Pyrolysis 103 (2013) 102 – 111. doi:10.1016/j.jaap.2013.03.011.

[143] J. Lehmann, S. Joseph, Biochar for Environmental Management. Science and Technology, Earthescan, UK and USA, 2009, Ch. 1: Biochar for Environmental Mangement: An Introduction, pp. 1–12, ISBN: 978-1-84407-658-1.

[144] E.-D. Schulze, C. Körner, B. E. Law, H. Haberl, S. Luyssaert, Large-scale bioenergy from additional harvest of forest biomass is neither sustainable nor greenhouse gas neutral, GCB Bioenergy 4 (2012) 611–616. doi:10.1111/j.1757-1707.2012.01169.x.

[145] A. Alessandro, G. Jacopo, B. Aikaterini, Carbon accounting of forest bioenergy, Tech. rep., European Commission, Joint Research Center, Intitute for Energy and Transport, EUR 25354 EN. ISBN: 978-92-79-25100-9 (2013).

[146] L. Montanarella, E. Lugato, The Application of Biochar in the EU: Challenges and Opportunities, Agronomy 3 (2013) 462–473. doi:10.3390/agronomy3020462.

[147] K. Y. Chan, Z. Xu, Biochar for Environmental Management. Science and Technology, Earthescan, UK and USA, 2009, Ch. 5: Nutrient Properties and Their Enhancement, pp. 67–84, ISBN: 978-1-84407-658-1.

[148] A. Downie, A. Crosky, P. Munroe, Biochar for Environmental Management. Science and Technology, Earthscan, UK and USA, 2009, Ch. 2: Physical Properties of Biochar, pp. 13–32, ISBN: 978-1-84407-658-1.

[149] J. Lehmann, C. Czimczik, D. Laird, S. Sohi, Biochar for Environmental Management. Science and Technology, Earthescan in the UK and USA, 2009, Ch. 11: Stability of Biochar in the Soil, pp. 183–205, ISBN: 978-1-84407-658-1.

[150] P. Conte, H. P. Schmidt, G. Cimo, Agricultural and Environmental Application of Biochar: Addvances and Barriers, SSSA, 2015, Ch. Research and Application of Biochar in Europe. doi:10.2136/sssaspecpub63.2014.0050.

[151] International Biochar Initiative, Online available at: www.biochar-international.org. Last accessed 09.06.2015.

[152] C. Kamman, H.-P. Schmidt, Biochar in Europe, The Biochar Journal, Arbaz, Switzerland, ISSN 2297-1114Online available at: www.biochar-journal.org/en/ct/34. Last accessed 16.03.15.

[153] Interreg IVB North Sea Region project "Biochar: climate saving soils", Website, Online available at: http://www.biochar-interreg4b.eu/. Last accessed 09.06.2015.

[154] Refertil. Reducing mineral fertilisers and cchemical use in agriculture by recycling treated organic waste as compost for bio-char products, Website, Online available at: http://www.refertil.info/. Last accessed 27.11.2015.

[155] Fertiplus. Reducing mineral fertilisers and agro-chemicals by recycling treated organic waste as compost and bio-char, Website, Online available at: http://www.fertiplus.eu/. Last accessed 27.11.2015.

[156] W. Trimble, On Charring wood, Plough, the Loom and the Anvil, Vol. 3, 513-516, 1851.

[157] J. Morley, Following through with grass seeds, The National Greenkeeper 1 (1) (1927) 15.

[158] J. Morley, Compost and charcoal, The National Greenkeeper 3 (9) (1929) 8–26.

[159] E. Tyron, Effect of charcoal on certain physical, chemical and biological properties of forest soils, Ecological Monographs 18 (1948) 81–115. doi:10.2307/1948629.

[160] B. Glaser, L. Haumaier, G. Guggenberger, W. Zech, The "Terra Preta" phenomenon: a model for sustainable agriculture in the humid tropics, Naturwissenschaften 88 (2001) 37–41. doi:10.1007/s001140000193.

[161] J. Lehmann, J. Gaunt, M. Rondon, Bio-char sequestration in terrestrial ecosystems - a review, Mitigation and Adaptation Strategies for Global Change 11 (2006) 403–427. doi:10.1007/s11027-005-9006-5.

[162] R. Brown, Biochar for Environmental Management. Science and Technology, Earthescan in the UK and USA, 2009, Ch. 8: Biochar Production Technology, pp. 127–146, ISBN: 978-1-84407-658-1.

[163] J. Manya, Pyrolysis for biochar purposes: A review to establish current knowedge gaps and research needs, Environmental Science & Technology 46 (2012) 7939–7954. doi:10.1021/es301029g.

[164] J. Libra, K. Ro, C. Kamman, A. Funke, N. Berge, Y. Neubauer, T. M.M., C. Führner, O. Bens, K. J., K.-H. Emmerich, Hydrothermal carbonization of biomass residuals: a comparative review of the chemistry, process and application of wet and dry pyrolysis, Biofuels 2 (1) (2011) 89–124. doi:10.4155/BFS.10.81.

[165] E. Cetin, B. Moghtaderi, R. Gupta, T. Wall, Influence of pyrolysis conditions on the structure and gasification reactivity of biomass chars, Fuel 83 (2004) 2139–2150. doi:10.1016/j.fuel.2004.05.008.

[166] M. Guerrero, M. Pilar Ruiz, A. Millera, M. Alzueta, R. Bilbao, Characterization of biomass chars formed under different devolatilization conditions: Differences between rice husk and eucalyptus, Energy & Fuels 22 (2008) 1275–1284. doi:10.1021/ef7005589.

[167] H. Marsh, F. Rodriguez-Reinoso, Chapter 2 - activated carbon (origins), in: H. M. Rodriguez-Reinoso (Ed.), Activated Carbon, Elsevier Science Ltd, Oxford, 2006, pp. 13 – 86. doi:10.1016/B978-008044463-5/50016-9.

[168] L. Pulido-Novicio, T. Hata, Y. Kurimoto, S. Doi, S. Ishihara, Y. Imamura, Adsorption capacities and related characteristics of wood charcoals carbonized using a one-step or two-step process, Journal of Wood Science 47 (1) (2001) 48–57. doi:10.1007/BF00776645.

[169] R. A. Brown, A. K. Kercher, T. H. Nguyen, D. C. Nagle, W. P. Ball, Production and characterization of synthetic wood chars for use as surrogates for natural sorbents, Organic Geochemistry 37 (3) (2006) 321 – 333. doi:10.1016/j.orggeochem.2005.10.008.

[170] J. Guo, A. C. Lua, Characterization of chars pyrolyzed from oil palm stones for the preparation of activated carbons, Journal of Analytical and Applied Pyrolysis 46 (2) (1998) 113 – 125. doi:10.1016/S0165-2370(98)00074-6.

[171] T. Zhang, W. P. Walawender, L. T. Fan, M. Fan, D. Daugaard, R. C. Brown, Preparation of activated carbon from forest and agricultural residues through co2 activation, Chemical Engineering Journal 105 (2004) 53 – 59. doi:10.1016/j.cej.2004.06.011.

[172] K. A. Spokas, Review of the stability of biochar in soils: predictability of o:c molar ratios, Carbon Management 1 (2) (2010) 289–303. doi:10.4155/CMT.10.32.

[173] H. Knicker, K. U. Totsche, G. Almendros, F. J. Gonzalez-Vila, Condensation degree of burnt peat and plant residues and the reliability of solid-state vacp mas 13c nmr spectra obtained from pyrogenic humic material, Organic Geochemistry 36 (10) (2005) 1359 – 1377. doi:10.1016/j.orggeochem.2005.06.006.

[174] G. Almendros, H. Knicker, F. J. Gonzalez-Vila, Rearrangement of carbon and nitrogen forms in peat after progressive thermal oxidation as determined by solid-state 13c- and 15n-nmr spectroscopy, Organic Geochemistry 34 (11) (2003) 1559 – 1568. doi:10.1016/S0146-6380(03)00152-9.

[175] E. S. Krull, J. A. Baldock, J. O. Skjemstad, R. J. Smernik, Biochar for Environmental Management. Science and Technology, Earthescan in the UK and USA, 2009, Ch. 4: Characteristics of Biochar: Organo-chemical Properties, pp. 53–65, ISBN: 978-1-84407-658-1.

[176] S. Schimmelpfennig, B. Glaser, One step forward toward characterization: Some important material properties to distinguish biochars, Journal of Environmental Quality 41 (4) (2012) 1001–1013. doi:10.2134/jeq2011.0146.

[177] J. A. Baldock, R. J. Smernik, Chemical composition and bioavailability of thermally altered pinus resinosa (red pine) wood, Organic Geochemistry 33 (9) (2002) 1093 – 1109. doi:10.1016/S0146-6380(02)00062-1.

[178] J. Lehmann, J. J. Pereira da Silva, C. Steiner, T. Nehls, W. Zech, B. Glaser, Nutrient availability and leaching in an archaeological Anthrosol and a Ferralsol of the Central Amazon basin: fertilizer, manure and charcoal amendments, Plant and Soil 249 (2) (2003) 343–357. doi:10.1023/A:1022833116184.

[179] K. Y. Chan, L. Van Zwieten, I. Meszaros, A. Downie, S. Joseph, Agronomic values of greenwaste biochar as a soil amendment, Australian Journal of Soil Research 45 (2007) 629–634. doi:10.1071/SR07109.

[180] B. Liang, J. Lehmann, D. Solomon, J. Kinyangi, J. Grossman, B. O'Neill, J. O. Skjemstad, J. Thies, F. J. Luizao, J. Petersen, E. G. Neves, Black Carbon Increases Cation Exchange Capacity in Soils, Soil Science Society of America Journal 70 (5) (2006) 1719–1730. doi:10.2136/sssaj2005.0383.

[181] J. Lehmann, Bio-energy in the black, Front. Ecol. Environ. 5 (7) (2007) 381–387. doi:10.1890/1540-9295(2007)5[381:BITB]2.0.CO;2.

[182] T. H. DeLuca, M. D. MacKenzie, M. J. Gundale, W. E. Holben, Wildfire-Produced Charcoal Directly Influences Nitrogen Cycling in Ponderosa Pine Forests, Soil Science Society of America Journal 70 (2) (2006) 448–453. doi:10.2136/sssaj2005.0096.

[183] C.-H. Cheng, J. Lehmann, J. E. Thies, S. D. Burton, M. H. Engelhard, Oxidation of black carbon by biotic and abiotic processes, Organic Geochemistry 37 (11) (2006) 1477 – 1488. doi:10.1016/j.orggeochem.2006.06.022.

[184] A. Mukherjee, A. Zimmerman, W. Harris, Surface chemistry variations among a series of laboratory-produced biochars, Geoderma 163 (3-4) (2011) 247 – 255. doi:10.1016/j.geoderma.2011.04.021.

[185] J. W. Gaskin, C. Steiner, K. Harris, K. C. Das, B. Bibens, Effect of low-temperature pyrolysis conditions on biochar for agricultural use, Transactions of the Asabe 51(6) (2008) 2061–2069. doi:10.13031/2013.25409.

[186] C.-H. Cheng, J. Lehmann, M. H. Engelhard, Natural oxidation of black carbon in soils: Changes in molecular form and surface charge along a climosequence, Geochimica et Cosmochimica Acta 72 (6) (2008) 1598 – 1610. doi:10.1016/j.gca.2008.01.010.

[187] A. Garcia Rueda, Characterization of biochar for soil amendment purpose, Master's thesis, Technische Universität Berlin (2013).

[188] J. Rouquerol, D. Avnir, C. W. Fairbridge, D. H. Everett., J. H. Haynes, N. Pernicone, J. D. F. Ramsay, K. S. W. Sing, K. K. Unger, Recommendations for the characterization of porous solids, Pure & Appl. Chem. 66 (8) (1994) 1739–1758. doi:10.1351/pac199466081739.

[189] IUPAC. Compendium of Chemical Terminology, 2nd ed. (the Gold Book), Blackwell Scientific Publications, Oxford, 1997, Compiled by A. D. McNaught and A. Wilkinson. ISBN 0-9678550-9-8. doi:10.1351/goldbook.

[190] S. Lowell, J. E. Shields, Powder Surface Area and Porosity. Third edition, Chapman & Hall Ltd., 1991, ISBN: 978-90-481-4005-3.

[191] J. Rouquerol, F. Rouquerol, P. Llewellyn, G. Maurin, K. Sing, Adsorption by Powders and Porous Solids: Principles, Methodology and Applications, Elsevier Science, 2013, ISBN: 9780080970363.

[192] S. Brunauer, L. S. Deming, W. E. Deming, E. Teller, On a Theory of the van der Waals Adsorption of Gases, Journal of the American Chemical Society 62 (7) (1940) 1723–1732. doi:10.1021/ja01864a025.

[193] I. Langmuir, The adsorption of gases on plane surfaces of glass, mica and platinum, J. Amer. Chem. Soc. 40 (1918) 1361–1402. doi:10.1021/ja02242a004.

[194] S. Brunauer, P. H. Emmett, E. Teller, Adsorption of Gases in Multimolecular Layers, J. Amer. Chem. Soc. 60 (2) (1938) 309–319. doi:10.1021/ja01269a023.

[195] L. G. Gurvich, Physico-chemical attractive force, Zh. Russ. Fiz-Khim. Obshchestva Chem. 47 (1915) 805–827.

[196] J. de Boer, B. Lippens, B. Linsen, J. Broekhoff, A. van den Heuvel, T. Osiga, The t-curve of multimolecular N2 adsorption, Journal Colloid Interface Science 21 (1966) 405–414. doi:10.1016/0095-8522(66)90006-7.

[197] E. P. Barrett, L. G. Joyner, P. P. Halenda, The determination of pore volume and area distributions in porous substances. i. computations from nitrogen isotherms, Journal of the American Chemical Society 73 (1) (1951) 373–380. doi:10.1021/ja01145a126.

[198] Quantachrome Instruments, NOVA operation manual. High speed gas sorption analyzer. Versions 10.0 and above, P/N 05069 Rev L (2008).

[199] N. Seaton, J. Walton, N. Quirke, A new analysis method for the determination of the pore-size distribution of porous carbons from nitrogen adsorption measurements, Carbon 27 (1989) 853–861. doi:10.1016/0008-6223(89)90035-3.

[200] J. Landers, G. Gor, A. Neimark, Density functional theory mmethod for characterization of porous materials, Colloids and Surfaces, A: Physicochemical and Engineering Aspects 437 (2013) 3–32. doi:10.1016/j.colsurfa.2013.01.007.

[201] J. E. Amonette, S. Joseph, Biochar for Environmental Management. Science and Technology, Earthescan, UK and USA, 2009, Ch. 3: Characteristics of Biochar: Microchemical Properties, pp. 33–52, ISBN: 978-1-84407-658-1.

[202] S. Sohi, E. Krull, E. Lopez-Capel, R. . Bol, Chapter 2 - a review of biochar and its use and function in soil, in: D. L. Sparks (Ed.), Advances in Agronomy, Vol. 105 of Advances in Agronomy, Academic Press, 2010, pp. 47 – 82. doi:10.1016/S0065-2113(10)05002-9.

[203] H. P. Boehm, E. Diehl, W. Heck, R. Sappok, Surface oxides of carbon, Angew. Chem. internat. Edit. 3 (10) (1964) 669–677. doi:10.1002/anie.196406691.

[204] S. L. Goertzen, K. D. Theriault, A. M. Oickle, A. C. Tarasuk, H. A. Andreas, Standardization of the boehm titration. part i. {CO2} expulsion and endpoint determination, Carbon 48 (4) (2010) 1252 – 1261. doi:10.1016/j.carbon.2009.11.050.

[205] l. Tsechansky, E. R. Graber, Methodological limitations to determining acidic groups at biochar surfaces via the Boehm titration, Carbon 66 (2014) 730–733. doi:10.1016/j.carbon.2013.09.044.

[206] G. Ojeda, S. Mattana, M. BonmatÃ, S. K. Woche, J. Bachmann, Soil wetting-drying and water-retention properties in a mine-soil treated with composted and thermally-dried sludges, European Journal of Soil Science 62 (5) (2011) 696–708. doi:10.1111/j.1365-2389.2011.01378.x.

[207] D. Fabbri, A. G. Rombola, C. Torri, K. A. Spokas, Determination of polycyclic aromatic hydrocarbons in biochar and biochar amended soil, Journal of Analytical and Applied Pyrolysis 103 (0) (2013) 60 – 67, pyrolysis 2012. doi:10.1016/j.jaap.2012.10.003.

[208] D. Fabbri, C. Torri, K. A. Spokas, Analytical pyrolysis of synthetic chars derived from biomass with potential agronomic application (biochar). relationships with impacts on microbial carbon dioxide production, Journal of Analytical and Applied Pyrolysis 93 (0) (2012) 77 – 84. doi:10.1016/j.jaap.2011.09.012.

[209] A. R. Zimmerman, Abiotic and microbial oxidation of laboratory-produced black carbon, Environ. Sci. Technol. 44 (2010) 1295–1301. doi:10.1021/es903140c.

[210] B. T. Nguyen, J. Lehmann, Black carbon decomposition under varying water regimes, Organic Geochemistry 40 (8) (2009) 846 – 853. doi:10.1016/j.orggeochem.2009.05.004.

[211] M. Carrier, A. G. Hardie, A. Uras, J. Görgens, J. H. Knoetze, Production of char from vacuum pyrolysis of South-African sugar cane bagasse and its characterization as activated carbon and biochar, Journal of Analytical and Applied Pyrolysis 96 (0) (2012) 24 – 32. doi:10.1016/j.jaap.2012.02.016.

[212] J. W. Lee, M. Kidder, B. R. Evans, S. Paik, A. C. B. III, C. T. Garten, R. C. Brown, Characterization of Biochars Produced from Cornstovers for Soil

Amendment, Environmental Science & Technology 44 (20) (2010) 7970–7974. doi:10.1021/es101337x.

[213] G. Ojeda, S. Mattana, A. Avila, J. M. Alcaniz, M. Volkmann, J. Bachmann, Are soil-water functions affected by biochar application?, Geoderma 249-250 (2015) 1 – 11. doi:10.1016/j.geoderma.2015.02.014.

ISBN 978-3-945682-22-7

Alba Dieguez Alonso 2015

961